A Peel Adhesion Test For Thermal Spray Coatings

by

Michael Sexsmith

BASc., The University British Columbia 1993

A Thesis Submitted in Partial Fulfillment of
The Requirements for the Degree of
Master of Applied Science

in

The Faculty of Graduate Studies
Department of Metal And Materials Engineering

We Accept this thesis as conforming to the required standard

The University of British Columbia
July 1995

In presenting this thesis in partial fulfilment of the requirements for an advanced degree at the University of British Columbia, I agree that the Library shall make it freely available for reference and study. I further agree that permission for extensive copying of this thesis for scholarly purposes may be granted by the head of my department or by his or her representatives. It is understood that copying or publication of this thesis for financial gain shall not be allowed without my written permission.

Department of Metals and Materials Engineering

The University of British Columbia
Vancouver, Canada

Date Oct 12 1995

Abstract

In order for the thermal spray industry to progress, informative and reliable coating evaluation techniques are needed. The measurement of adhesion is an important problem and existing tests have severe limitations. A peel adhesion test has been adapted to thermal spray coatings from the adhesives industry which should address this problem. In a peel test, a thin metal foil is coated by plasma spraying. The foil is then peeled off of the coating at a constant speed. The force required for separation is monitored as a function of crack position. The force is than converted into a peel strength which is equivalent to the energy required for separation. The test allows the detection of variations in adhesion within a single sample. Interface defects were detected and correlated with features of the peel test curve. The measured parameter of energy per unit area of fracture, was found to be representative of interfacial fracture toughness. The peel test was used to determine interface toughnesses in the range of 10 to 60 J/m^2 for ceramic coatings, 150 to 250 J/m^2 for cermet coatings and 160 to 300 J/m^2 for metal coatings.

A literature review of interfacial fracture mechanics revealed the complexity of determining the interface stress intensities so an energy balance approach is used to determine the energy consumed in separating the coating from the substrate. The balance accounts for the energies associated with adherand deformation, friction, applied loads, and residual stress. Both a numerical and experimental method of determining the work of deformation in the substrate were developed. The numerical method allowed the calculation of the work of deformation based on an arbitrary elastoplastic stress-strain curve for the foil material. The experimental method measured the energy of deformation by imitating the peeling process without an interface. Both methods were in agreement for the adherand materials tested. The deformation work was found to be a significant fraction of the total energy. Deformation energies, when normalized to the foil area, were found in the range 30 J/m^2 to 400 J/m^2 depending on the material. Friction was also measured experimentally so that all of energies consumed in the test could be determined independently. It was found to add about 10 to 15% to the measure loads.

The adhesion of a range of different thermal spray coatings (TSCs) was measured. The adhesion of the spray pattern profile was studied as well as the adhesion of uniform coatings. The results were compared with the ASTM standard for TSC adhesion measurement, the expected range of interface toughnesses and the Vickers hardness of the coating. The comparisons indicate that the measurement is self consistent and produces results comparable to other toughness measurements. A comparison between the ASTM standard test and the peel test was not possible due the fact that the ASTM test is unable to test coatings stronger that 70 MPa. Most of the coatings studied were much stronger than this limit. Comparison with hardness showed that harder and more brittle coatings adhered with lower energies than softer coatings. This is consistent with our understanding of the fracture of materials. It was found that the adhesion of a uniform coating was comparable to the adhesion of the central region of the spray pattern. This indicates that the poor adhesion of the periphery particles does not significantly affect the adhesion of a coating.

The need to do further work in understanding the effects of residual stress on bonding was identified. The residual stress in a coating can alter the type of loading which the interface experiences and can reduce the adhesion of a coating to very low values as shown. A complete mechanical description of the peeling process should be developed which includes the effects of residual stress. In order to allow the relationship between the peel test and the service life of a coating, performance comparisons should be made between the tested coatings. The peel test was found to be a simple inexpensive method for reliably determining the adhesion of a thermal spray coating.

Key Words

Thermal Spray Coatings, Adhesion, Peel testing, Fracture Mechanics, Interface toughness.

Table of Contents

List of Tables

List of Figures

Acknowledgment

The author wished to thank Dr. Tom Troczynski for his motivating guidance in this work. The assistance of HS Tools, NW Mettech, Metcon Services and Norton in the production of coatings for this research was greatly appreciated. The author wishes to thank the staff, students and faculty of the Department of Metals and Materials Engineering at UBC for maintaining the stimulating environment under which this work was completed. The finical support of The British Columbia Science Council is gratefully acknowledged

1. Introduction

Many processes which degrade the performance of materials are associated with surface phenomena. These processes include corrosion, wear, friction and combinations of these. Due to the large costs associated with repairing or preventing this degradation, many techniques have been developed which modify the surface properties of materials. One of the most promising techniques of surface modification is thermal spraying. In this process a torch is used to produce a thermal plasma either by an electric arc or combustion process. This plasma is an ionized gas which can have temperature up to 15000K. Material is introduced into the plasma, in the form of wire, rod or powder, where it is rapidly heated. The material is accelerated by the plasma towards a substrate where it impacts and cools. For a single particle, the process occurs in less than a millisecond. In this time some of the material evaporates, some melts and chemical reactions may occur. All of these processes occur too quickly for equilibrium to be reached. A coating is formed by the buildup of many of these small particles.

Thermal spray coatings offer an economical opportunity to improve the surface of engineered components. This opportunity will only be realized if the problems associated with processing, evaluating and utilizing the special properties of the coating in a cost efficient and meaningful manner can be solved. One of the major problems involved in the use of coatings is their adhesion. The coating cannot perform its function if it does not remain in place. Thus an understanding of adhesion is fundamental to the progress of this technology. In order to understand adhesion, measurement techniques which are both informative and reliable are needed. This study was undertaken to develop a peel adhesion test which would improve our fundamental knowledge of coatings and simultaneously allow a simple industrial evaluation of coating quality.

1.1 Thermal Spraying

Thermal spraying is a process by which a wide variety of substrates can be coated with various metals, ceramics and polymers. In this process a torch is used to produce a hot plasma flame which is accelerated away from the nozzle. The coating material is injected into the flame at the nozzle, either in the form of powder, rod or wire. The material melts rapidly and is accelerated towards the substrate where it impacts and rapidly solidifies. The coating produced has a very unique microstructure which consists of individual splats stacked upon one another other. A complete discussion of the process was presented by Boulos [1].

The process has several advantages over conventional coating techniques. The first is that a wide variety of materials including polymers, ceramics, metals and composites can be sprayed onto the same range of substrates. This flexibility means that a manufacturer can change the coating material without significantly altering the equipment needed. A second advantage of the process is its portability. The required equipment is usually small in size. Most torches can be handheld or mounted on robotic arms. Some systems are portable and can be easily moved to a jobsite. Accompanying this small size is a correspondingly low capital cost. Large expensive tanks, vacuum chambers and furnaces are not needed.

Because of these advantages, the process has attracted attention from many industries, which can be divided into three categories: manufacturing (e.g. automotive), infrastructure repair (e.g. petrochemical plants) and high technology (e.g. aircraft). There are three classes of materials which are commonly sprayed: metals (e.g. super alloys), oxide ceramics (e.g. alumina) and cermets (e.g. tungsten carbide and cobalt.) The coatings are usually used to modify the surface properties to improve wear resistance, corrosion resistance or thermal conductivity over a wide range of environmental conditions. Table I lists some of the common coatings and their uses.

Table I. Thermally Sprayed Materials and Their Uses

Metals	**Uses**	**Examples**
Aluminum	Corrosion Resistance	Cylinder Bores
Stainless Steel	Sliding Wear Resistance	Valve Seats
Chromium	Erosion Resistance	Chemical Process Plants
Titanium	Surface Repair	Sealing Surfaces
	High Temperature Wear	Concrete Protection
Cermets	Thermal Barriers	Crankshaft Repair
WC-Co	Electrical Barriers	Pump Impellers
Ti-TiN	Spray Casting	Diesel Piston Caps
Al-SiC		Printing Rolls
Ceramics		
Cr_2O_3		
Al_2O_3		
ZrO_2		

The thermal spray coating (TSC) process is a violent, inhomogeneous technique and poses several problems in materials evaluation. Test samples must survive grit blasting, an extremely hot plasma flame, and the impact of hot, small and high velocity particles. The coating produced is far from thermodynamic equilibrium and contains complex residual stress patterns due to the rapid quenching of particles upon impact. Coatings contain many features including microcracks, pores, impurities, *in situ* oxidation, and particles with a wide variety of thermal histories. The coating-substrate interface is rough and bonding depends greatly on surface preparation and a multitude of deposition parameters [2,3,4].

The properties of TSCs often differ greatly from the properties of an ordinary bulk material and thus characterization must take place in the as-deposited state. As coatings become more specialized, existing standard measurement techniques cease to be adequate. New standard techniques for characterizing these coatings must be developed so that deposition processes can be improved and coatings can be compared. The adhesion of the coating material to

the substrate is an important property of the system, for which the existing measurement techniques are not adequate.

1.2 Problem Specification

The adhesion of thermal spray coatings is an important problem facing engineers who design coated components. Adhesion is affected by a host of variables including: powder and torch parameters, surface preparation and substrate heating. An understanding of how these variables interact is necessary in order for coating users to have confidence in the product. Traditional adhesion measurement techniques are useful for comparing coating quality, but are limited in their ability to be used for predictions. A new peel adhesion test is proposed which attempts to address the need for a more informative test.

A fundamental problem in investigating adhesion is to define or select a parameter which characterizes the strength of an interface. Normally the choice of parameter is limited by the accepted tests [4] and it is difficult to convince a conservative industry that a new parameter is a better measure of adhesion. Because of these constraints, there are several requirements which any adhesion test should attempt to meet. The test should be easy to perform and should not require expensive equipment or sophisticated analysis. Industry will not be willing to accept sophisticated tests which require substantial employee training or capital investment. The tested component should be representative of the actual components sprayed. Most destructive tests are performed on coupons which have a very different size and shape than the engineered components. The test should be sensitive only to adhesion and not to other closely related variables such as residual stress. This will allow the effects of these other variables to be understood independently. The measured parameter should be useful in predicting service limitations. This is equivalent to saying, that the cause of failure in the test should

be understood, and that a theory describing failure in the test sample can be used to predict failure in an engineered component.

In order to understand adhesion, the variables which affect bonding must be identified. With most adhesive systems this list can be divided into three categories. The first is the chemical compatibility of the two materials. This is usually characterized by the types of chemical bonds which can form between them. In systems where one material was liquid at the time of bonding the chemical interaction with the surface is characterized by the wetting angle. Low wetting angle interfaces would be more strongly adherent than high angle interfaces. The cleanliness of the surface is very important in determining wetting angle and thus the bonding. The second category is the mechanical nature of the interface. In thermal spraying the surface is grit blasted before coating to provide a rough surface into which the coating can mechanically lock. Grit blasting disturbs any layer on the surface and exposes the more active material underneath. The impact of the particles assists in this interlock process and processes with high speed particles tend to produce better bonding. The ductility of the surface controls the nature of this roughening process. The third category is the loading on the interface. The applied external loads can be aggravated by the internal residual stresses generated during processing. The residual stresses are caused by the rapid quenching of the particles and by the large thermal gradients produced during spraying. For thick coatings the residual stresses can be high enough to fail the coating either by spalling or cracking.

2. Current Techniques for Adhesion Measurement

Several adhesion tests for TSCs have been recently reviewed by Lin [5] and by Brown [2]. Three general classes of tests can be considered, each of which has its merits and problems.

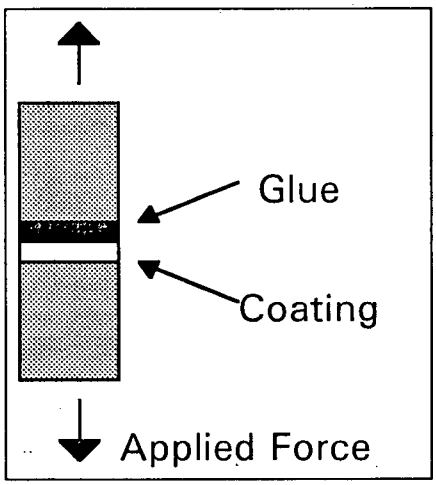

Figure 1. The basic principle of the tensile adhesion test (TAT) as defined by ASTM Standard C633-79. A coated cylinder is glued to a matching cylinder and then the assembly is pulled apart. The failure may occur in the coating, at one of three interfaces, in the glue or through a combination of these.

2.1 Stress Based Tests

Several test methods, such as ASTM C633-79, tensile adhesion test (TAT) shown in Figure 1 detect the load or stress required to fail a standard joint. The samples are designed to test shear and tensile stresses. Most of these tests require a strong bonding agent to attach the coating to a loading fixture. These tests have the limitation that they can only test the bond strength up to the strength of the adhesive used. Many coatings are stronger than the available adhesives and thus their adhesion cannot be tested with these techniques. It has also been shown [6] that the stress distribution in the joint is far from uniform and depends on sample size. Because most thermal spray coatings are brittle these tests are flaw sensitive and

generally show a wide scatter in their results. Failure is sudden and can occur at the interface, within the coating, or within the bonding agent. This means that it is not always adhesion which is measured. These tests are often technique sensitive and depend largely on sample alignment. The main advantage of these tests is that they are simple to perform and the calculation of the stress is straight forward. It is for these reasons that they are the most popular methods used.

2.2 Fracture Mechanics Techniques

In order to try to relate the measured external forces at failure to the stresses at the interface, the concepts of linear elastic fracture mechanics (LEFM) have been used to quantify adhesion. A whole class of tests can be used to quantify the fracture toughness or interfacial energy of a specimen [5]. The advantage of these techniques is that the LEFM theory can be used to determine the stress intensities in an engineered component, and determine if they exceed the intensity causing failure in the test coupon. This category includes double cantilever beam tests [3] and notched beam tests [5]. These tests usually attempt to detect the load at which a crack begins to propagate and relate that macroscopic load with a stress intensity at the crack tip. This requires knowledge of the elastic behavior of the entire system and usually assumptions about the elastic properties of the coating. TSCs can be heavily microcracked and thus may not be linearly elastic. These techniques are justified for homogenous isotropic materials, but the analysis becomes very complex for orthotropic composite systems such as coated beams. A recent review by Hutchinson [7] reveals the complexity of measuring and interpreting interfacial toughness in two material systems. With most fracture mechanics tests there is a large amount of stored energy in the sample, making it difficult to control the crack, and to know its true location. As with the stress based tests failure does not always occur at the interface and thus the result can be ambiguous. In order to accurately measure the important strains and displacements, expensive instrumentation is needed. Because of the complexity of the test analysis and the equipment required, these tests are best suited to research environments.

2.3 *Nondestructive Tests*

The third class of measurement techniques is perhaps the most desirable. This is the class of nondestructive techniques. By measuring adhesion directly on the engineered component all of the considerations of how well the sample reflects reality are not necessary. The application of these techniques to thermal spray coatings is still relatively unexplored but several researchers [8,9] have developed ultrasound techniques which successfully evaluate adhesion. These techniques suffer from the disadvantage that the measured parameter (usually wave intensity) is not useful in making quantitative predictions about service failure. A calibration technique must be used to compare measured strength with measured ultrasound intensity. These techniques are however, useful as quality monitoring methods once a range of acceptable measurements is experimentally determined. Further exploration of the whole range of available nondestructive tests is warranted.

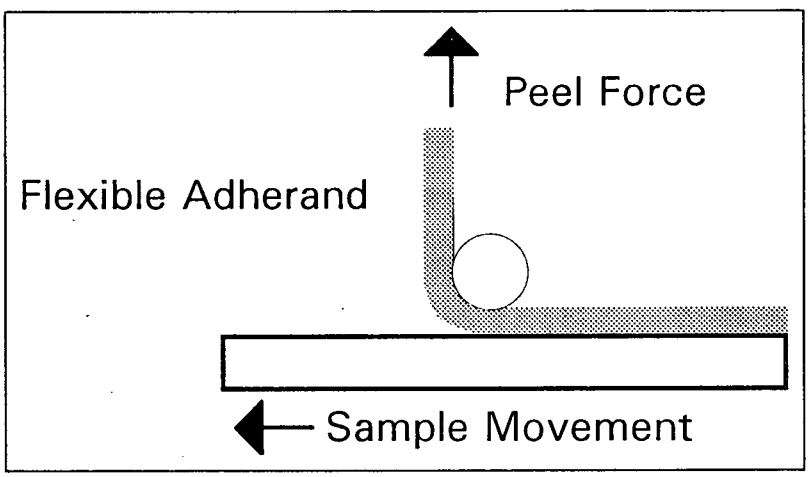

Figure 2. The basic principle of the peel test. A thin flexible adherand is pulled from its substrate and the force is measured as a function of crack position.

2.4 Peel Testing For Adhesion

An adhesion test is needed which has the predictive ability of the fracture mechanics tests and the simplicity of the force based tests. The peel test has the qualities of both. Several standard test configurations exist [10,11]. Because of its wide spread use in the adhesives industry, a great deal of study into the mechanics of the test system has been undertaken, [12-15] giving more confidence in the technique. In a peel test, a thin adherand is pulled from its substrate, in this case a coating, with a fixed geometry. The crack propagates in a stable manner at the peel speed. The basic principle is shown in Figure 2. The force required to continue cracking is monitored as a function of crack position and time. The peel test produces a force versus displacement curve which represents the adhesion of the coating. The resulting peel strength represents the incremental energy per unit width per increment peeled and has the units of N/m. This is equivalent to the surface energy with units of J/m^2. Because very little energy is stored in the bent foil, crack propagation is stable and controlled by the displacement of the sample.

The peel test essentially measures the average adhesion along the line of the crack tip. As the crack progresses a different portion of the interface is loaded. By measuring the load as a function of crack position the test can be used to map the adhesion in the direction perpendicular to the crack front. This allows the detection of surface inhomogeneities which affect adhesion. The resolution of the test depends on the size of the area of foil which is loaded, which in turn depends on the geometry of the peel test.

2.4.1 Peel Test Applications

Peel testing has traditionally been used to measure the adhesion of tapes and glue [12-14] and most manufacturers of adhesives list the peel strength of their products alongside

lap shear and tensile strength. Because of the simplicity of the test, attempts have been made to apply the peel test to other coating systems. In the microelectronics industry a peel test is used to evaluate the bonding of metal films to ceramics [16]. The test has also been applied to thin film coating systems where the coating is peeled from the substrate [15]. In these tests the coating itself is peeled from the substrate. The peel stresses and forces were found to depend largely on the coating properties and stable peeling was not always possible.

2.4.2 Peel Test Types

Amongst all of the available peel tests, two basic forms exist. They are similar in terms of sample preparation and procedure but can generate very different crack tip stresses.

The first is one in which the compliant adherand is peeled from the substrate at a specified angle. In most cases the angle is 90 degrees (T-Peel) from or close to parallel to the substrate plane. The shape of the adherand is controlled by its properties and the properties of the interface and substrate. The stress intensity at the crack tip and the amount of plastic work done to bend the adherand for a given peel load is a function of all the materials properties of the system and the peel angle. This geometry is very similar to a double cantilever beam test, but one beam is extremely compliant and the other is considered to be infinitely stiff.

In the second form (used in this work) the compliant adherand is bent around a rotating mandrel (Figure 2). The shape of the deformed adherand is controlled. In this test the torque required to rotate the mandrel or the tensile force in the adherand is measured. The strains in the adherand are usually much smaller than in the free peeling tests. In this case the amount of plastic work depends on the adherand properties only and can be controlled by changing the mandrel size. The stress intensity at the crack tip depends on the properties of all of the materials involved but because of the smaller strains the mechanical description of the system is simpler.

3. An Overview of Interface Fracture Theory

In order for a material or process to be accepted by the engineering community there must be methods of making performance predictions based on simple laboratory tests. This is due to the prohibitive costs of performance testing. Currently most adhesion test techniques do not relate in a simple way to performance conditions and thus extrapolation of laboratory results to engineered components is difficult. An attempt to relate the peel test mechanics to the mechanics of coated components would allow designers to relate test results to service conditions. While it is beyond the scope of the current work to develop a complete mechanical description of the peel test as applied to thermal spray coatings, it is appropriate to outline the basic considerations and techniques.

3.1 The Fracture Mechanics of Isotropic Materials

Fracture mechanics attempts to relate the external loads to the stress intensity at a crack tip. This is generally accomplished by describing the stress fields as a series expansion about the crack tip. For a planar crack the expansion is of the form:

$$\sigma = \sum K(2\pi r)^{-\frac{1}{2}} f_1(\theta) + A_2(2\pi r)^{\frac{1}{2}} f_2(\theta) + A_3(2\pi r)^{\frac{3}{2}} f_3(\theta)... \qquad (3.1)$$

Where r is the distance form the crack tip, (θ) is the angle for the crack plane. The functions ($f_i(\theta)$) and the constants are determined by the geometry, loading and the elastic properties. All terms except the first disappear when r is small. Thus the stresses at the crack tip can be specified by K and $f_I(\theta)$. K is called the stress intensity factor, and $f_I(\theta)$ has been found for standard geometries [17]. The crack will propagate when K reaches a critical value usually referred to as K_C. Three types of stress can exist. Mode I stress is tensile across the crack. Mode II is shear stress in the direction of the crack, and Mode III is shear stress along the line of the crack front. The stress intensity for each type of loading is given a separate

intensity factor. Most materials are weakest under tensile stresses and thus the toughness of a material is specified as the tensile stress intensity require to propagate a crack (K_{IC}). It can also be shown [17] that a crack will propagate when the strain energy released for an increment of cracking reaches a critical value the crack will propagate (G_{IC}). These two conditions are equivalent and are related in plane stress by:

$$G_{IC} = \frac{K_{IC}^{\ 2}}{E} \tag{3.2}$$

A more thorough description of fracture mechanics theory can be found in [17].

3.2 The Mechanics of Interface Cracks

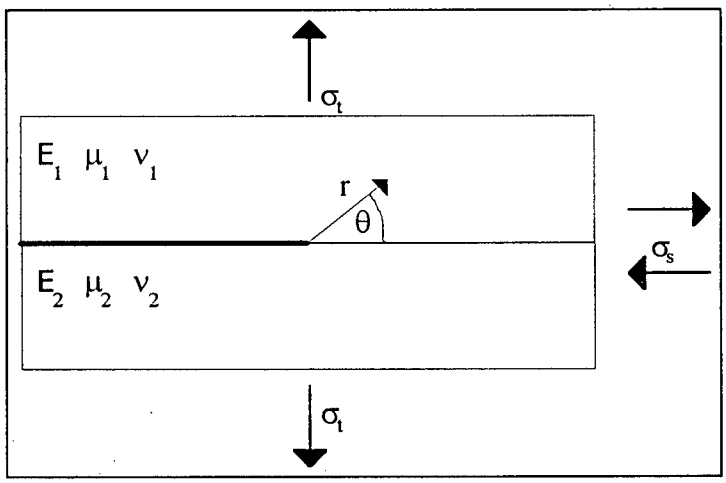

Figure 3. A schematic of a typical interface crack. A polar coordinate system about the crack tip is used. Stresses across the interface are referred to as σ_t and stresses along the interface in the crack direction are referred to as σ_S.

The mechanics of interfacial cracks has become an important problem in recent years because of the development of many new composite and coating technologies. Much effort [7, 18,19] has been put into applying the theory of fracture mechanics to interfaces. In general due to the difference in the elastic properties of the joined materials, the plane of the interface will have mixed mode loading. In coatings there is not likely to be a significant mode III component

so only tensile and in plane shear stresses will be examined. Hutchinson [7] summarizes much of this work with respect to two material systems. Several general observations can be drawn from this body of theoretical work, which are relevant to the peel test.

Dundurs [19] showed that, for problems with plane stress or plane strain, the elastic stress fields can be characterized by two non-dimensional parameters (α,β) which are functions of the material properties of the bonded materials and describe the elastic mismatch between the two materials. A general schematic of an interface is shown in Figure 3 and the labeling conventions shown are used in this discussion.

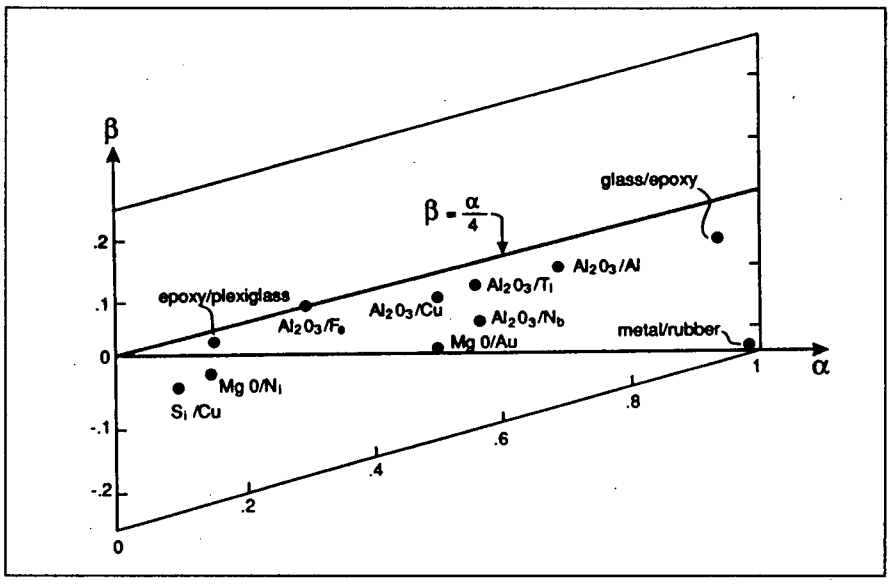

Figure 4. A plot of Dundurs parameters for several interfaces between two materials, including ceramic metal interfaces. Plot is taken from reference [7].

For two isotropic materials, (subscripts 1 and 2) characterized by a Young's modulus (E), shear modulus (μ) and a Poisson's ratio (ν) these parameters are given in plane stress by:

$$\alpha = \frac{(E_1 - E_2)}{(E_1 + E_2)} \tag{3.3}$$

$$\beta = \frac{1}{2} \cdot \frac{\mu_1\left(\frac{1-\nu_2}{1+\nu_2}\right) - \mu_2\left(\frac{1-\nu_1}{1+\nu_1}\right)}{\frac{\mu_1}{1+\nu_2} + \frac{\mu_2}{1+\nu_1}} \tag{3.4}$$

A chart of these values for several material combinations is shown in Figure 4. It is often convenient to write the β parameter in the form:

$$\varepsilon = \frac{1}{2\pi} \ln\left(\frac{1-\beta}{1+\beta}\right) \tag{3.5}$$

For an interface crack, the dominant term in the expansion for the stress field near the crack tip in the crack plane becomes:

$$\sigma_t + i\sigma_s = \left[Kr^{i\varepsilon}\right](2\pi r)^{-\frac{1}{2}} = (K_1 + iK_2)r^{i\varepsilon}(2\pi r)^{-\frac{1}{2}} \tag{3.6}$$

Note that the tensile and shear stresses are coupled through a complex valued stress intensity factor (K), whose amplitude oscillates as r becomes smaller. K_I and K_2 are the real and imaginary components of K, and if there is no mismatch, the Dundurs parameters vanish and the K values become the conventional mode I (K_I) and mode II (K_{II}) stress intensity factors. The ratio of mode II to mode I loading at the crack tip can be defined as the phase angle of the complex coefficient:

$$\psi = \arg\left(Kr^{i\varepsilon}\right) \tag{3.7}$$

Because this value oscillates as r changes, this value can only be calculated if some arbitrary length is used for r or if $\beta=0$. Argument exists as to what type of length scale should be used [7], but if it is assumed that since ε is small the contribution of the $r^{i\varepsilon}$ term is insignificant, then the phase angle is approximately:

$$\psi \approx Arc\tan\left(\frac{K_2}{K_1}\right) \tag{3.8}$$

The strain energy release rate for interface crack propagation in plane stress is given by:

$$G = \frac{2\left(1-\beta^2\right)}{\left(\frac{1}{E_1}+\frac{1}{E_2}\right)}\left|Kr^{i\varepsilon}\right|^2 \tag{3.9}$$

Again this is only physical when an arbitrary length scale is selected for r.

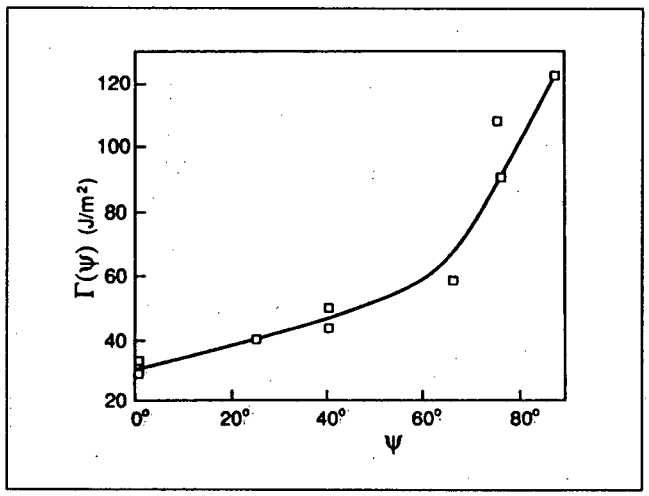

Figure 5. A typical plot taken from reference [7] of G_C against phase angle for a glass epoxy interface. With the notation used in reference [7] Γ is equivalent to G_C. .

Because it is difficult to achieve pure mode I or mode II on the interface and most interface cracks propagate in a mixed mode fashion. It is thus meaningless to try to characterize an interface only in terms of a single toughness parameter such as K_{IC} or G_{IC}. It is usually necessary to specify the toughness as a function of the phase angle (Ψ). The interface toughness is normally an increasing function of Ψ because interfaces tend to be stronger in shear than in tension. A typical plot of toughness (G_C) versus Ψ is given in Figure 5.

Because of the disturbance of the stress fields near the interface, a crack is usually forced to propagate parallel to the interface but it may run through the interface or one of the two materials. This depends on the loading, and elastic mismatch as well as the relative toughnesses of the interface and the two materials. This explains in part why some adhesion tests fail to cause the crack to exactly follow the interface.

3.3 Application of Theory to TSCs

When attempting to apply this body of theoretical work to the peel adhesion test for TSCs, several questions must be answered.

3.3.1 The Elastic Properties of Coatings

The elastic properties of TSCs strongly depend on the processing conditions. The particles are rapidly quenched and are thus might not be fully crystalline. The degree of porosity and microcracking can reduce the modulus of a coating material to 10 to 50% of that of the fully dense coherent material. Several methods for measuring the elastic properties have been suggested [20,21], but they are time consuming, expensive and/or unreliable. Further research into this is necessary.

3.3.2 Interface Roughness

In TSCs the scale of the interface roughness is a significant fraction of the coating thickness and thus cannot be ignored in stress field calculations. Some attempts [17, 22, 23, 24] have been made to explain high surface energies and R Curve behavior with non planar cracks. In these treatments the roughness is considered to be much smaller that the scale of the cracks. They only examine the effect of interlock behind the crack tip and do not examine the modification

to the stress field as a crack constantly changes direction. Presently no theory deals with this important problem.

3.3.3 The Effects of Residual Stresses

The relaxation of residual stresses can provide energy for crack propagation during peeling. The magnitude and distribution of residual stress in a coating is not generally known. Recently methods have been proposed which allow the evaluation of residual stress [25]. An examination of these stresses and their effect on the peel test remains to be done. These stresses are caused by differential shrinkage in the plane of the coating. They can be represented by an interface shear stress and a moment about a crack tip or free edge [7]. In order to balance this moment a tensile stress must develop across the interface near the edge. The extent and magnitude of this local stress field depends on the inplane stress and the coating thickness. The interface stress, however, must take the form shown in Figure (6b) for force equilibrium to be satisfied. This stress can cause spalling because the interface is loaded in tension. The magnitude and direction depend on the material properties and spray conditions and must be determined experimentally. Regardless of the direction of the residual stress, the loading causes a stress across the interface when a free edge or crack exists.

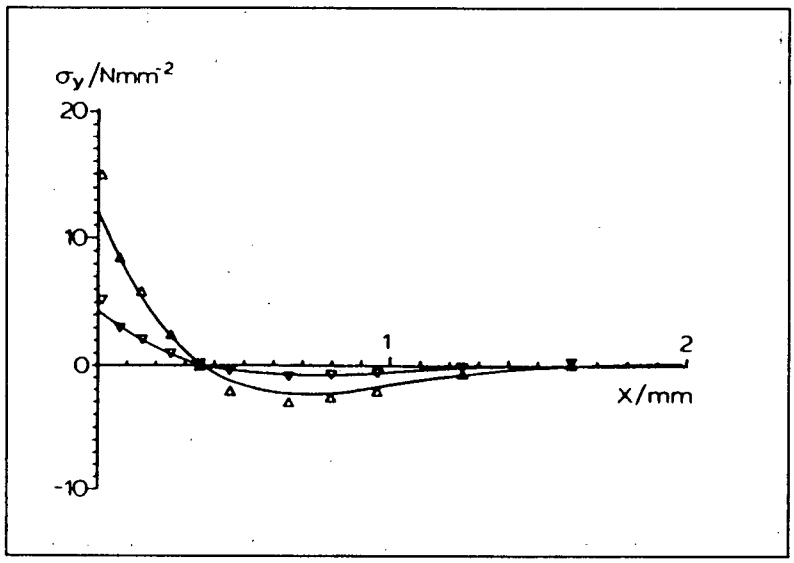

(a)

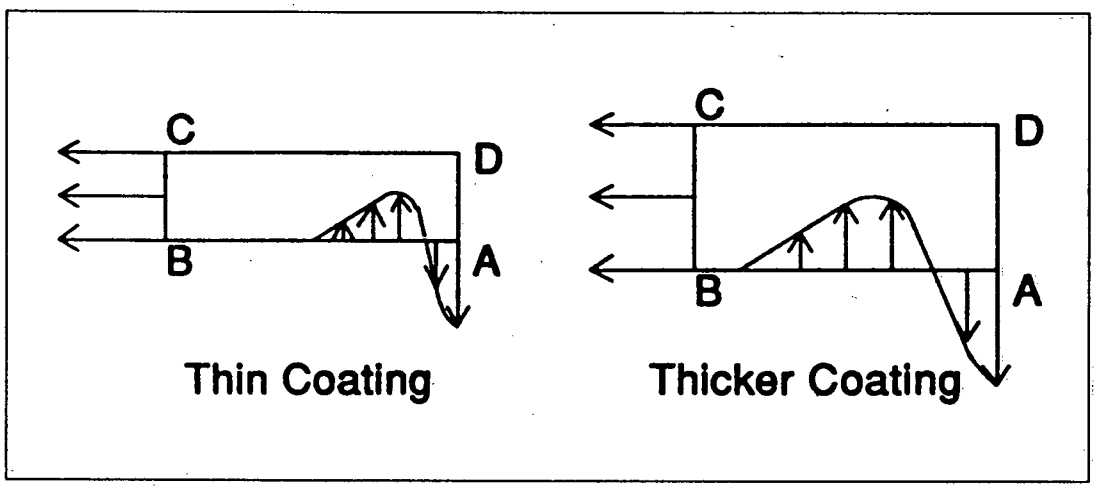

(b)

Figure 6. Tensile stresses across the interface (a) during peeling [13] and for an interface under in plane residual stress [26]. The moments about the arbitrary point B must be balaced so a tensile interface for developes at a free edge.

3.3.4 Relationship Between Peel Force and Crack Tip Stress Intensity

Because the foil is long and slender, beam theory can be used to describe its mechanical response to loading. Since the force at the foil end and the foil material properties are known the constraint at the crack tip on the foil can be calculated from the geometry. In free peeling the deflections in the foil are large enough that large displacement beam theory must be used [12-14]. For a mandrel type test, small displacement theory is adequate. Crocombe and Adams [12,13] have used an FEM model of the peel test, which allowed plasticity in both the foil and substrate to examine the stresses in the foil and substrate near the interface. They found that the typical phase angle (Ψ) for peeling was in the range of 30 to 50 degrees and that the crack tip stresses take the form shown in Figure 6a.

A second possible method of solution would be to examine the foil like a cantilever beam. Using this method, Thoules [14] developed an analytical solution for the phase angle during the peeling of an elastic film and substrate. The phase angles were found to be in the same range of 30 to 50 degrees. They were found to be relatively independent of peeling geometry and peel force, but could be shifted by inplane residual stresses. This indicates that further analysis of the residual stresses in necessary for a complete understanding of the process. Kim and Kim [15] have developed an analytical solution for the energies associated with the deformation of an elastoplastic film with this method but did not extend the solution to calculate crack tip stresses.

It should be noted that peeling produces phase angle values in the 30 to 50 degree range. This is the same range expected [7] for debonding under residual stress. Munz [27] shows similar stress fields at free edges due to differential shrinkage in brazed metal ceramic/joints. The stress field across the interface at a crack tip or sample edge under residual stresses is very similar to the stress field generated by the peel force (Figure 6). This indicates that the peel test mimics the types of load to which a coated system would be subjected.

3.4 Mechanics Summary

The above discussion represents a general picture of how a theoretical understanding can be used to interpret the peel test. The important aspects can be summarized as follows. The measured interfacial energy (U_I) can be considered to be equivalent to G_C for the stress intensity phase angle of the test. The phase angle is affected, however, in an unknown way by the material properties and residual stresses in the system. While two different tests on similar materials are likely to have similar phase angles, they will not have failed under identical crack tip conditions. This problem occurs in all adhesion tests to an unknown degree. The test does however allow the comparison of different coatings under the same macroscopic loading conditions, while giving a reasonable estimate of the fracture mechanics parameter in important engineering range of stress intensity phase angles. It thus maintains some semblance to both traditional fracture mechanics tests and force based tests and can be used to bridge the gap between them.

4. Peel Test Development: Theory and Calibration

Because the stress intensity at the crack tip during peeling can not easily be defined, an energy balance was applied to the system to determine the energy required for failure. The analysis is much simpler than stress intensity calculations and is more easily applied to complicated geometries in both the test sample and engineered components.

4.1 Definition of Peel Strength in Terms of Energy

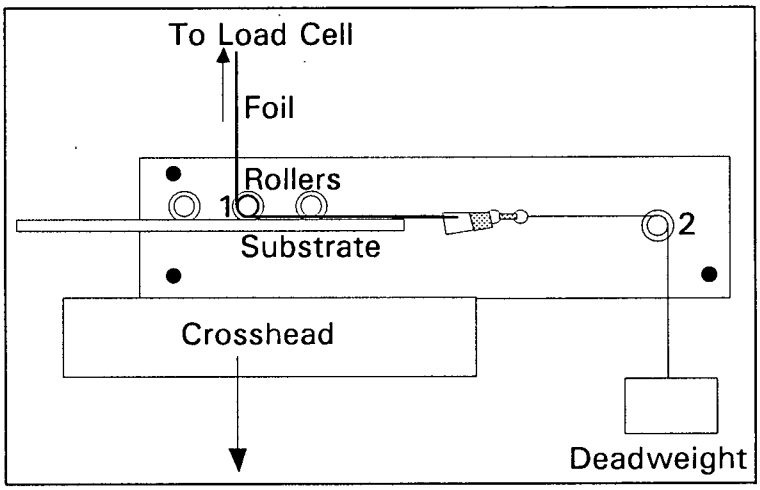

Figure 7. A schematic of the peel test jig. As peeling progresses the deadweight is raised and the substrate moves to the left.

The total energy dissipated during the peel test (U_{tot}) can divided into the 3 categories: the work to separate the two materials (U_I), the work to overcome jig friction (U_f), and the work of bending the foil (U_b). This is stated as :

$$U_{tot} = U_I + U_f + U_b \tag{4.1}$$

The interfacial energy (U_I) includes: chemical bonding, asperity friction, the energy required to deform or break asperities in the crack wake and any other interface toughening mechanisms [3, 18, 22, 23]. U_I Represents the energy which must be supplied to a coating to cause it

to fail under any loading condition with the same stress intensity phase angle (Ψ).

There are two sources of energy available to drive cracking during peeling: The energy from the relaxation of residual stresses (U_S) and the energy supplied by the peel force. In the peel test a deadweight (D) is used to hold the sample in place (Figure 7) and it must be subtracted from the measured force (F_m). Since energy supplied is equal to energy consumed, the measured force (F_m) is related to the energy of the system by:

$$\frac{U_s}{w \cdot dx} + \frac{(F_m - D)}{w} = \frac{U_{tot}}{w \cdot dx} \tag{4.2}$$

Where w is the film width, and dx represents a length element along the foil. The frictional loss can be modeled as a constant drag force which is proportional to the dead weight:

$$U_f = \mu D \tag{4.3}$$

From Eq. (4.1) Eq. (4.2) and Eq. (4.3) the interfacial energy can be expressed as a function of measured peel force, energy of deformation (U_b), residual stress energy (U_S) and frictional losses (μD):

$$\frac{U_I - U_s}{wdx} = \frac{F_m - (1+\mu)D}{w} - \frac{U_b}{wdx} = Peel\_Strength \tag{4.4}$$

The frictional and bending work can be found experimentally or analytically using a calibration technique discussed below. The residual stress energy is unknown and thus cannot be separated from the interfacial energy. Thus, from a measurement of the peel force the interfacial energy less the residual stress energy can be obtained. This parameter is defined as the peel strength and represents the energy required to fail the interface.

4.2 Work of Deformation and Friction During Peeling

In order to obtain the peel strength from the peel load a calibration is necessary to determine the amount of energy consumed by friction and plastic work during peeling.

This can be accomplished by directly measuring the friction and plastic work in a free standing foil. The work can also be calculated from the tensile stress-strain curve of the foil material.

4.2.1 Numerical Calculation of the Work of Deformation

In order to understand the deformation energy dissipated in a peel test some understanding of the mechanics is needed. From the elastoplastic characteristics of the adhesive and foil the deformations in the foil can be determined. The energy required to deform the material is then determined.

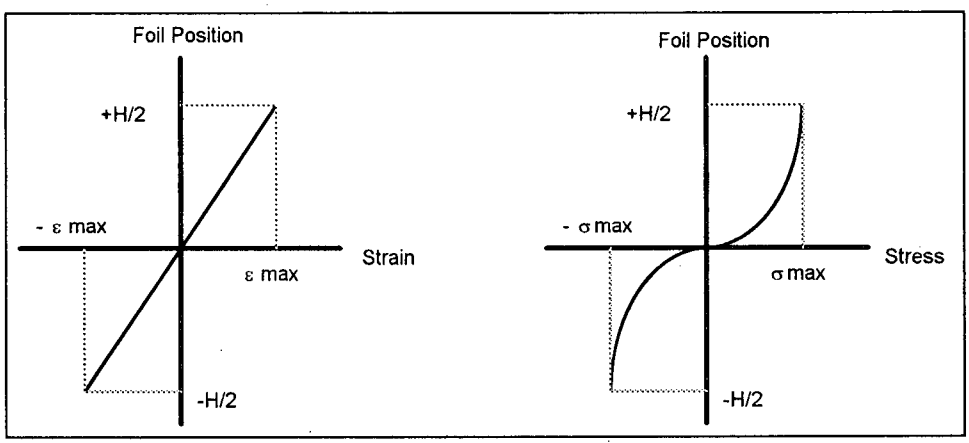

Figure 8. The distribution of stress and strain across the foil width. The strain varies linearly with distance for the foil center and the stress is an arbitrary function of strain.

For the sake of discussion the calculation will be based on bending the foil to a mandrel. Because the calculation is path independent, the method applies to any peeling configuration where the minimum curvature is known. The deformation energy is obtained by calculating the total energy required to strain the foil against the stresses supported by the foil. For simplicity it will be assumed that the stress-strain characteristics of the material are the same in compression and tension. Thus the inside portions of the bent foil which are in compression must overcome the same stresses as the outside portions which are in tension (Figure 8).

This assumption is made in order to take advantage of symmetry and is not necessary. The procedure could be easily modified to use a different stress-strain relationship in compression than in tension, with a corresponding increase in the complexity of the final integrals.

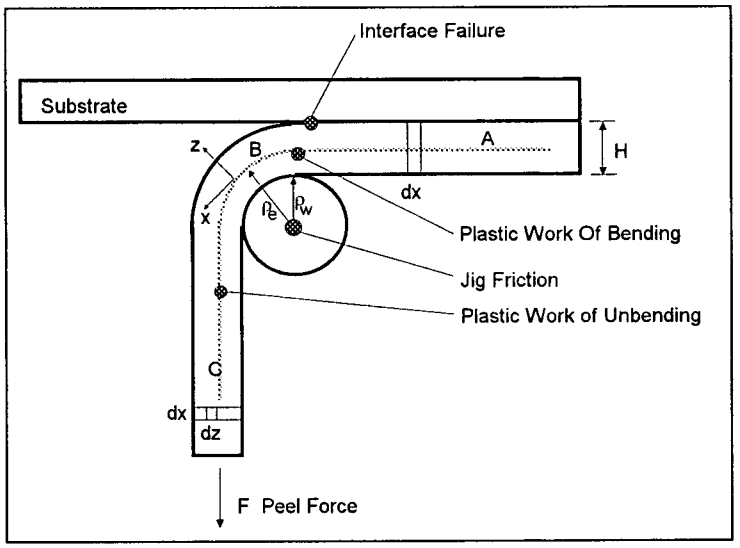

Figure 9. A schematic representation of the energy dissipated during a peel test. Plastic work, jig friction and interface failure all contribute to the total energy consumed. The coordinate system depicted is used in deriving an analytical method of calculating deformation work.

When examining the energy of the system three states are considered. The first is the unbent foil which is considered to have zero energy (area A in Figure 9). The second is the foil bent to the minimum radius (i.e. the mandrel radius) which corresponds to the maximum strain or area B in Figure 9. The third state is the straightened foil a large distance from the bend (area C in Figure 9). This ligament of foil has experienced a permanent deformation and in order to be straight must be held in tension. A constant amount of elastic energy per unit length is thus added to the foil.

Beam theory will be used to model the bending of the foil strip. The assumptions of small deformation beam theory require that strain be a linear function of distance from the neutral axis of the beam. This is a valid assumption for beams which are thin compared to their radius

of curvature [28]. As long as the minimum radius of curvature is significantly greater than the foil thickness the theory is valid. This is valid for the foils used because they were 0.05 to 0.2 mm thick and the bending radius was 3.13mm. Consider an element of foil *wdxdz* located at a position *z* from the neutral axis of the foil, as shown in Figure 9. For each element entering the bend there is an equal element leaving it. Thus the energy per unit length processed is the sum of the energy used to bend the entering element and the energy used to unbend the exiting one. In the fully bent foil, the strain (ε) is distributed linearly across the foil as shown in Figure 8a. The maximum strain (ε_m) is given by:

$$\varepsilon_m = \frac{z}{\rho_e} \tag{4.5}$$

Where *z* is the position across the foil and ρ_e is the radius of the bent foil. The stress-strain curve is some characteristic function for a given foil, and thus the stress variation across the foil will have the form shown schematically in Figure 8b. In order to calculate the energy requirement for each element (*dx*) the stress must be integrated over all the strains experienced by that element. These integrals are simply the areas under the stress-strain curve.

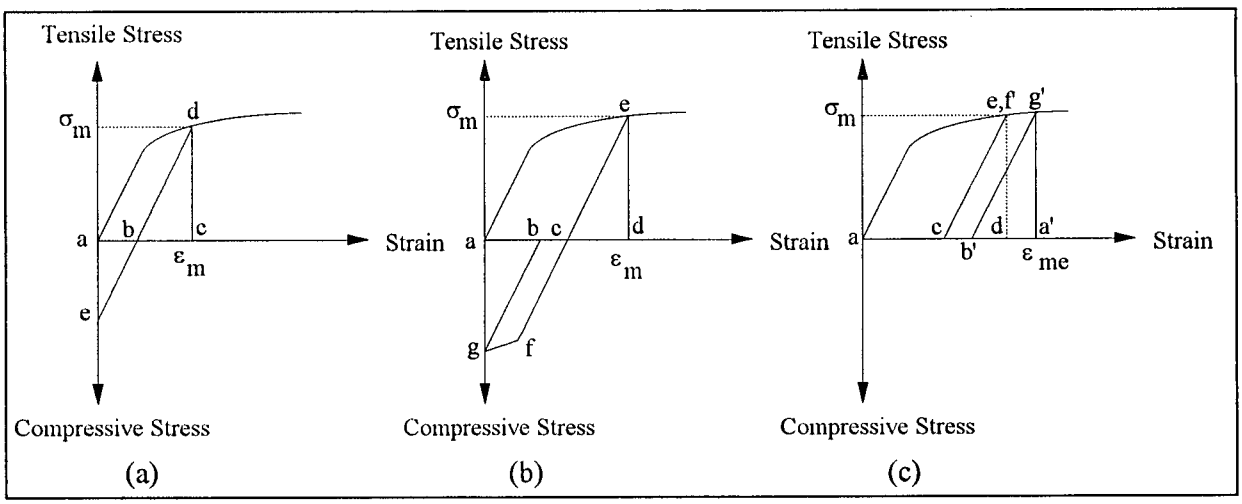

Figure 10. The stresses and strains experienced by different elements of foil during bending. The area under the curve represents the energy consumed (a) Bending plastically but unbending elastically. (b) Bending plastically and unbending plastically. (c) The superposition of the lower portion of curve (b) showing how the effective maximum strain is determined.

Figure 10 shows two possibilities for the bend unbend hysteresis loops for an element. The elements close to the neutral axis will behave as shown in Figure 10a and the elements at the foil surface will behave as shown in Figure 10b. The work of deformation is the areas under the curve. Figure 10a shows the energy for an element which is bent to its maximum strain (ε_m) with both plastic and elastic work, but returns to straight with only elastic work. These elements are called Case I elements and the energy required to process them is called U_{tot1}. Note that elements which experience no plastic work (i.e. the elements close to the neutral axis of the foil at z=0) do not consume energy during peeling, as the elastic energy stored in bending is released upon unbending. The following calculation applies to them as well, with the total energy being summed to zero. As the element is bent it encounters an increasing stress (σ) until it reaches its maximum strain. The energy per unit volume required to reach maximum strain is the area {acd} in Figure 10a and is given by:

$$U' = \int_0^{\varepsilon_m} \sigma \partial \varepsilon \tag{4.6}$$

The element now begins to unbend. From point {d} to {b} it relaxes elastically releasing energy. The amount of energy is the area of triangle {bcd} and is given by:

$$U'' = -\frac{\sigma_m^{\,2}}{2 \cdot E} \tag{4.7}$$

Where E is the elastic modulus of the material and σ_m is the stress at the maximum strain (ε_m). The element reaches a point of zero stress at {b} which corresponds to a strain of:

$$\varepsilon = \varepsilon_m - \frac{\sigma_m}{E} \tag{4.8}$$

It must now work elastically against a stress to reach the point of zero strain at {e}, which corresponds to a straight foil. The total work per unit volume done in unbending is the area of triangle {abe} given by:

$$U''' = \frac{E}{2} \cdot \left[\varepsilon_m - \frac{\sigma_m}{E} \right]^2 \tag{4.9}$$

The total energy (U_{tot1})associated with the element is given by the sum of the energies defined by Eq. (4.6), (4.7) and (4.9):

$$\frac{U_{tot1}}{w \cdot \partial x \cdot \partial z} = \int_0^{\varepsilon_m} \sigma \partial \varepsilon - \frac{\sigma_m^{\,2}}{2E} + \frac{E}{2}\left(\varepsilon_m - \frac{\sigma_m}{E}\right)^2 \tag{4.10}$$

The second possibility is shown in Figure 10b. In this case plastic work must be done to return the foil to straight. This is referred to as reverse bending. The elements processed in this manner are referred to as Case II elements and the total energy required is called U_{tot2}. Examination of the hysteresis loop shows that, since the material behaves in compression as it does in tension, the lower part of the curve can be superimposed on the upper curve by matching the lines {cf} and {ce}. This procedure eliminates the triangle {cde} which represents the elastic energy stored on bending and subsequently released on unbending. The system can be modeled as having an effective maximum strain (ε_{me}) This strain is equivalent to twice the strain at point {c}, which is found from the maximum stress and the elastic modulus.

$$\varepsilon_{me} = 2 \cdot \left[\varepsilon_m - \frac{\sigma_m}{E}\right] \tag{4.11}$$

The elemental energy is given by:

$$\frac{U_{tot2}}{w \cdot \partial x \cdot \partial z} = \int_0^{\varepsilon_{me}} \sigma \partial \varepsilon \tag{4.12}$$

The transition strain (ε_{mt}) between Case I and Case II occurs when the effective maximum strain equals the maximum strain. From the similarity of triangles {abg} and {cde} in Figure 10b and Eq (4.11):

$$\frac{\varepsilon_{mt}}{2} = \frac{\sigma_{mt}}{E} \tag{4.13}$$

Where σ_{mt} is the stress at the transition strain. Equation (4.13) is implicit and its solution requires knowledge of stress-strain relationship. The strain at which this occurs is a material characteristic.

The position ($z=z_t$), across the foil thickness, at which the transition occurs is given by Eq. (4.5) as:

$$z_t = \varepsilon_{mt} \cdot \rho_e \tag{4.14}$$

Foils which are thinner than twice z_t do not have any elements for which the second case solution is necessary and thus only the first solution is used. The more complicated Case II problem is presented here but the procedure for the simple Case I problem is the same. The total energy consumed per unit length processed is found by integrating over all of the elements in z. Since the strains are symmetrical the integral is twice the integral over all positive z:

$$\frac{U_b}{w \cdot \partial x} = 2\left\{\int_0^{z_t} U_{tot1}\partial z + \int_{z_t}^{\frac{H}{2}} U_{tot2}\partial z\right\} \tag{4.15}$$

$$\frac{U_b}{w \cdot \partial x} = 2\left\{\int_0^{z_t}\left[\int_0^{\varepsilon_m} \sigma\partial\varepsilon - \frac{\sigma_m^{\,2}}{2 \cdot E} + \frac{E}{2}\cdot\left(\varepsilon_m - \frac{\sigma_m^{\,2}}{E}\right)^2\right]\partial z + \int_{z_t}^{\frac{H}{2}}\left[\int_0^{\varepsilon_{mt}} \sigma\partial\varepsilon\right]\partial z\right\} = \Omega \tag{4.16}$$

Where Ω is the work of deformation per unit width per increment peeled and has the same units as peel strength (J/m^2 or N/m). In general the integrals in Eq. (4.16) must be evaluated numerically. In many cases the stress-strain relationship for the foil of interest must be measured. It is then possible to fit a polynomial to the measured curves and this function can be used in the numerical solution.

4.2.2 Verification of Calculation

In order to verify the prediction of the above theory, the work of bending for four types of foil was tested. The foils were selected to represent different types of plastic response. A soft aluminum foil was chosen to represent nearly ideal plastic behavior. A nickel foil was selected to represent a nearly linear work hardening material. Brass and stainless steel foils were

chosen to represent power law work hardening. The stress-strain relationship for each foil was measured and this information was used to calculate the work of bending for each material. Each foil was then bent to a mandrel in a similar fashion to the peel test, (Figure 7) and the work of bending was measured.

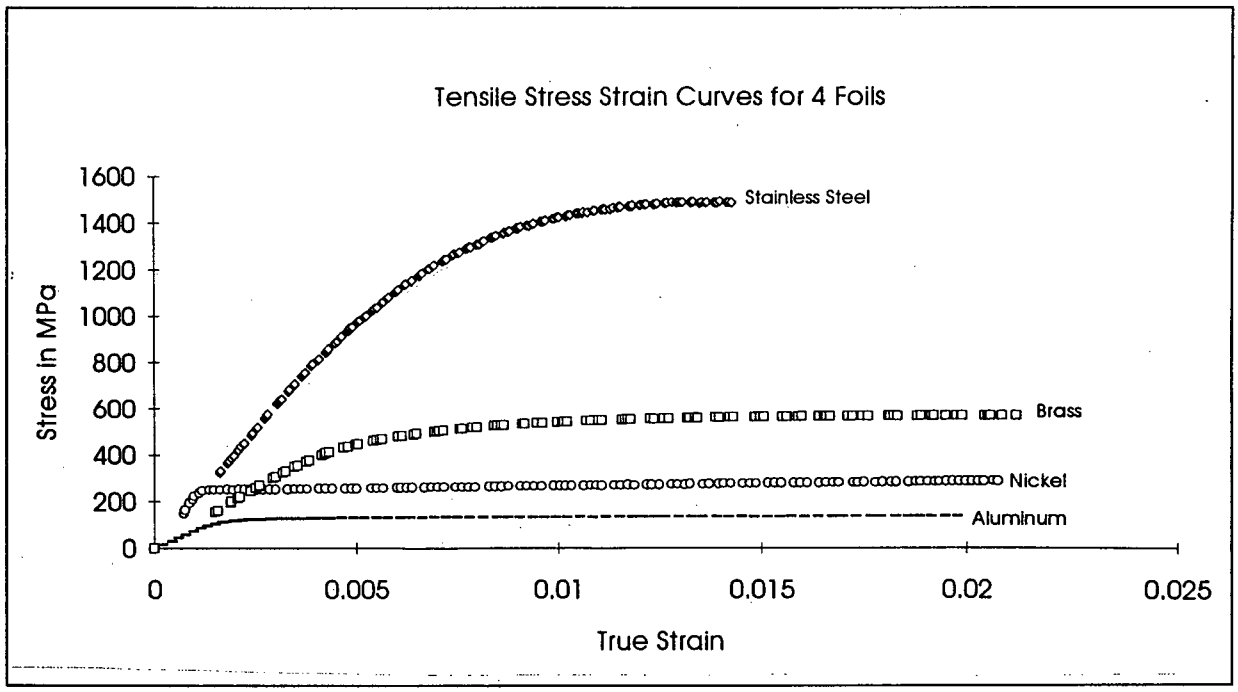

Figure 11. The true stress strain curves for the four foils used to calculate plastic deformation energy. Polynomials were fit to this measured data to allow numerical integration.

The stress strain curve for each foil was measured using a tensile test. Strips of each foil were cut and aluminum tabs were glued to each end. In order to simplify the verification experiments the foil was not grit blasted or soldered like the foils used in the peel tests. The samples were then placed in the grips of a standard Instron testing machine. The elongation of the sample was measured using an LVDT type extensometer which was mounted on the grips. The crosshead was displaced at a constant rate of 0.125 mm/min. which corresponds approximately to a strain rate of 0.003/min. The load and extension were recorded on a PC. From the measured loads and displacements the corresponding stresses and strains

were calculated. Sample stress strain curves for the foils are shown in Figure 11.

In order to use the above theory it is necessary to integrate the stress strain relationship. In order to make this simple, a curve fitting technique was used to obtain polynomials to use in the integrals. A linear regression was used to match a function to the elastic region of each curve. The slope was then taken to be the elastic modulus. A third order polynomial was then fitted to the work hardening region of each curve.

$$\sigma = A\varepsilon + B\varepsilon + C\varepsilon^2 + D\varepsilon^3 \qquad (4.17)$$

The intersection point of the two curves was then taken as the yield point. The functions were then used to predict the work of bending. The curve fitting data is summarized in Table II.

Table II. Summary of the Elastoplastic Foil Behavior

	Nickel	Brass	Aluminum	Stainless Steel
Modulus	210 GPa	102 GPa	70 GPa	202 GPa
A coefficient	2.45×10^8	1.17×10^8	1.19×10^8	-2.13×10^8
B coefficient	1.66×10^9	9.23×10^{10}	2.83×10^9	3.00×10^{11}
C coefficient	4.04×10^{10}	-6.44×10^{12}	-1.94×10^{11}	-2.06×10^{13}
D coefficient	-1.35×10^{12}	1.50×10^{14}	4.86×10^{12}	5.06×10^{14}
Account for	Reverse Bending	Reverse Bending	Reverse Bending	Bending Only
Calculated Deformation Energy Ω	178 N/m	142 N/m	76.2 N/m	131 N/m

All the calculations were done for 0.0762mm thick foil bent to a minimum 3.175mm radius. It should be noted that the stiff stainless steel foil was the only material for which the effects

of plastic work during unbending could be ignored. This confirms the observation of Kim and Kim [15] that the plastic work required for reverse bending is significant. The amount of plastic work is not linked only to yield stress and thus methods of work estimation must account for work hardening. Models assuming ideal plasticity will likely underestimate the amount of work.

The measurement of friction can be a problem. The magnitude of the frictional loss is proportional to the forces holding the mandrel against it bearings, which is in turn related to the peel forces. An increase in adhesion will cause an increase in foil tension and an increase in frictional losses. Any calibration for friction must describe friction as a function of tension in the foil. Friction also depends on environmental variables such as temperature, cleanliness and amount and type of lubrication used. Care must be taken to control these variables in such a way as to minimize friction or maintain it at a constant level.

In order to measure the plastic work and friction in the jig, a procedure similar to the one proposed by Adams [12] was used. A foil sample was mounted in the peel jig as shown in Figure 7. The jig is rigidly mounted on the crosshead of an Instron universal testing machine, with the edge of mandrel #1 aligned with the center of the load cell grip. This causes a constant peeling angle. The right edge (as shown in the figure) is connected to a thin nylon cord with a universal joint. This cord bends 90 degrees over mandrel #2 and a deadweight is attached to the end. Initially sufficient weight is added until the foil is forced to conform to the mandrel. The crosshead is then lowered at 1.25 mm/min. and the tension in the foil is monitored. The force is averaged over 10mm of crosshead displacement. After 10mm the crosshead is stopped and more weight is added and the test is repeated. By varying the load an empirical description of the friction and plastic work can be obtained.

The force measured by the load cell (F_m)is the sum of the deadweight (D), the friction force (f) and the deformation work (U_b) per increment peeled (dx).

$$F_m = D + f + \frac{U_b}{dx} \tag{4.18}$$

The friction in the jig (f) is rolling friction in the bearings and is proportional to the applied load (D). Equation (4.18) can thus be written as:

$$F_m = (1+\mu)\cdot D + \frac{U_b}{dx} \tag{4.19}$$

where μ is the coefficient of friction. By dividing the intercept by the sample width a value for the parameter Ω is obtained experimentally This the value of this parameter is predicted by Equation (4.16) allowing a comparison between the numerical method and an experiment.

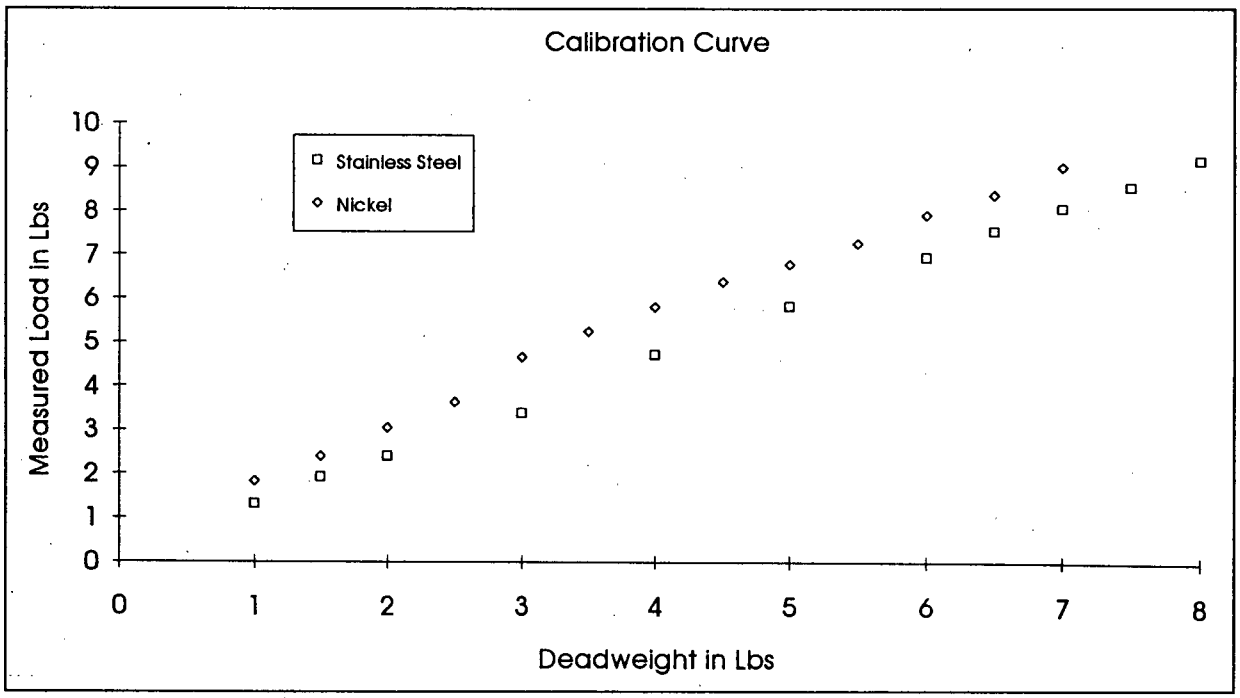

Figure 12. A friction and deformation work calibration curve for a nickel and a stainless steel foil. The slope and intercept are used to calculate the friction coefficient and the deformation work.

For a foil of a given width the friction coefficient and Ω can be found from a plot of deadweight (D) versus measured load (F). Figure 12 shows this relationship for nickel and stainless steel foils, and Table III summarizes experimental results for several foil materials. A spreadsheet regression program was use to predict the intercept and the slope ($1+\mu$). The confidence in U_b is exemplified by the excellent linear fit between load cell force and deadweight shown in Figure 12. The peel strength can now be found from Equation (4.4):

$$PeelStrength = \frac{F_m - (1+\mu)D}{w} - \Omega \qquad (4.20)$$

Equation (4.20) can be used to calculate the peel strength as defined in equation (4.4) from a peel test based on the friction and plastic work determined in the calibration step.

Table III Comparison of Predicted and Measured Work

	Nickel	Brass	Aluminum	Stainless Steel
Friction Coefficient (±.01)	.09	.12	.11	.12
Measured Ω(±20)	205 N/m	113 N/m	92.9 N/m	121 N/m
Predicted Ω	178 N/m	142 N/m	76.2 N/m	131 N/m

4.2.3 Calibration of Peel Test Foils

Since the calibration technique was shown to be reliable, calibrations were performed on foils which were more representative of the ones used for peeling. Along with each set of peel test samples, calibration sample were made in the same manner as the coated specimens. The calibration samples were soldered and grit blasted, but not coated or bonded to an aluminum plate. The solder was then removed from the copper block in the same manner as the

coated samples. The edges were trimmed off with shears to provide clean edges. The work and friction were then calculated for the foils in each sample set using the experimental procedure outlined above. Table IV shows the results of the calibrations on grit blasted foils. These were significantly different than the values for the unworked foils discussed in the first part of this section, because the grit blasting works the surface of the foil..

Table IV Calibration Summary

	.005 Ni foil	.003 Ni foil	.003 SS foil	.004 SS foil
Ω	400 N/m	203N/m	42 N/m	142 N/m
μ	.12	.11	.14	.13

5. Peel test Development: Experiments

Several experimental procedures were developed in this work. They are all described in detail in Appendix B. A brief description of the peeling procedure, the tensile adhesion test procedure (TAT), and the hardness measurement technique are given here.

5.1 Peeling Procedure

In order to adapt the peel test to thermal spray coatings several new procedures were developed to coat and test a thin foil. These procedures evolved during the initial stages of the experimental program. The development was stopped when a repeatable useful procedure was found. Further development is warranted which would allow the testing of foils without soldering and would allow more severe grit blasting.

5.1.1 Geometry

The geometry of peeling has a significant effect on the failure of the interface. By changing the foil loading, the crack tip stresses change and thus the measured parameter changes its meaning. The relationship between crack tip stresses and foil loads is discussed below. For a constant peeling geometry however, the type of stress is not expected to vary much with the level of adhesion [13]. It is easier to control the geometry with a mandrel type test and thus the geometry used was based on the ASTM 3167 floating roller peel test. In order to ensure controlled crack propagation along the interface the loaded region should be small. A small radius mandrel (6.35 mm in diameter) was thus utilized to maximize foil strain at the interface within a small, well defined region. Thin foils reduce the amount of plastic work dissipated in the test and make it easier to ensure that the foil conforms to the mandrel. Thin foils however are fragile and difficult to handle. Several foil thicknesses were examined. The test can work

for foils between 50 and 250 microns and a 75 micron foil was found to be the easiest to use.

5.1.2 Substrate Selection

The selection of a suitable substrate is difficult because of the limited number of available foil materials. The thin foil test substrate should behave mechanically and chemically like the bulk substrate. Because of the wide variety of substrate materials sprayed it is impossible to find a single foil type which would be representative of the bonding to these materials As most of these materials are not available in a thin foil form, a 302 stainless steel foil was chosen as a substrate in this work. In order to explore the effect of substrate material on bonding, several other foils were examined including pure nickel, brass and aluminum. The brass and aluminum foils were difficult to work with and while it was possible to use them they were not tested extensively. The pure nickel foil was found to be an excellent substrate for this test.

Peel tests require that one adherand is sufficiently compliant and that negligible energy is lost to bending the adherand compared to the bonding energy. With TSCs the interface tends to fail in a brittle manner. They must also be sprayed onto stiffer substrates than those normally used. Because test conditions are outside the usual range for peel tests some theoretical understanding of how these problems will affect the test is needed.

5.1.3 Preparation

In order to provide mechanical backing and a thermal sink, the foil was soldered to a copper block (Figure 13a). This was accomplished by coating the foil with solder using an electric soldering iron and liquid acid flux. After the solder coating was applied, the foil sample was thoroughly cleaned, and a new layer of flux was applied. A copper block was heated on a hot plate and a layer of solder was applied to the surface. The foil was then placed onto

the liquid solder and pressed down with a steel weight. The assembly was removed form the hot plate and allowed to cool. Figure 13a shows a schematic of the prepared samples. The samples were then cleaned, degreased and tape was used to mask all but a rectangular area (50 mm by 20 mm) on the foil. This area was grit blasted with 100 grit Al_2O_3 at 80 psi at a distance of 80 mm at 45 degrees from the surface. Care was taken to grit blast each sample in an identical fashion. The samples were then cleaned with a dry nylon toothbrush.

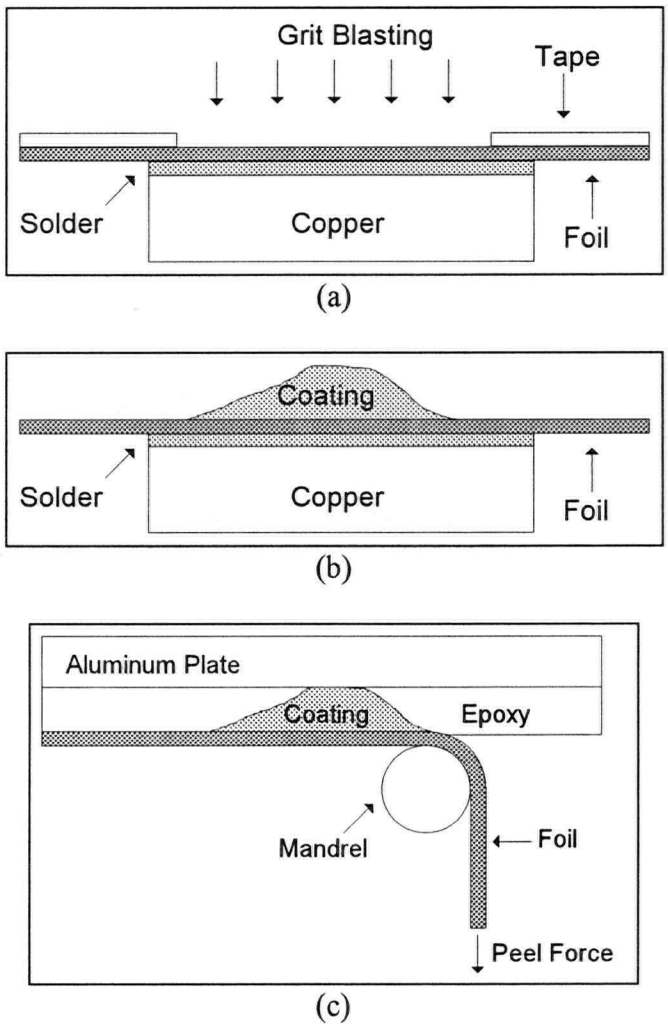

Figure 13. The main steps in preparing a peel test sample. (a) A foil is soldered to a copper block and grit blasted. (b) The assembly is coated. (c) The copper and solder are removed and the foil is peeled from the coating. The Gaussian shaped coating shown is produced by moving the torch in only one direction along the same path for each pass.

5.1.4 Spraying

The coatings were applied using several different torches at different companies. This allowed a range of coating processes to be explored, and the development of links with local industry. The first company, HS Tools, is a machine and repair shop servicing the aircraft industry. As part of that service they operate a Metco MBN (30 kW) radial feed plasma torch. This type of torch represents the current level of technology found in industry today. The second company Northwest Mettech sells a proprietary high power axial injection plasma torch. It represents the forefront in computer controlled high performance torches. The third company Metcon Services operates a proprietary axial injection plasma torch, which is again a leader in torch technology. The fourth company is Norton which sprayed several materials with their Rokide oxygen/acetylene torch. This technology has been in industrial use for 15 years. The powders and coating types sprayed at each facility were different and thus comparisons between them are both undesirable and impossible.

The samples were mounted on rotating drum. The drum rotated at speeds up to 500 rpm, and the torch was moved vertically to provide full coverage. Cooling air was directed at the drum from two nozzles at the rear of the jig. In order to further shield the samples aluminum masks are used to cover all but a small portion of the foil. The rotational speed and traverse speed were selected by each spray company to suit their process.

Two types of sample were sprayed for each coating type. The first sample was called the profile sample and is made by holding the torch stationary and rotating the jig. A Gaussian shaped band of coating is formed. This is shown in Figure 13c. This geometry allows the variation in adhesion between different portions of the plasma stream to be measured. The second type of sample was an ordinary uniform coating. As well as the peel test samples several mild steel bars and several ASTM C633 [29] cylinders were coated. From these extra

samples other traditional evaluations could be made such as hardness, microstructure and a comparative bond strength test.

5.1.5 Post Preparation

The sprayed samples were cleaned with alcohol and glued, using a thermoset epoxy, to a clean, grit blasted, 1 mm thick aluminum plate. After the glue was cured the samples were placed on an electric hot plate until the solder melted. The aluminum, glue, coating and foil sandwich was separated from the copper block (Figure 13c) and the melted solder was quickly brushed off the foil using steel wool. The edges of the sandwich were ground parallel on a wet SiC wheel. This step reduces the possibility of edge effects. By grinding with successively smaller grits the size of the damage zone was minimized. The sandwich was allowed to dry before it was threaded through the test jig.

5.1.6 Peeling

The sample was mounted in the jig, (shown in Figure 7) and the starting tab was clamped into the jaw. The foil was pulled from the coating at a constant rate of 2.5 mm/min. The load and cross-head displacement were monitored and recorded digitally. From the load displacement curve the peel strength as a function of crack position was calculated using the calibration procedure discussed above.

5.2 ASTM Bond Strength Test

In order to compare the peel test with an industrially accepted test, the ASTM standard C633-79 test [29] (TAT) was carried out on all coatings. The procedures and specifications for the test are discussed in detail in Appendix B and are outlined here. A cylinder of mild steel

is grit blasted and coated along with the peel samples. A second identical cylinder is glued with a thermoset epoxy to the coated face and cured in a kiln. A special V-block jig is used to ensure alignment during curing. The two cylinders are then pulled apart in tension (Figure 1). The system may fail in the glue, at the coating/substrate interface or inside the coating. If the sample fails in the glue then it is only known that the bond strength is higher than the measured stress. If the sample fails in the coating it is only known that the adhesive strength in tension is higher than the cohesive strength. The load at which failure occurs is divided by the area of the surface and a crude estimate of the failure stress is obtained. The samples were one inch in diameter and two inches in length in order to homogenize the stress distribution over the test area.

5.3 Metallography and Hardness

Each coating was cut so that a cross section could be evaluated for microstructure and hardness. Each coating was vacuum impregnated with a low viscosity two part epoxy under a vacuum of -30 mm Hg. After the epoxy was cured, the samples were sectioned on an abrasive blade saw and mounted in a standard epoxy. The cross section was then ground with special metal bonded diamond disks to a 10 micron finish. As TSCs are usually difficult to polish special finishing procedures were used for each material [30]. After finishing the microstructure was visually examined to ensure that the polished surface was acceptable for the hardness tests. The hardness was then measured at five locations in each coating with a Vickers microhardness tester. The applied load was 300 grams. The average hardness was reported.

5.4 Examples

The peel curves for all of the coatings studied are given in Appendix A and Table V shows a summary of the results. For this work the peel strength of a uniform coating is averaged over 30 mm of peeling and the result is reported. This arbitrary distance was chosen because

it is larger than the usual width of the spray pattern and thus is larger than the scale of the expected variability. For profile coatings the entire curve must be reported because the variation is the important information.

Table V. Summary of Test Data

Type	Sprayer	Name	Thickness in mm (±0.005)	Hardness Vickers (±10%)	ASTM Bond Stress Mpa (±20%)	Peel Strength (N/m) on SS Foil (±20)	Peel Strength (N/m) on Ni Foil (±20)
Cr_2O_3	Metcon	05/23/95 AB	.08	822	>70	40	193
Cr_2O_3	Rokide	05/16/95 BC	0.128	1067	>70	36	254
Cr_2O_3	Mettech	01/01/95 bob	0.23		45		
NiCr-Al_2O_3	Rokide	05/16/95 DE	0.3	247	46	280	486
Fe Bond Coat	Mettech	05/26/95 AB	0.121	122.8	>70	213	718
Titanium	Metcon	05/23/95 CD	0.08	247	>70	224	967
WC-Co	Mettech	05/06/95 A	0.08	780	>70	162	659
WC-Co	Metcon	04/07/95	0.14	548	46	227	732

Many peel tests have been performed on a variety of coatings on both nickel and stainless steel substrates. In order to elucidate the meaning of each curve, two examples are discussed in terms of how they indicate coating quality and process features.

5.4.1 Metco 447 Bondcoat

Figure 14 shows the variation in bond strength across a profile sample of a Ni-Al-Mo composite powder sprayed with a Metco radial feed torch at HS Tools on an annealed, unsoldered foil (76 μm thick). This test was undertaken to determine if soldering the foil to a heat sink was necessary. The foil was held to a block by clamping it at both ends. During spraying, thermal gradients caused kinking and warping in the foil. As can be seen in the figure the profile between two samples was repeatable despite the kinking problem. Many of the large spikes on the curve correspond to individual kinks in the foil where non-uniform peeling occurred. The flaws in the coating were detected by the test in a manner which allowed each flaw to be located and examined on the fracture surface. This ability to locate flaws is considered a major advantage of the peel test over other adhesion tests.

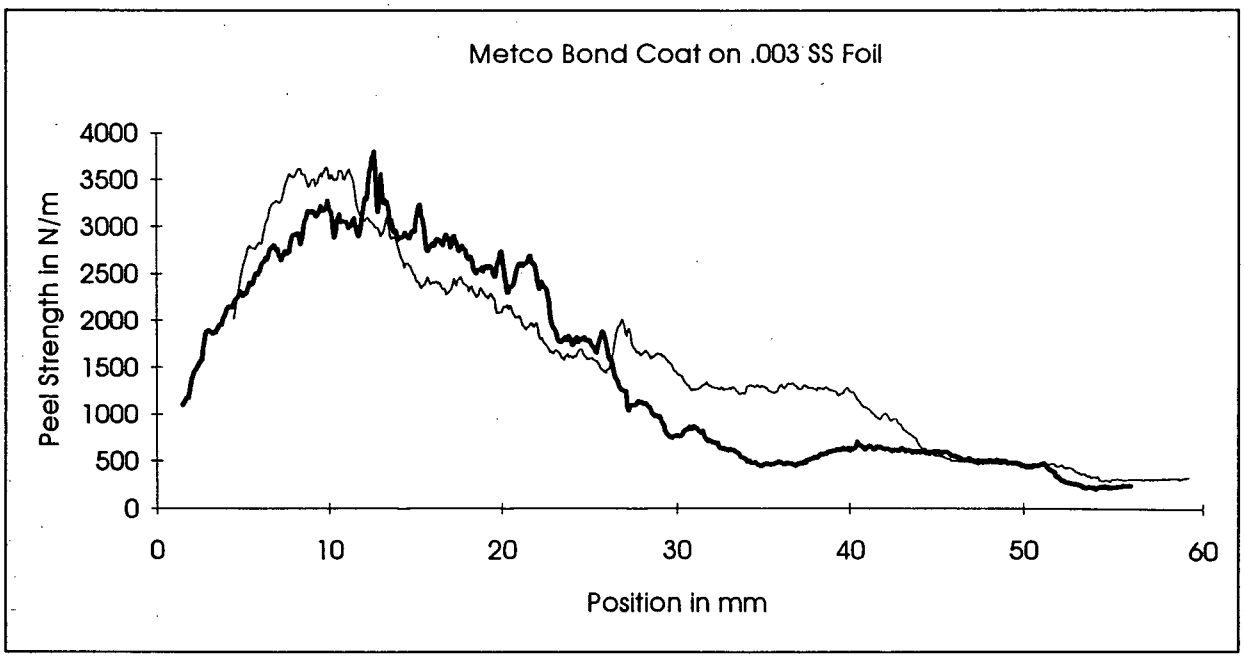

Figure 14. Peel strength profile of a Metco bondcoat.

A distinctive non-symmetry of the peel strength curve is observed. The non-symmetric distribution of mass, momentum and temperature in a radial feed plasma plume is quoted in literature [31]. Using the peel test we are able to show the combined effect of these skewed distributions on the level of local adhesion. The peel strength changes by a factor of seven between the peak where the "best" particles arrived and the periphery where the coldest, and slowest particles deposited.

5.4.2 Metcon WC-Co

Figure 15 shows the peel curve for a WC -Co coating sprayed at Metcon Services. Both a profile and a uniform coating were tested. The curves shown are for a nickel substrate but the curves for the stainless steel substrate have the same basic features. Figure 15a shows the peeling curve for the uniform coating sample. Note that the adhesion drops in the direction of the torch traverse. This drop is accompanied by a visible color change on the fracture surface. The drop is likely due longer exposure time of the low adhesion region to the spray environment. The surface would have been exposed to more of the fume in the spray booth than the regions covered earlier. Fume is the term used to refer to the dust present during spraying. It consists mainly of original powder fines, entrapped dust, and condensed material from evaporated particles. No visible differences are apparent. The region would also have been hotter than regions sprayed earlier. A second explanation for the low adhesion would be that region was not adequately grit blasted and thus had a smaller amount of mechanical bonding. These types of observations are not possible with any other adhesion test.

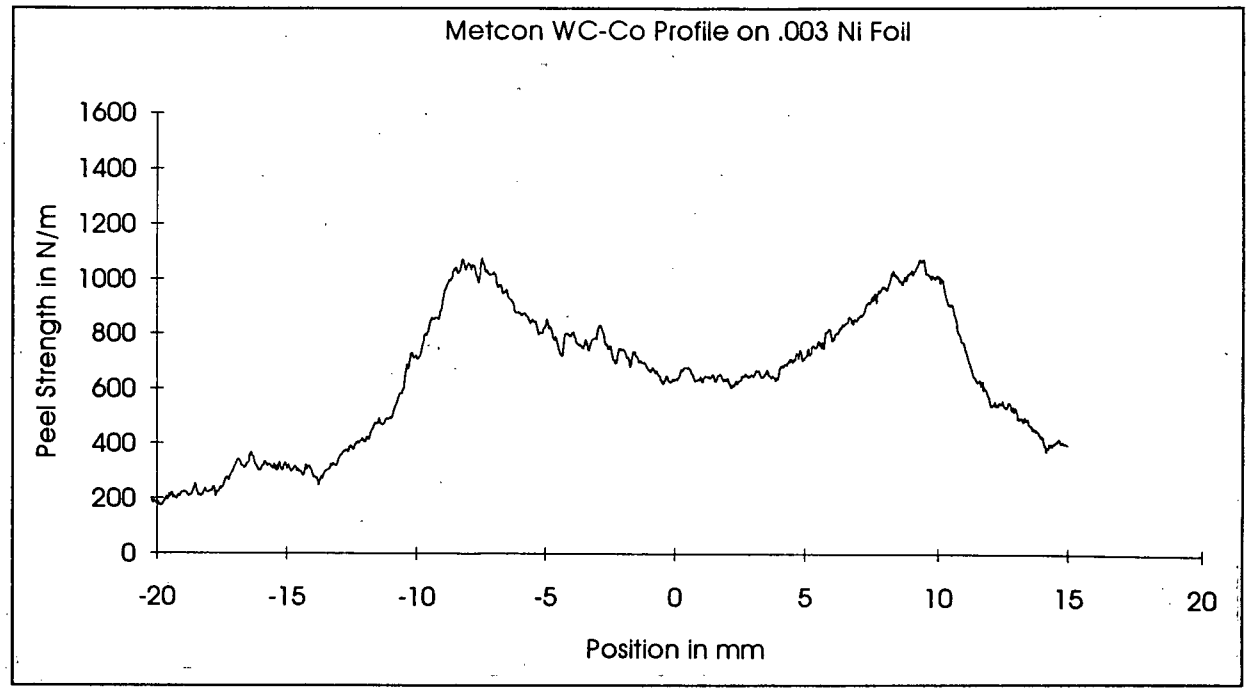

(a)

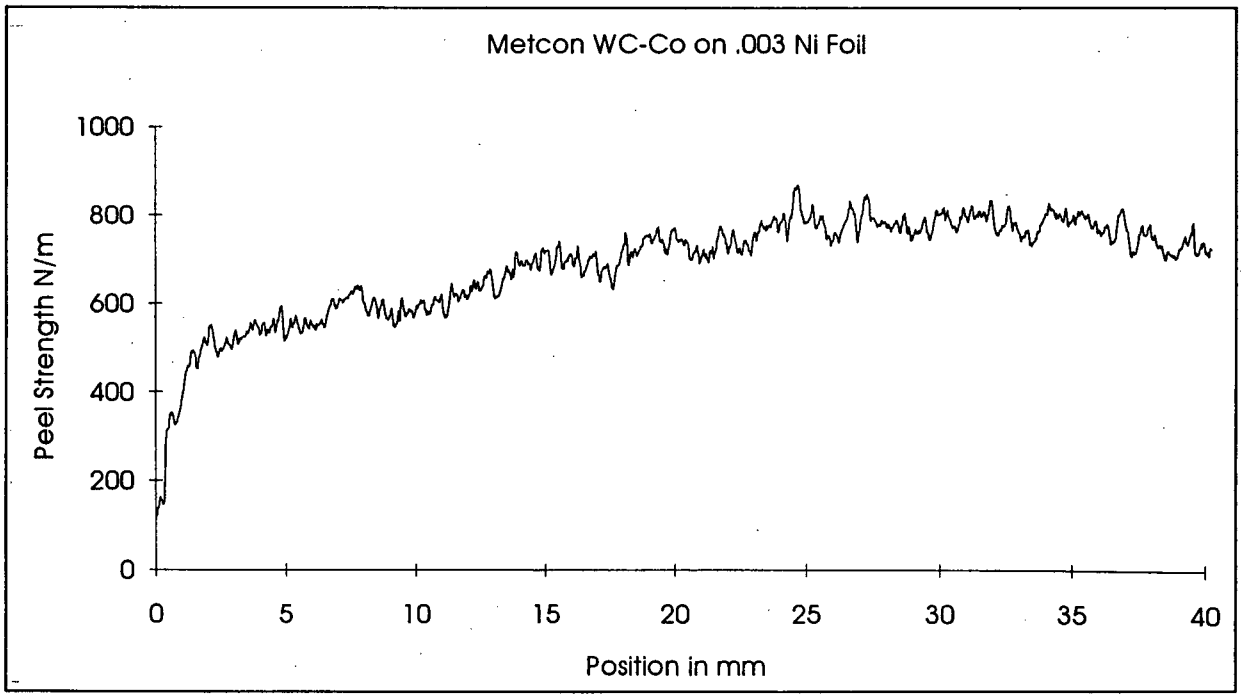

(b)

Figure 15. The peel strength curves for a Metcon WC-Co coating. (a) The spray profile, and (b) the uniform coating.

The adhesion profile of the coating shows a much larger variation than the uniform coating. The adhesion curve is symmetrical about the spray pattern center where the deposit is thickest. In the peripheries the adhesion slowly increases as one move towards the center and reaches a maximum or of 1000 N/m at 7mm from the center. The adhesion then drops to 580N/m in the center. This pattern may be due to the expected increase in residual stress with coating thickness. In the periphery the coating is thin and residual stresses are low. The peel strength increases towards the center due to the better processing of particles in more central parts of the pattern [31], but begins to decrease when residual stresses become large enough to assist in interfacial cracking. A second explanation is that the spray process has not been properly optimized for adhesion and that the majority of the particle traveling through the central portion of the pattern are too hot or fast to bond properly. Again these observations are not possible with any other test method.

5.4.3 Rokide Chromia

Figure 16 shows the peel strength curve for a Rokide chromia coating sprayed onto a nickel foil. As expected for a brittle ceramic it show a much lower interfacial energy than the metal and cermet coatings. The uniform coating curve (Figure 16b) shows a constant bonding across the whole sample of ~220 N/m. Some small scale variations are present, which show no pattern and can be linked with surface features. The profile is shown in Figure 16a. The adhesion at the edges of the profile is high and is very close to the level of adhesion of the epoxy used to bond the coatings to the aluminum plate. The coating is very thin in these regions and the glue penetrates to the interface. As the coating becomes thicker, the adhesion drops as less glue is able to penetrate. The minimum adhesion is ~140 N/m. The adhesion then begins to rise close to the center of the profile. The majority of the mass of the coating (~90%) is the region of rising adhesion. This is likely due to the better processing of the particle which travel through the central portion of the flame.

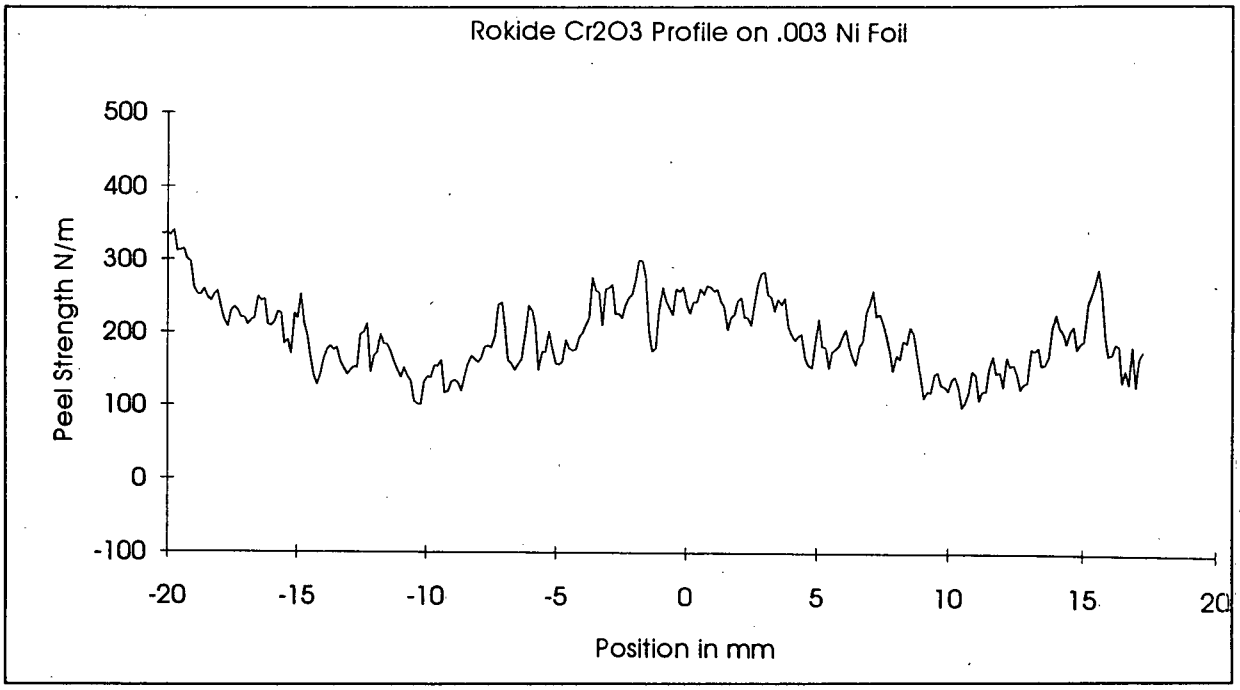

(a)

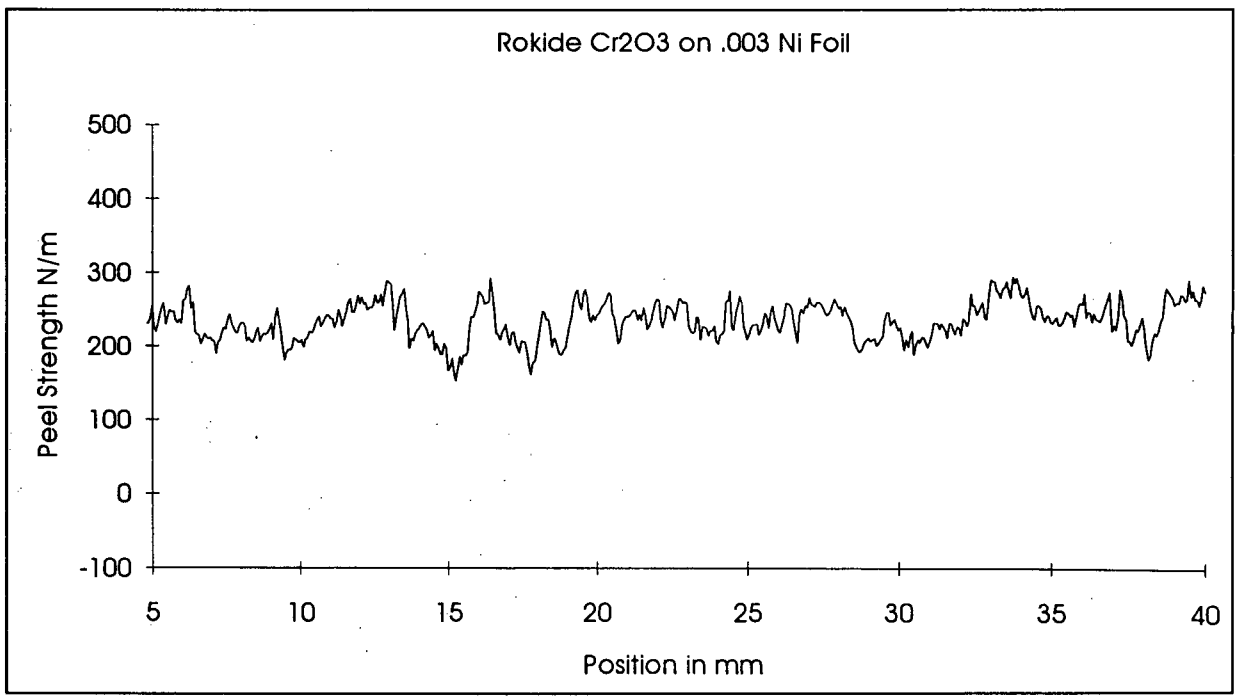

(b)

Figure 16. The peel strength curves for a Rokide Chromia coating. (a) The spray profile, and (b) the uniform coating.

The peak level of adhesion occurs at the center of the profile and is ~260 N/m. The adhesion of the uniform coating is much closer to the profile maximum than the profile minimum. This indicates that the poorly bonded periphery particles do not significantly reduce the adhesion of the coating.

6. Discussion

Several general observations about the peel test and thermal spray coatings can be drawn from the results of this study. The peel test propagates a crack in a controlled way along the coating substrate interface in a manner which can detect the location of bonding flaws, bonding changes with substrate material and the required energy for failure. The detected parameter is self consistent and can be correlated with other test results.

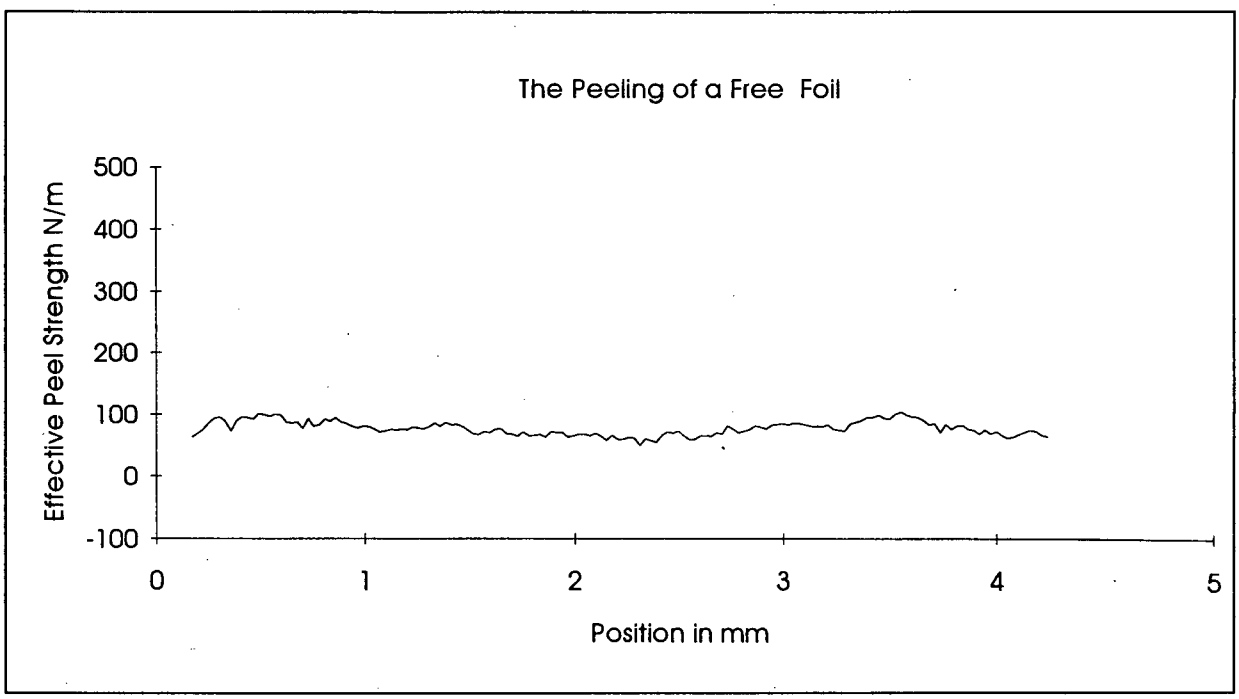

Figure 17. A portion of the curve generated during a calibration test. The deadweight is 3 lbs. Any additional force is due to plastic work or friction. Because the experimental conditions are identical when peel testing, the level of variation in this signal represents the expected level of experimental noise in the peel test.

6.1 Signal Variations

The peel curves are not smooth continuous curves and show significant variations. The test apparatus could be expected at worst to generate variations of 10%. A plot of the peel

force measured during a calibration shows the level of variation which the experimental apparatus would be expected to generate (Figure 17). This would include measurement system noise, drift and frictional variations. The variations larger than this must thus be considered significant, although there is no clear relationship between these variations and the crack propagation characteristics or microstructural features of the coating, substrate or interface. The noise is possibly indicative of a slip-stick type of crack propagation. The crack can only propagate a short distance before the stresses drop below the level required to continue cracking. Alternatively the noise may reflect the variation in bond strength on a small scale.

At the outset of this study it was expected that due to the large differences in coating properties across the spray pattern variations would exist in the adhesion of the coating. These variations should coincide with the torch path and would thus be periodic in the torch traverse direction. A second possibility was that on the first set of passes the poorly processed periphery particles would land first and cause a much lower adhesion than would be found in the center of the profile. The peel test did not indicate any periodic changes in adhesion and the adhesion of a uniform coating was not significantly lower than the maximum adhesion of the profile. Examination of the adhesion profiles indicates that the center of the profiles generally have a lower adhesion than the edges. This is likely due to the increased residual stress in the thicker, hotter portion of the profile. Thus strategies for improving adhesion should be based on reducing residual stress rather than improving the processing of periphery particles.

6.2 Peel Strength and Fracture Toughness

As the peel strength essentially represents the failure energy per unit area it can be compared to the fracture toughness of coating interfaces. Several researchers [3, 5, 32] have compiled a limited set of G_C values for various coating systems. These sources did not examine the phase angle (Ψ) at the interface. They have reported the values as G_{IC} because they

were the results of DCB tests which should produce mode I stress at the crack tip in homogeneous materials. Because the peel test has a significant amount of mode II stress at the crack tip the results are not comparable as would be desired. The crack paths were usually through the coating or close to the interface, whereas the peel test causes failure on the interface. Caution should be employed in their interpretation. It is expected however that these differences should not significantly affect the range of possible values. Table VI show the typical range of values found for the DCB test and the peel test for both nickel and stainless steel foil. The peel strengths are generally of the same order of magnitude as the reported toughnesses for the steel substrate, but are at the higher end of the range. The toughnesses for the nickel substrate are much higher than the other values by about a factor of 3. This difference is discussed below.

Table VI Comparison of Fracture Energies

Type of Coating	DCB TEST J/m^2	Peel Test on Stainless Steel J/m^2	Peel Test on Nickel Foil J/m^2
Ceramic	10 to 100	10 to 60	175 to 275
Cermet	20 to 60	150 to 250	600 to 750
Metal	80 to 350	160 to 300	450 to 980

For both the DCB tests and the peel test the interfacial energies for the ceramic materials are much higher than would be expected for a fully dense ceramic. Thus energy dissipation mechanisms must operate other than the creation of new surface. Figure 18 schematically shows some of the possible mechanisms which might cause the high peel strength. These include friction between asperities, local plastic work within asperities, and microcracking in the coating. Because these mechanisms are difficult to isolate it is not possible to obtain the true interfacial energy with this method. These mechanisms also operate in service and improve the

toughness of the coating interface. The measured peel strength is thus representative of the energy needed to fail the coating under similar loading conditions. This makes the test useful for understanding service failure.

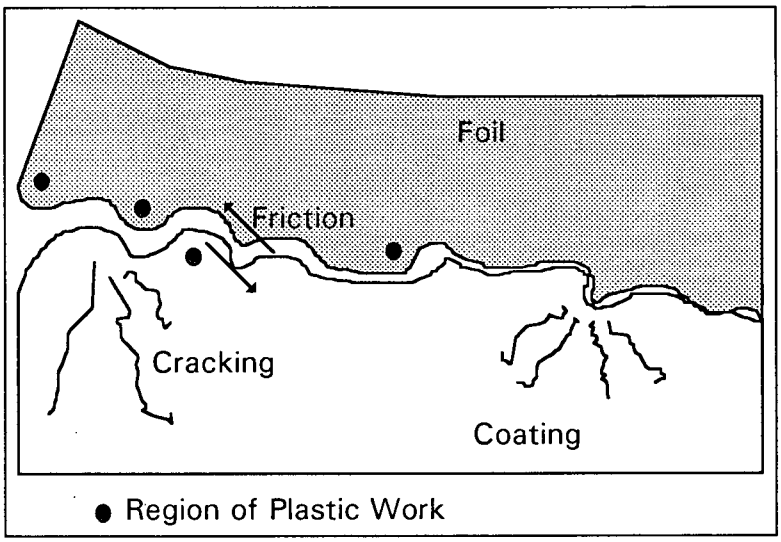

Figure 18. Possible energy dissipation mechanisms during cracking which would cause a high interfacial toughness.

6.3 Substrate Differences

In all cases the peel strength for the nickel foil was much higher than for the stainless steel foil. The foils were prepared and sprayed in exactly the same way and thus some material difference must account for this difference. The increased peel strength may be due to the difference in the substrate's surface chemistry. If this were the case, the difference would however not likely occur with all of the different coating materials. The peel strength on nickel foil was always higher. During thermal spraying molten splats cool in about 10^{-7}s [33]. This is commonly used as an argument that no chemical reactions have time to occur so the bonding of TSCs is independent of chemistry. A second possibility is that the lower yield strength and higher ductility of the nickel material allowed it to deform more easily upon particle impact, creating a better roughness during grit blasting and a better mechanical fit during spraying.

This ductility could also reduce the level of residual stress. It is unknown what a lower yield strength would do to the phase angle at the crack tip. Thus there may be a difference in the crack tip stresses because of the different substrate. During peeling the extra energy required to deform the surface asperities would be reflected in a higher interface energy and a more ductile fracture surface. SEM photographs of the fracture surface (Figure 19) show that both the nickel and stainless steel substrates had a brittle fracture pattern although the nickel has more signs of ductile deformation on a local scale. This is a qualitative evaluation and no quantitative methods were used to determine if more plastic deformation occurred. If the ductility of the nickel is drastically improving the bond strength, as indicated by the peel test, then this offers as strategy for improving bond coat materials. This hypothesis must however, be confirmed with other techniques. Currently most bond coats are complex alloys which are thermally sprayed. They are thus inherently brittle. A more ductile bond coat may improve bonding. Pure aluminum or other corrosion resistant ductile metals may thus be useful bond coats.

6.4 Crack Location

Examinations of the fracture surfaces formed in the peel test show that failure occurs exactly upon the interface. The SEM photographs, shown in figure 19, of the substrate side show no residue of the coating material. This was the case with all of the coatings tested. The geometry of the test is likely the cause. Because of the small mandrel size high foil strains are concentrated in a small region. The difference in the ability of the materials on each side of the interface to accommodate strain causes the stress field to be concentrated close to the interface. Models of the peel test [11,12] indicate that the peel test geometry causes stress fields which force the crack to propagate along the interface. The crack follows the local lowest energy path which is the interface. In this case the "extra" toughness may come from the mechanisms listed above which occur due to the rapidly increasing strains behind the crack tip. This explanation is overly

simple and a better understanding of crack propagation along highly strained rough interfaces is necessary. The experimental data indicates however, that high energies are measured and that failure occurs exactly at the interface. This is considered a significant advantage of using the peel adhesion test for the evaluation of thermal spray coatings.

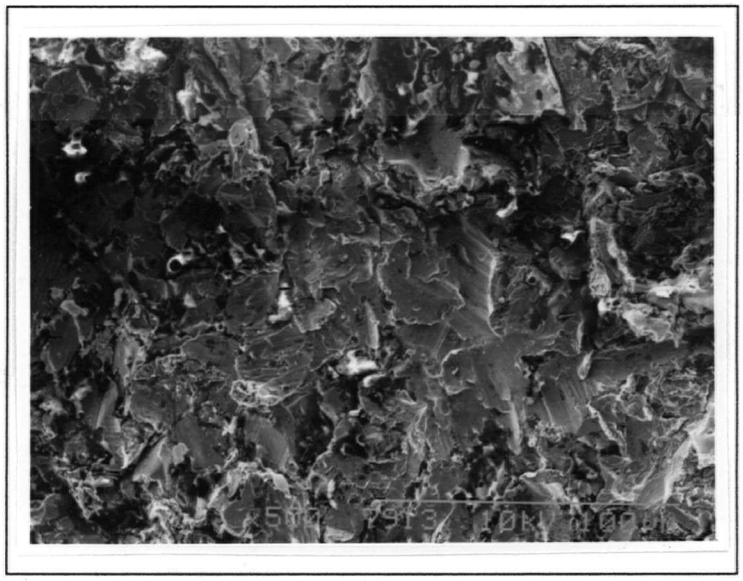

(a)

(b)

Figure 19. The substrate side of the interface fracture surface: (a) a nickel substrate and (b) a stainless steel substrate. Both exhibited brittle fracture, but the nickel foil is qualitatively more ductile.

6.5 *Correlations Between Test Results*

As many coatings were tested, it is possible to examine the types of correlations which the peel test has with both hardness and tensile bond strength. Table V summarizes the results of each of these tests for the various coatings. While a general quantitative relationship between tensile bond strength and peel strength is not currently available, it would be reasonable to expect that as tensile bond strength increases the peel strength should also increase. Because most of the TAT samples failed in the glue it is impossible to evaluate this relationship. The peel test is capable of testing coatings with much higher bond strengths than the TAT, such as those produced by the new generation of thermal spray processes.

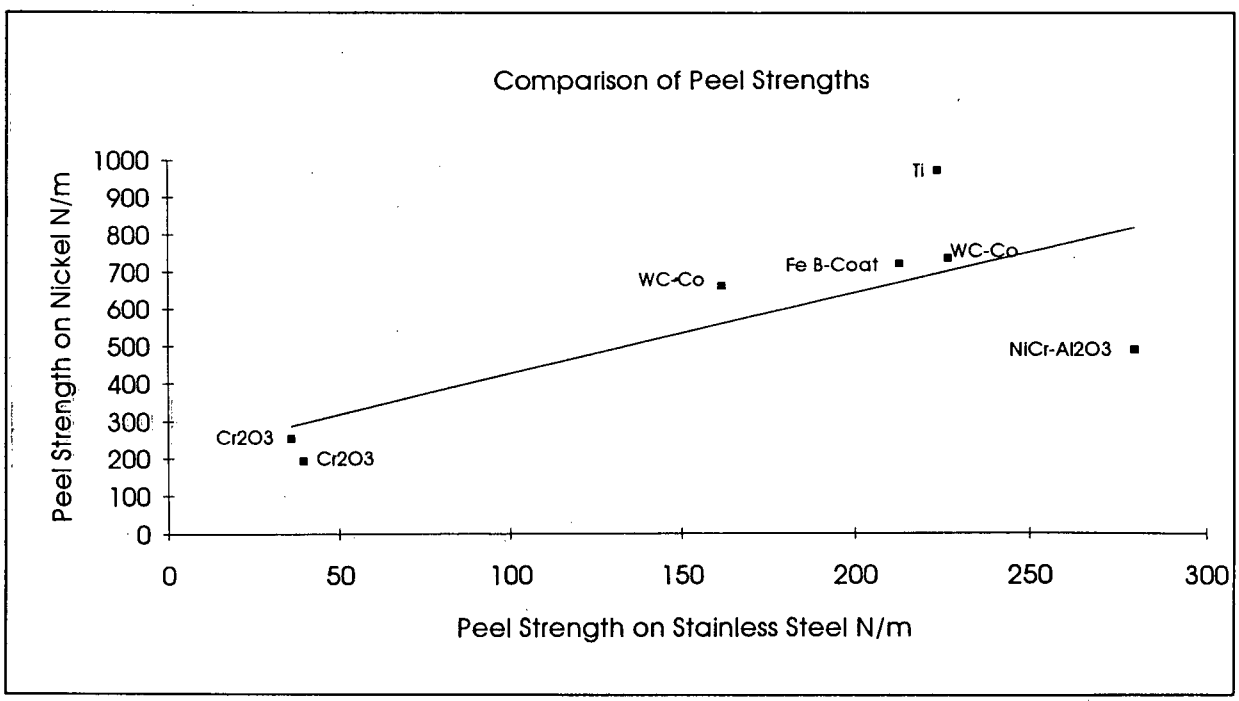

Figure 20. A plot of peel adhesion on stainless steel versus the peel adhesion on nickel foil; showing that an increase in adhesion to one substrate corresponds to an increase in adhesion to the other. Each point is labeled with the coating type.

A second consistency check is that in general the peel strength on nickel should increase when the stainless steel peel strength increases. This is shown in Figure 20. While it is not possible to develop a relationship between the two peel strengths it can be seen that they do increase with each other.

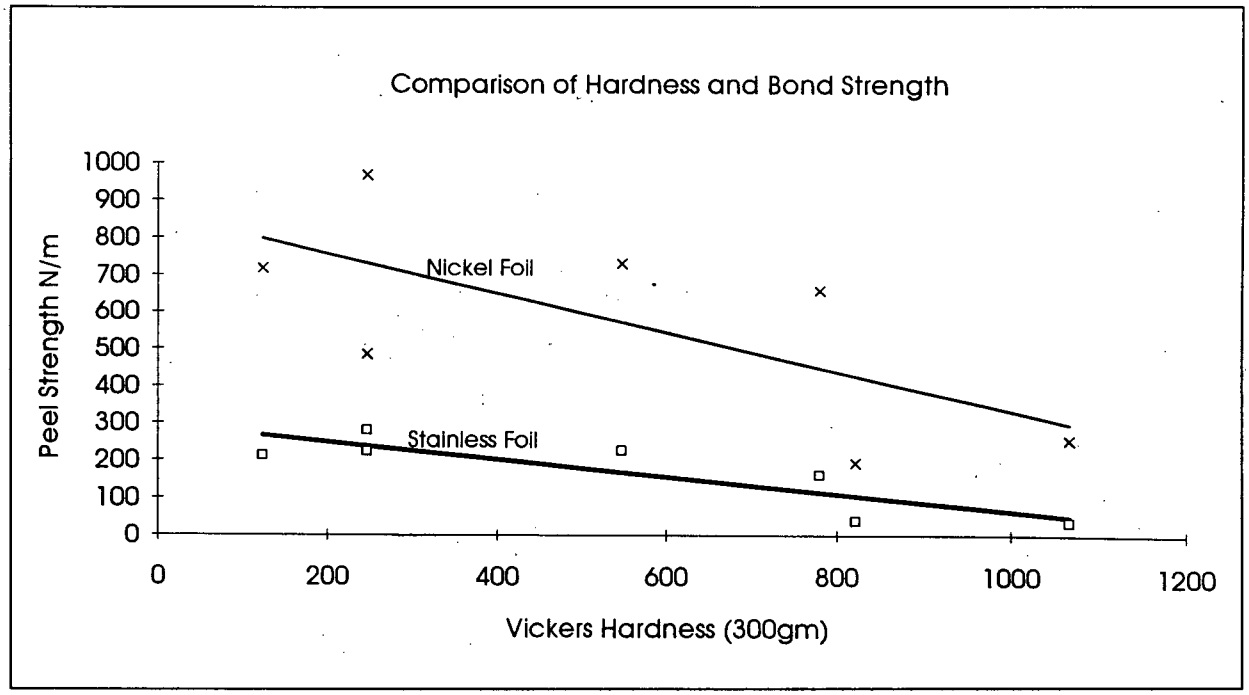

Figure 21. A plot of Vickers hardness versus adhesion, showing that an increase in hardness generally corresponds to a decrease in interfacial energy. Each point represents a different coating type.

A commonly used parameter for evaluating the general quality of a coating is Vickers hardness. This parameter reflects the properties of the coating material, the degree of porosity, the coherency and the degree of microcracking. Because the effects of these are all mixed in an unknown way, it is not a very useful measurement for engineering predictions. Harder coatings tend to adhere less well than softer coatings. For both the soft nickel substrate and the hard stainless steel substrate, the adhesion decreases as the hardness increases (Figure 21). These observations indicate that the peel test produces self consistent results which fit with the current state of knowledge about coatings.

7. Conclusions

Several types of conclusions can be drawn from the development of the peel test. The peel data produced has indicated several feature of TSCs. The test has also been shown to be useful for several types of evaluations. From this information several recommendations are made.

7.1 Summary of Results

In order for the peel test to be accepted, its results must be consistent with what is known about adhesion. The peel strengths measured here agree well with other measurements of G_C and thus can be considered to be reasonable measurements of this parameter for the stress intensity phase angle for the peel test. The peel test produces stress intensities similar to those encountered in coating service. The peel strength decreases with an increase in hardness. This is consistent with the fact that hard materials tend to fail in a low energy brittle manner. The peel strength is consistent with itself in that the peel strength on one substrate increases with the peel strength on another. This is despite the fact that the adhesion to the ductile nickel foil was much higher than adhesion to the hard stainless steel foil by about a factor of 3. As this is not likely due to chemistry the ductility of the nickel is likely the cause of the enhanced adhesion. This indicates that ductile bond coats may be advantageous over some of the harder alloys.

7.2 Utility of the Test

The peel test provides more information about how a coating can fail than most other destructive tests. It is thus a useful tool when doing developmental work on a coating. It allows the defects or regions of low adhesion to be precisely located and thus allows them to be studied as to their cause. Repeatable measurements of the variations in adhesion within a coating

were achieved which allows the test to be used for coating evaluation and comparison. The observed details of the variations may lead to a better understanding of the mechanism of failure along the coating/substrate interface. The failure occurs along the interface and thus the test is a true reflection of adhesion and not the cohesion of the coating. Because the test is not limited by the strength of a bonding agent it is capable if testing the adhesion of the high strength coatings which were previously untestable.

The test can also be useful as a quality assurance tool. Because it is less sensitive to sample size and alignment that TATs it provides a more reliable evaluation of the coating quality. The test is relatively easy to perform when compared to sophisticated fracture mechanics tests and it is thus possible for spray shops to do their own testing. The conditions of the test produce a stress intensity at the crack tip which is very similar to the type of stresses expected at an interface under bending loads or inplane residual stresses. This means that the test causes failure in a manner similar to the typical causes of failure in coating applications. The peel strength is thus more useful in predicting service constraints than either TATs, most fracture mechanics tests or ultrasonic adhesion measurements.

7.3 Future Work and Recommendations

Further work is required to fully characterize the test and to exploit its findings. This includes testing of a wider variety of coatings produce by the whole range of thermal spray processes. The test results should be compared to more DCB or 3 point bend toughness tests as well as to ultrasound interfacial integrity tests so that the relationships between these measurements can be determined. A comparison with some sort of performance test should also be undertaken. Both mechanical and thermal fatigue tests would be useful. Experiments such as the TAT test and the peel test should be performed on a variety of substrates which differ in their ductility. A more detailed model of the mechanics of the test should be formulated

which allows the determination of the applied loads and residual stresses on the stress intensity at failure. A mechanical description explaining the difference in bonding between the nickel and stainless steel is also needed. Such a model would have applicability in all industries which use the peel test.

The test itself can be improved. A major criticism of the test is the need to solder the foil substrate to a back plate. A scheme could be developed which allows the foil to be held and cooled during spraying without solder. This would allow the testing of substrates which are difficult or impossible to solder such as titanium. It would also reduce the preparation time associated with the test. In order to accomplish this thicker foils and larger bending mandrels would be needed. A second improvement would be the development of a simple bench top testing jig which does not require the expensive tensile machine and data acquisition system. A scaled down version of the existing system would be adequate.

The peel test has been proven to be a useful adhesion measurement technique for thermal spray coatings. It has several advantages over conventional testing techniques which make it useful for both quality assurance and developmental testing. It results can be related to the parameters of fracture mechanics and are thus useful in predictive work. Further work is needed to develop a complete mechanical description of the system, to use the test result to improve the spraying process and to determine the relationship between the test results and the performance of the coatings.

References

1 M. Boulos, P. Fauchais, E. Pfender, Fundamentals of Materials Processing using Thermal Plasma Technology, Notes From Short Course presented at *2nd National Thermal Spray Conference,* Cincinnati (1989)

2 S. Brown, B. Chapman, and G. Wirtz, Fracture Kinetics and the Mechanical Measurement of Adherence, in *Thermal Spray Technology - New Ideas and Processes*, Ed. D.L. Houck, Pub. ASM International, (1989), pp. 147-157

3 T. Troczynski and J. Camire, Resistance to Fracture of Thermal Sprayed Ceramic Coatings, *in Thermal Spray Industrial Applications,* Ed. C Berndt and S Sampath. Pub. ASM International, (1994), pp. 663-668

4 H.S. Ingham Jr., Adhesion of Flame Sprayed Coatings, *in Adhesion Measurement of Thin Films Thick Films and Bulk Coatings,* Ed. K.L. Mittal, Pub. ASTM, (1976), pp. 285-291,

5 C. K. Lin and C. C. Berndt, Measurement and Analysis of Adhesion Strength for Thermally Sprayed Coatings, *in Journal of Thermal Spray technology,* Vol. 3, No. 1, (1994), pp. 75-104.

6 W. Han, E Rybicki and J Shadley, An Improved Specimen Geometry for ASTM C633-79 to Estimate Bond Strengths of Thermal Spray Coatings, in *Journal of Thermal Spray Technology,* Vol. 2, No. 2, (1993), pp. 145-150

7 J. W. Hutchinson and Z. Suo, Mixed Mode Cracking in Layered Materials, *in Advances in Applied Mechanics*, Ed. J Hutchinson, Pub. Academic Press, Vol. 29, (1992), pp. 63-191

8 Y. Suga, Harjanto and J. Takahashi, Study on the Ultrasonic Test for Evaluating the Adhesion of Thermal Sprayed Coatings to a Substrate, in *Thermal Spray: International Advances in Coating Technology*, Ed. C.C. Berndt, Pub. ASM International, (1992), pp. 247-252

9 Y. Namba, H. Nakazato, and K. Honma, pp. 241-246 in "Thermal Spray: International Advances in Coating Technology", Ed. by C.C. Berndt, ASM International, (1992), pp. 241-245

10 ASTM D 903-49 (1983), Standard Test Method for Peel or Stripping Strength of Adhesive Bonds.

11 ASTM D 3167-76 (1986), Standard Test Method for Floating Roller Peel Resistance of Adhesives.

12 A. D. Crocombe and R. D. Adams, An Elasto-Plastic Investigation of the Peel Test, *in The Journal of Adhesion,* Vol. 13, (1982), pp. 241-267

13 A. D. Crocombe and R. D. Adams, Peel Analysis Using the Finite element Method, *in The Journal of Adhesion*, Vol. 12, (1981), pp. 127-139

14 M.D. Thoules and H.M. Jensen, Elastic Fracture Mechanics of the Peel Test Geometry, in *Journal of Adhesion*, Vol. 38, (1992), pp. 185-197.

15 K. Kim and J. Kim, Elasto-Plastic Analysis of the Peel Test for Thin Film Adhesion, *in Journal of Engineering Materials and Technology,* Vol. 110, (1988) , pp. 266-273

16 J. Holowczak, V Greenhut, and D. Shanefield, Peel Adhesion Bond Strength of Direct Bonded Copper Alumina as Affected by Alumina Sintering Aids, *In Metal Ceramic Joining,* Ed. P. Kumar and V. Greenhut, Pub. The Minerals and Metals Society, (1991), pp. 153-166

17 E. Gdoutos, Fracture Mechanics, Criteria and Applications, Kluwer Academic Publishers, Norwell Ma. (1990)

18 A. Evans and J Hutchinson, Effects of Non Planarity on the Mixed Mode Fracture Resistance of Bimaterial Interfaces, *in Acta Metallurgica,* Vol. 37, No. 3, (1989) , pp. 909-916

19 J. Dundurs, Effect of Elastic Constants on Stress In a Composite Under Plane Deformation, *in Journal of Composite Materials,* Vol. 1, (1967), pp. 310-321

20 H. Nakahira, K. Tani, K. Miyajima and Y Harada, Anisotropy of thermally Sprayed Coatings, *in Thermal Spray: International Advances in Coatings Technology,* Ed. C. Berndt, Pub ASM International, (1992), pp. 1011-1017

21 P. Xu, J. Stranart, and S. Meguid, Nondestructive Testing of Coatings Using Ultrasonic Leaky Rayleigh Waves, *in Thermal Spray Industrial Application,* Ed. C Berndt and S Sampath, Pub. ASM International, (1994), pp. 765-769

22 F. Tzschichholz and M. Pfuff, Influence of Crackpath Roughness on Crack resistance in Brittle Materials, *in Fracture Processes in Concrete, Rock,, and Ceramics,* Ed. J van Mier, J Rots, and A Bakker, Pub. E&F.N. Spon, London (1991) pp. 251-260

23 T. Troczynski, Stochastic Model of R-Curve due to Crack Bridging, *In Acta Metallurgica,* In Press for fall 1995

24 Y. Mai and B. Lawn, Crack-Interface Grain Bridging as a Fracture resistance Mechanism in Ceramics, *in Journal of The American Ceramic Society,* Vol. 70, No. 4 (1987), pp. 289-294

25 D. Greving, E. Rybicki, J. Shadly, Through Thickness Residual Stress Evaluations for Several Industrial Thermal Spray Coatings using a Modified Layer Removal Method, *in Journal of Thermal Spray Technology*, Vol. 3, No. 4, (1994), pp. 379-388

26 D. Greving, E. Rybicki, J. Shadly, Effects of Coating Thickness and Residual Stresses on the Bond Strength of ASTM C633-79 Thermal Spray Coating Test Specimens, *in Journal of Thermal Spray Technology*, Vol. 3, No. 4, (1994), pp. 371-378

27 D. Munz, M. Sckuhr, Y. Yang, Thermal Stresses in Ceramic-Metal Joints with an Interlayer, *in Journal of the American Ceramic Society,* Vol. 78, No. 2, (1995), pp. 285-290

28 D. Drucker, Introduction to The Mechanics of Deformable Solids, Pub. McGraw Hill, (1967), pp. 145

29 ASTM C633-79 (1979) Standard test Method for The Adhesion of Flame Sprayed Coatings.

30 G. Blann and D. Diaz, The Developement of ASTM Standards for Metallographic Preparation Practices for Thermal Spray Coatings, in *Thermal Spray Industrial Applications,* Ed. C. Berndt and S. Sampath, Pub. ASM International, (1994) pp.721-726

31 J.R. Finke, W.D. Swank, Simultaneous Measurement of Ni-Al Particle Size, Velocity, and Temperature in Atmospheric Thermal Plasmas, in *Thermal Spray: International Advances in Coating Technology*, Ed. C.C. Berndt, Pub. ASM International, (1992), pp. 39-43.

32 C. Berndt and R. McPherson, The Adhesion of Plasma Sprayed Ceramic Coatings to Metals, in *Materials Science Research*, Vol. 14, (1981), pp. 618-628

33 V.E. Belaschenko, Thermal Conditions of Formation of Hot Sprayed Coatings on Flat Surfaces *in Fizika i Khimiya Obrabotki Materialov*, Vol. 20, No. 3, (9186), pp. 82-87.

Appendix A Sample Peel Curves

A peel curve for each of the coatings tested is presented here. Each uniform coating is accompanied by a profile test on the same material. The average peel strength of each curve is reported in Table II. Some sample sets were not complete and missing data is indicated.

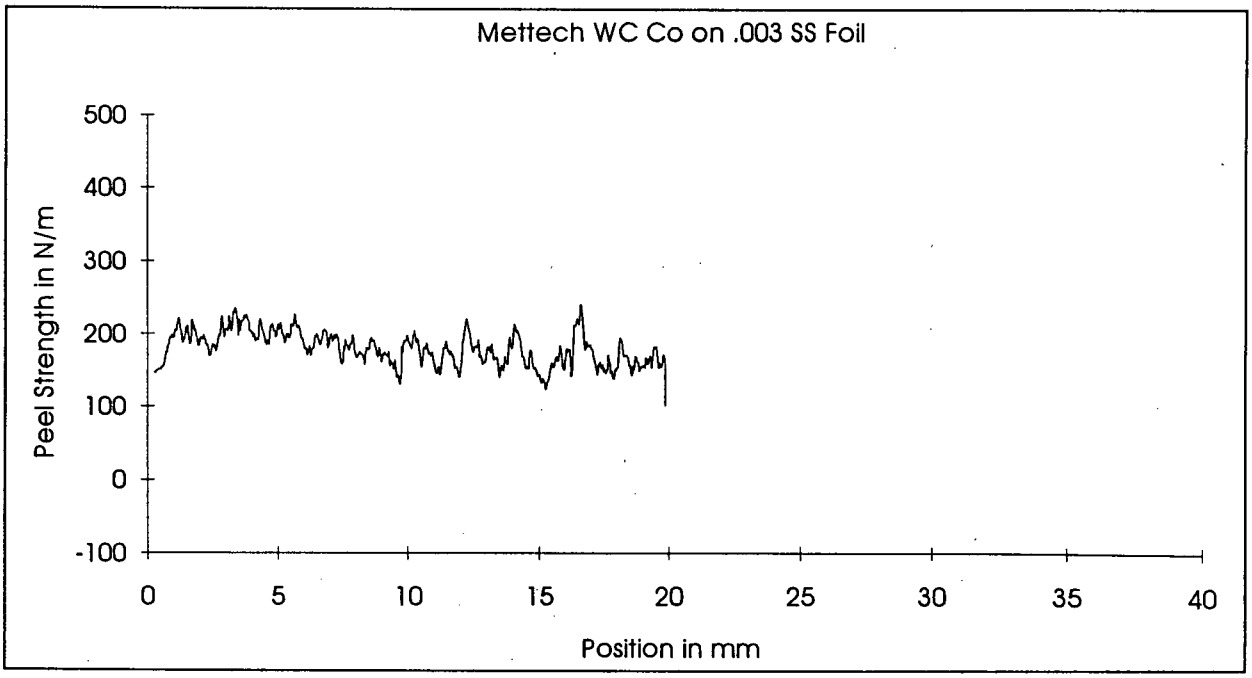

Mettech WC Co on .003 SS Foil (040695a)

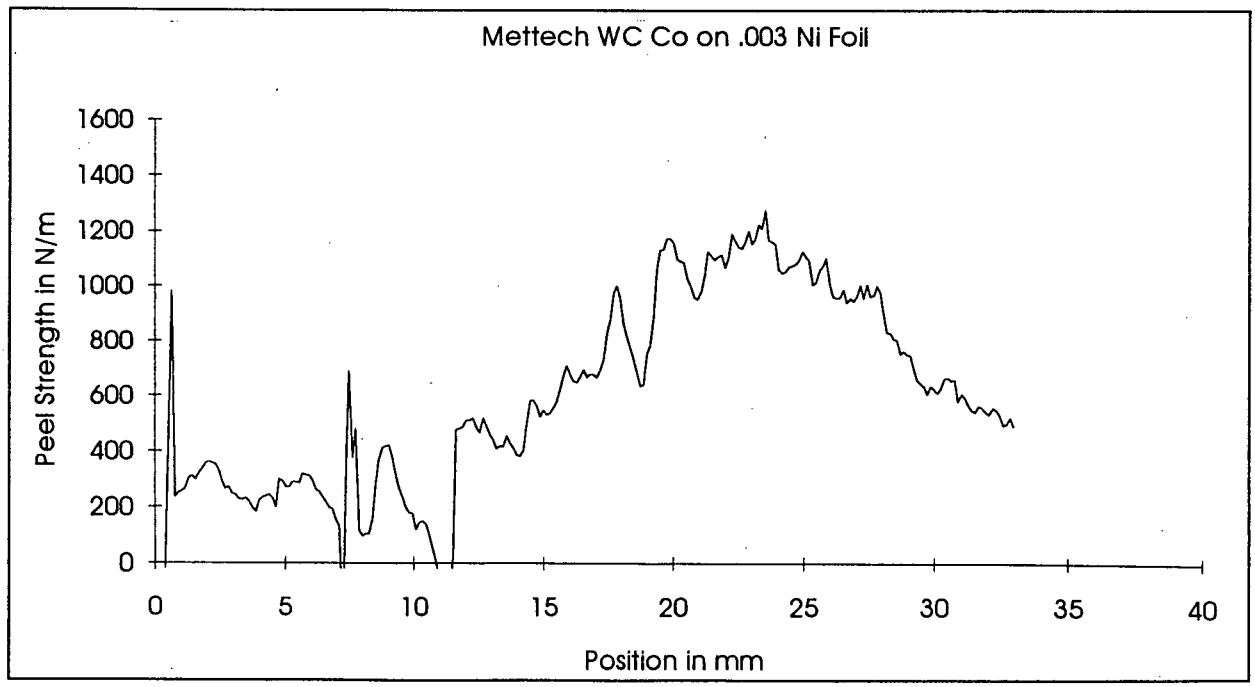

Mettech WC Co on .003 Ni Foil (040695a)

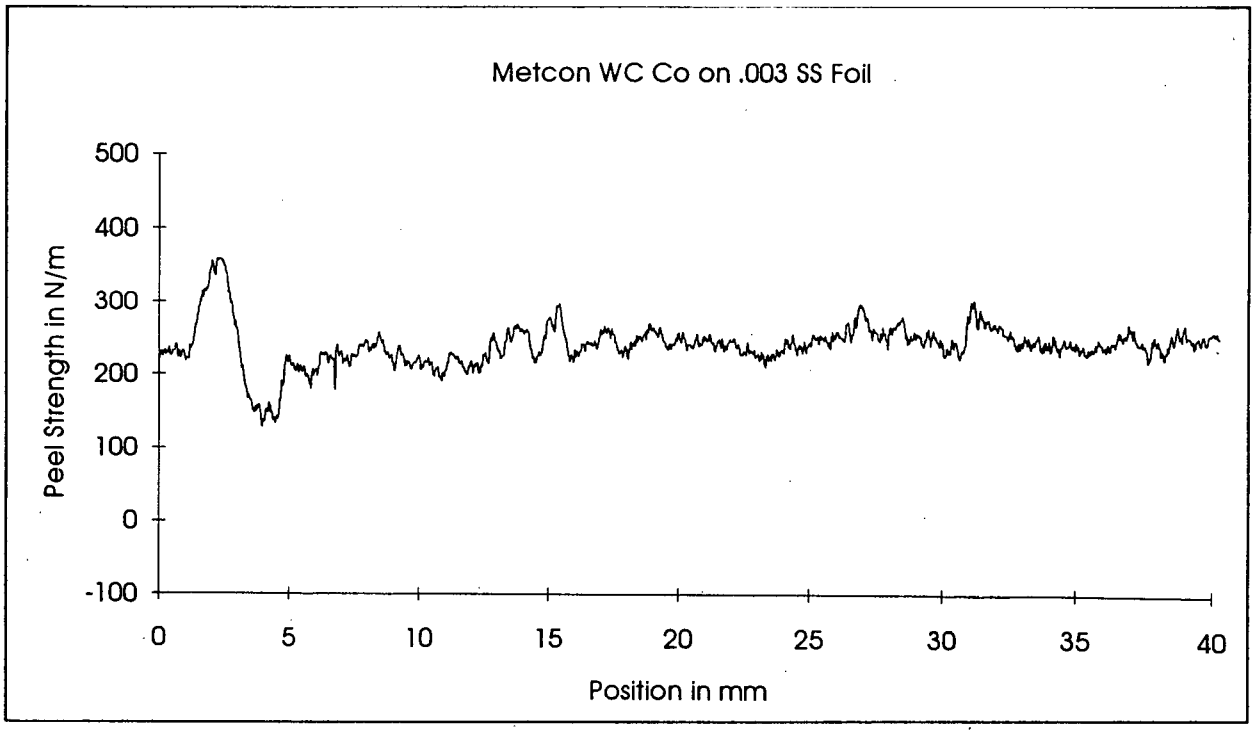

Metcon WC-Co on .003 SS Foil (040795a)

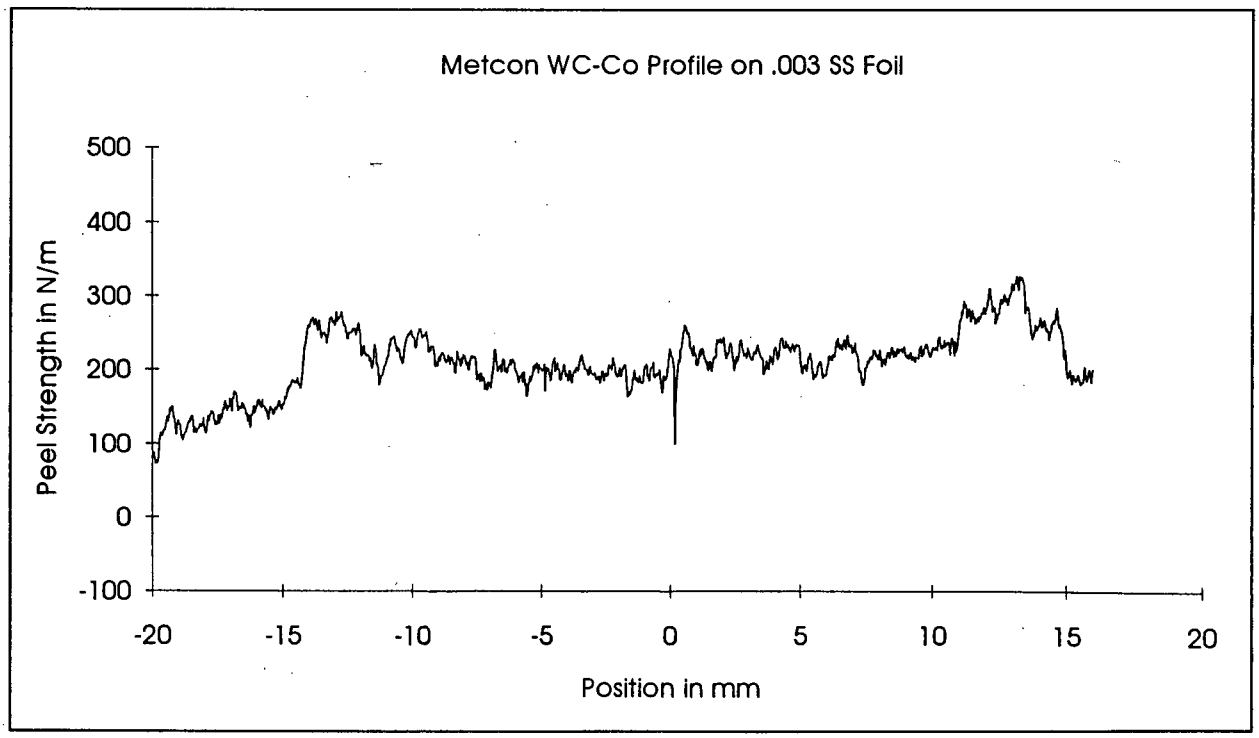

Metcon WC-Co on Profile on .003 SS Foil (040795ap)

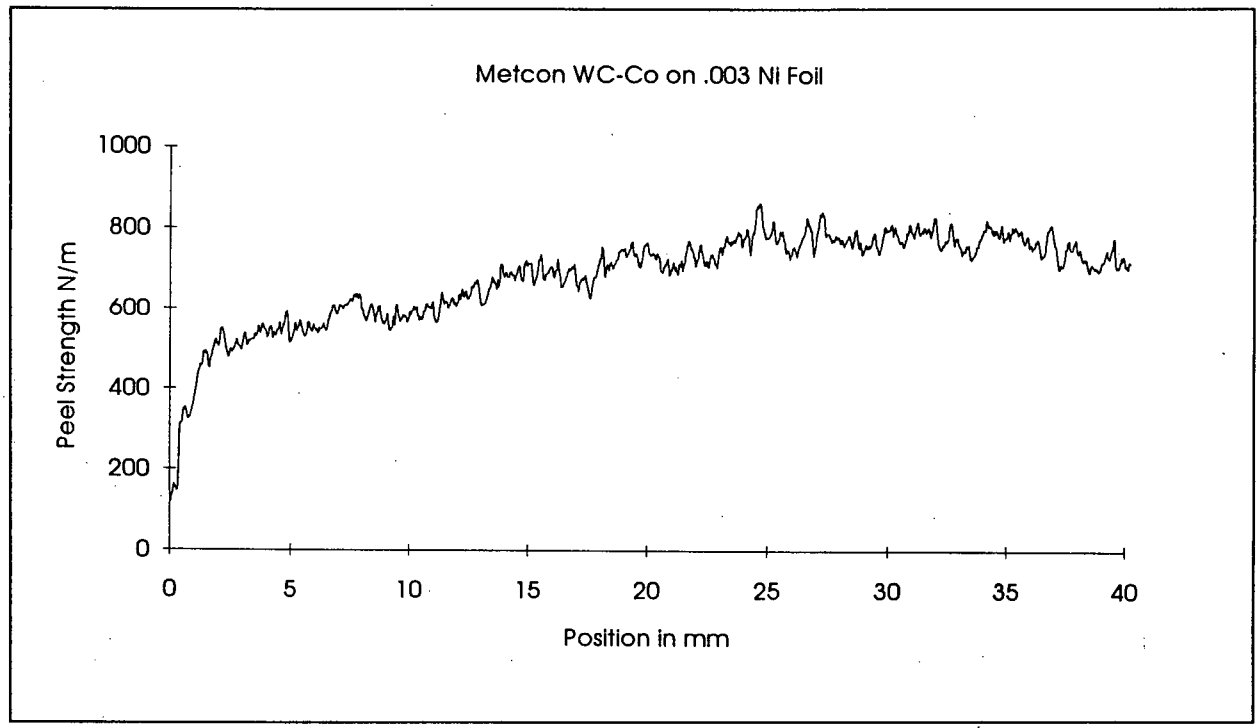

Metcon WC Co on .003 Ni Foil (040795a)

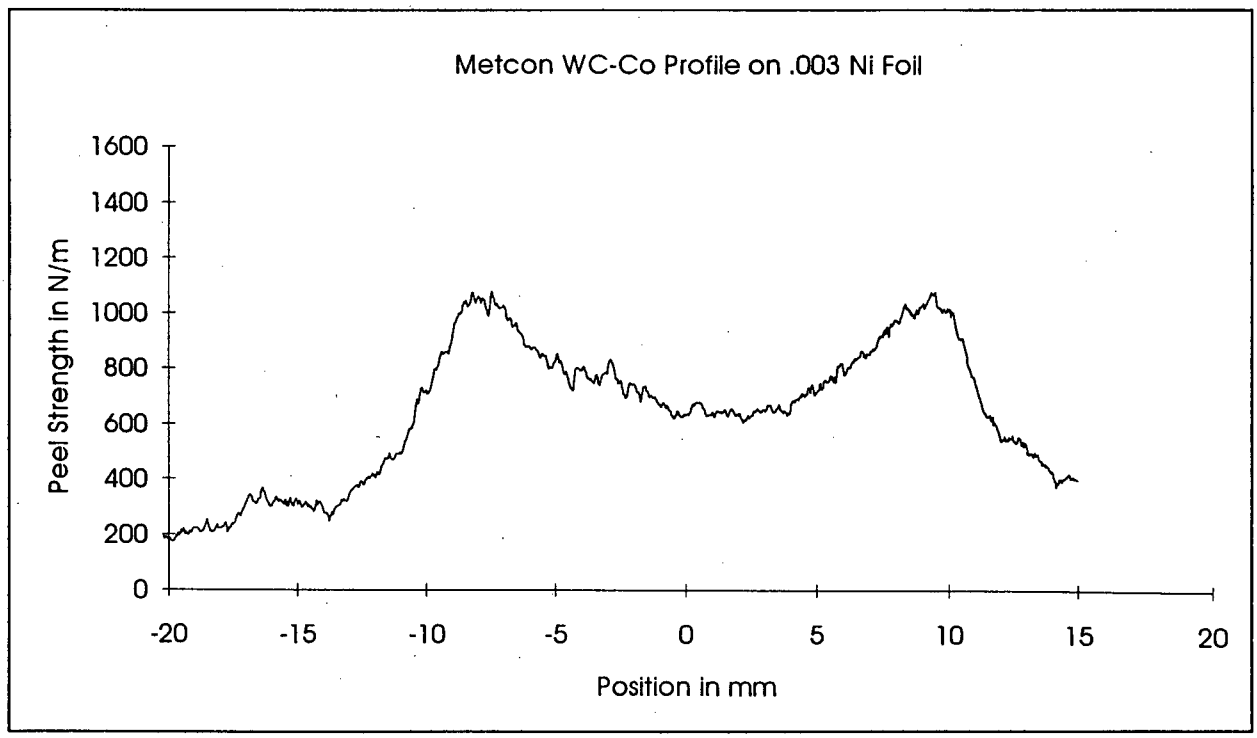

Metcon WC Co Profile on .003 Ni Foil (040795ap)

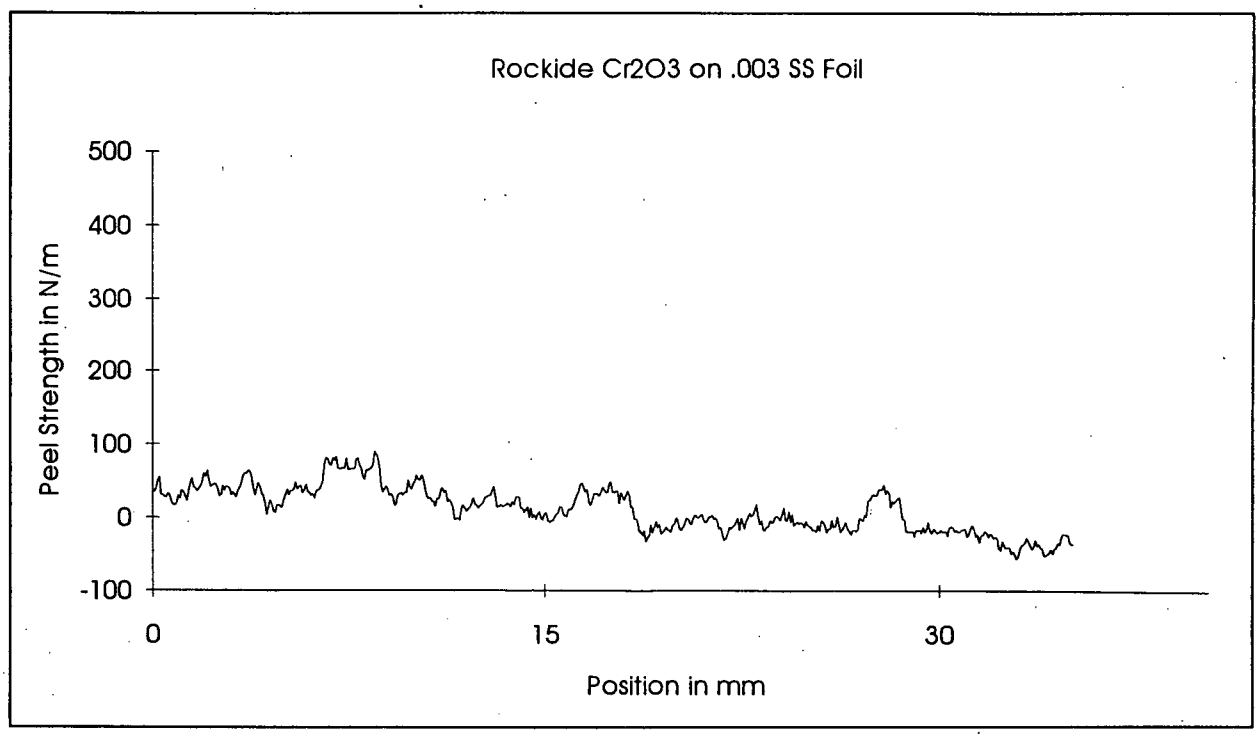

Rokide Cr_2O_3 on .003 SS Foil (051695c)

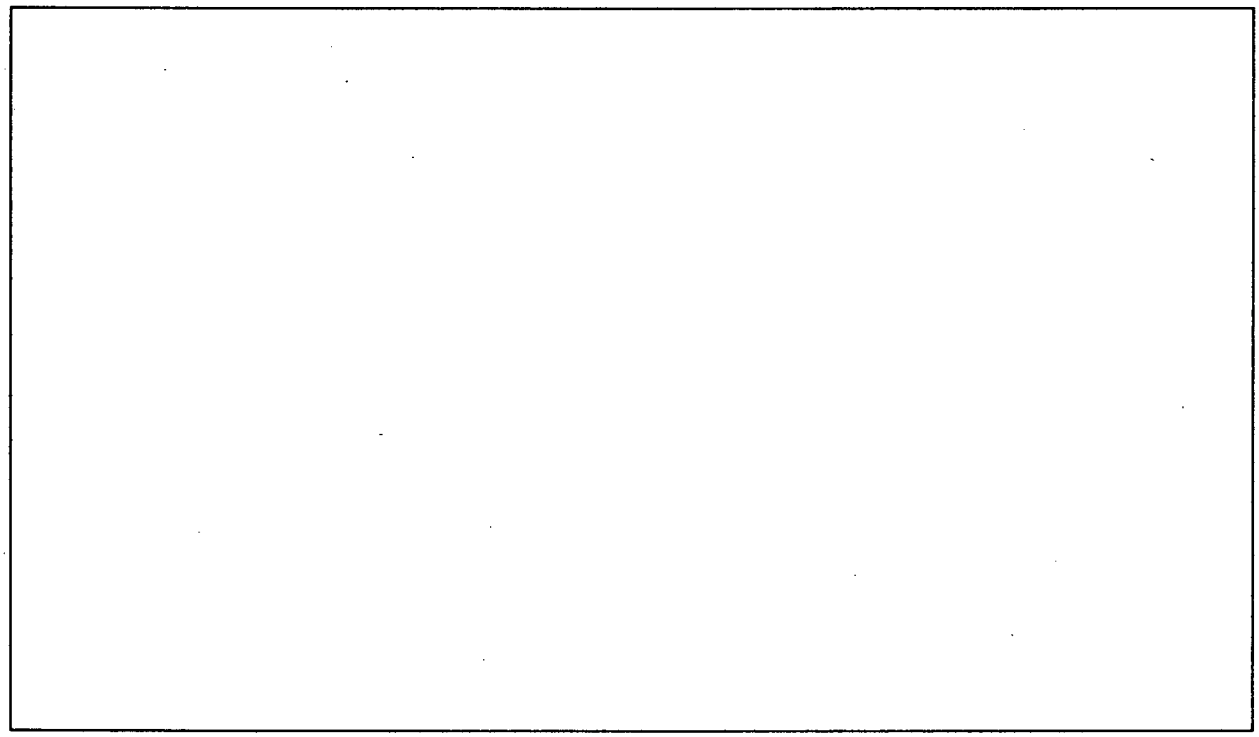

Rokide Cr_2O_3 Profile on .003 SS Foil **Test not Performed**

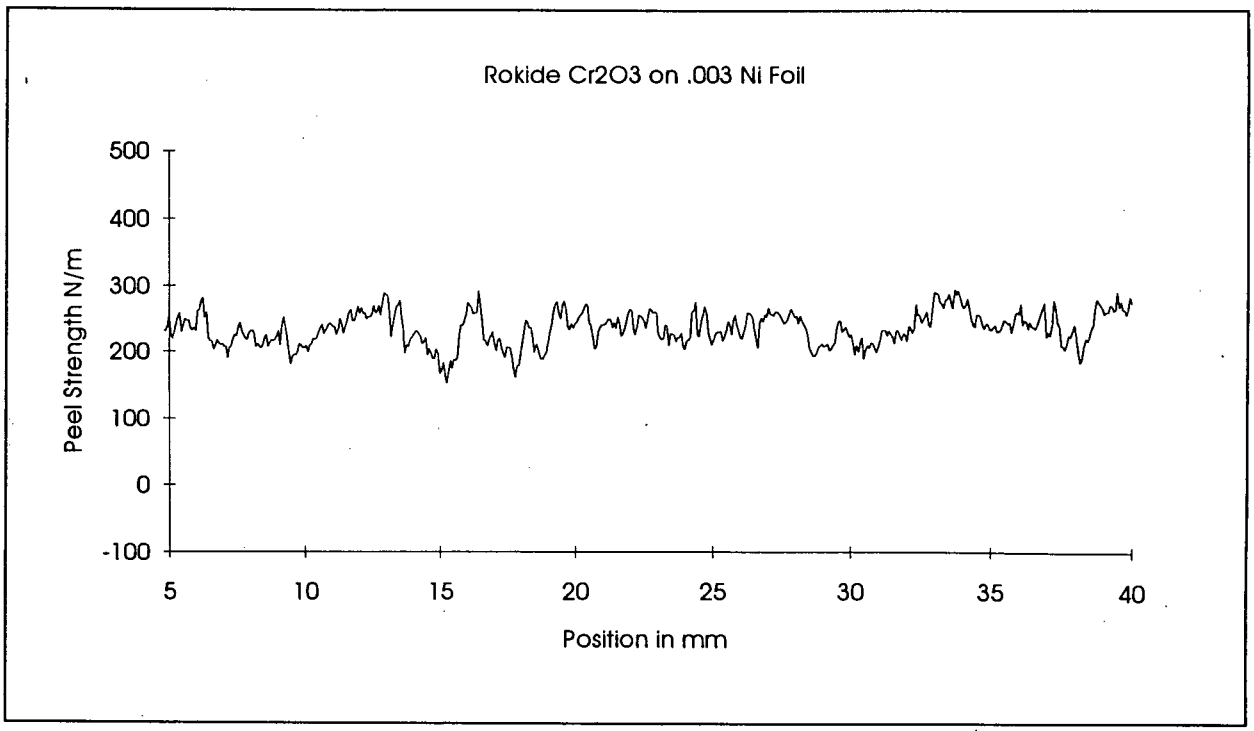

Rokide Cr_2O_3 on .003 Ni Foil (051695c)

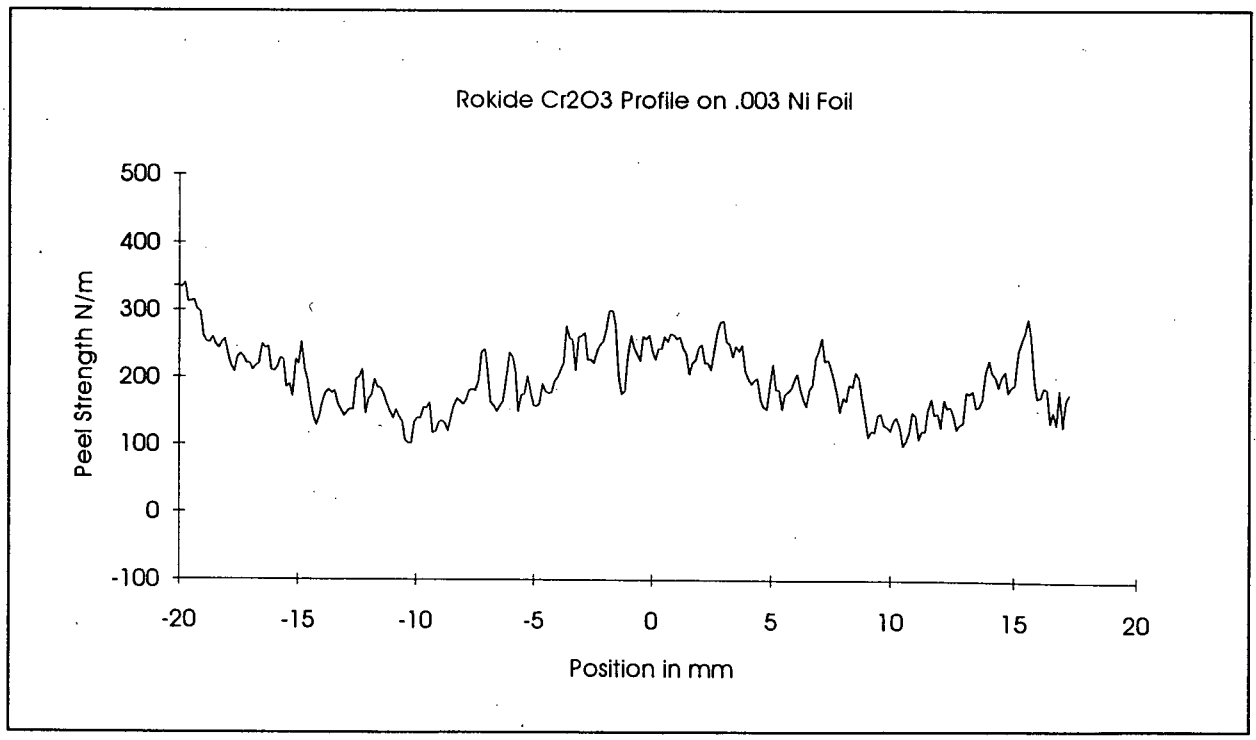

Rokide Cr_2O_3 Profile on .003 Ni Foil (051695b)

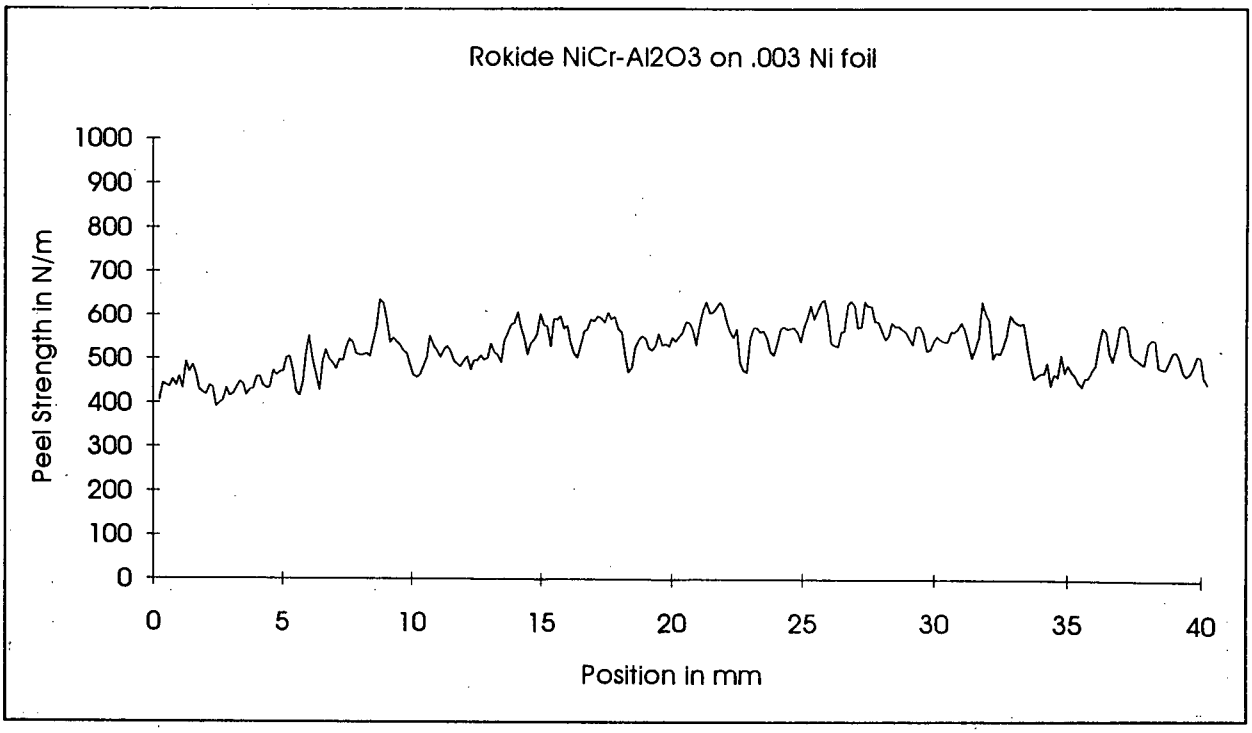

Rokide NiCr Al_2O_3 on .003 Ni Foil (051695e)

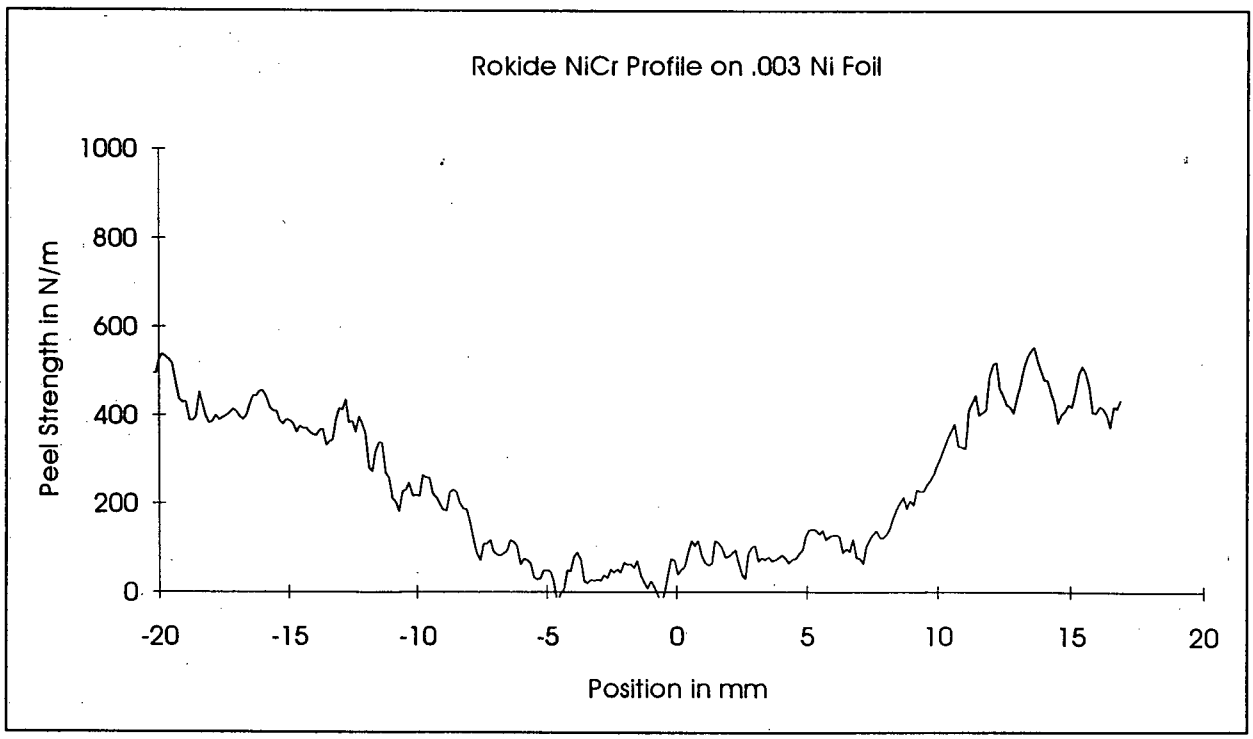

Rokide NiCr Profile on .003 Ni Foil (051695d)

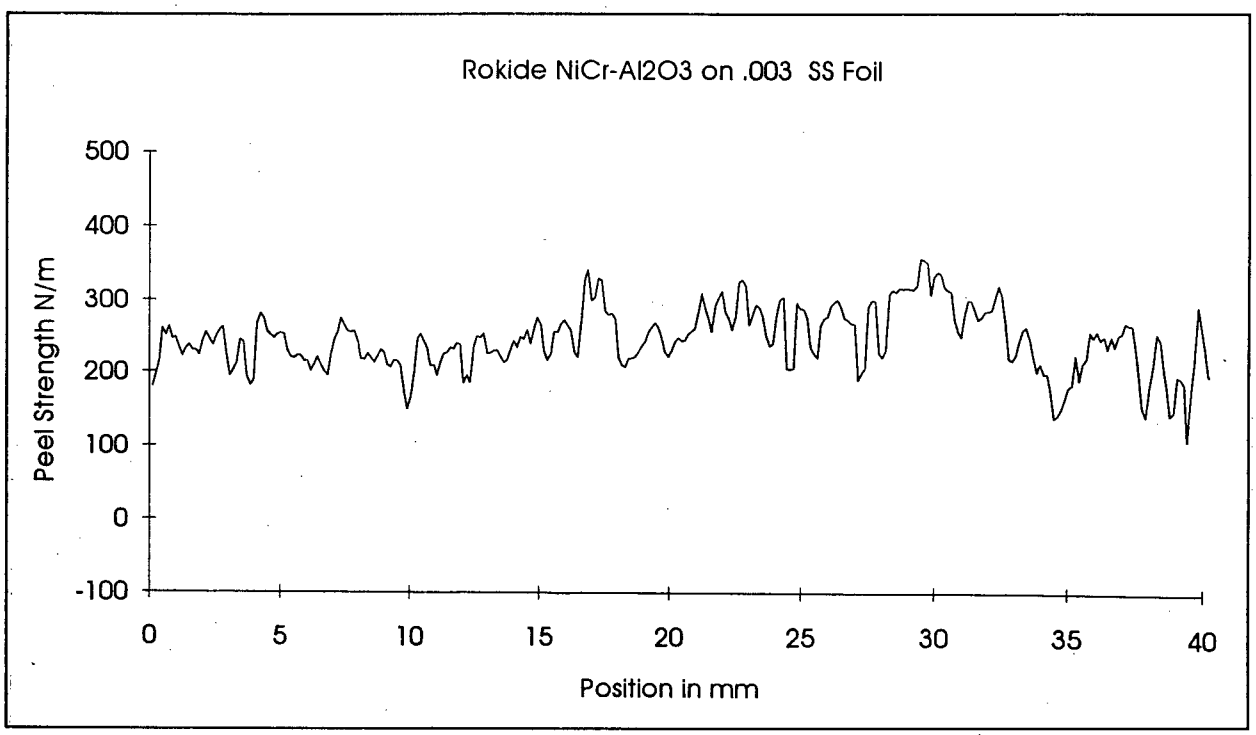

Rokide NiCr Al_2O_3 on .003 SS Foil (051695e)

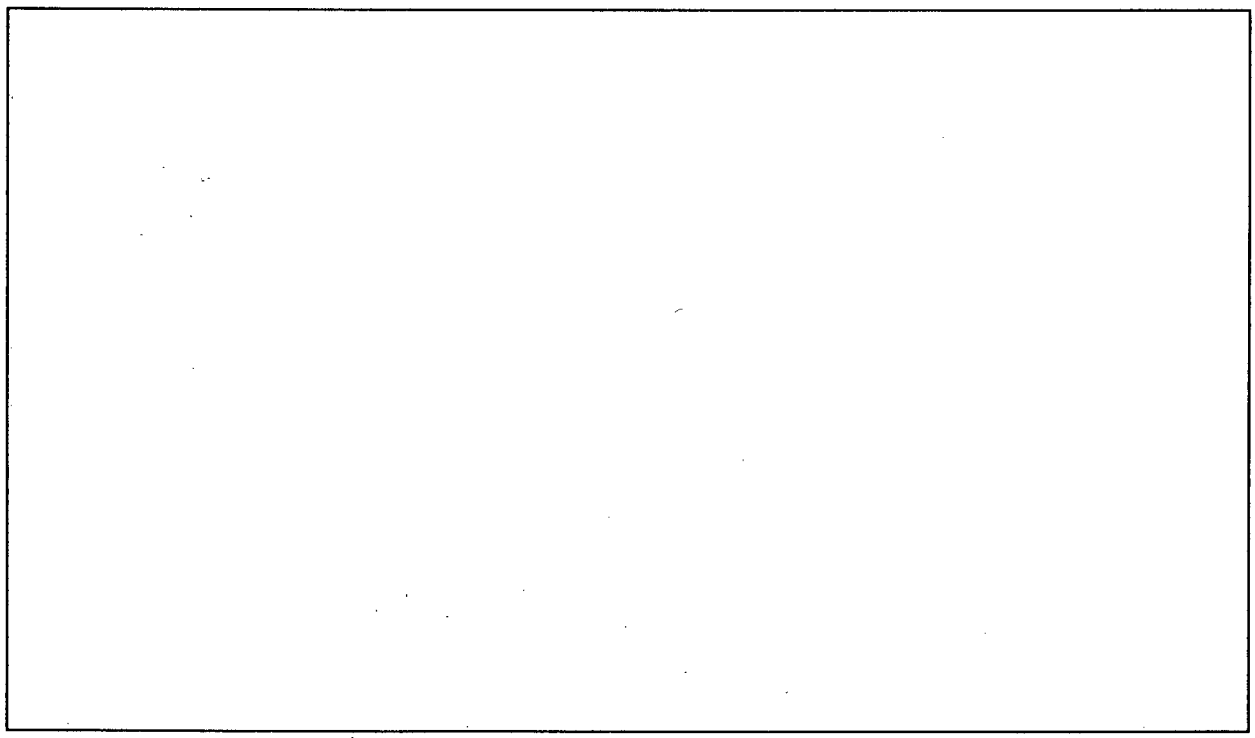

Rokide NiCr Al_2O_3 Profile on .003 SS Foil (051695d) **Test not Performed**

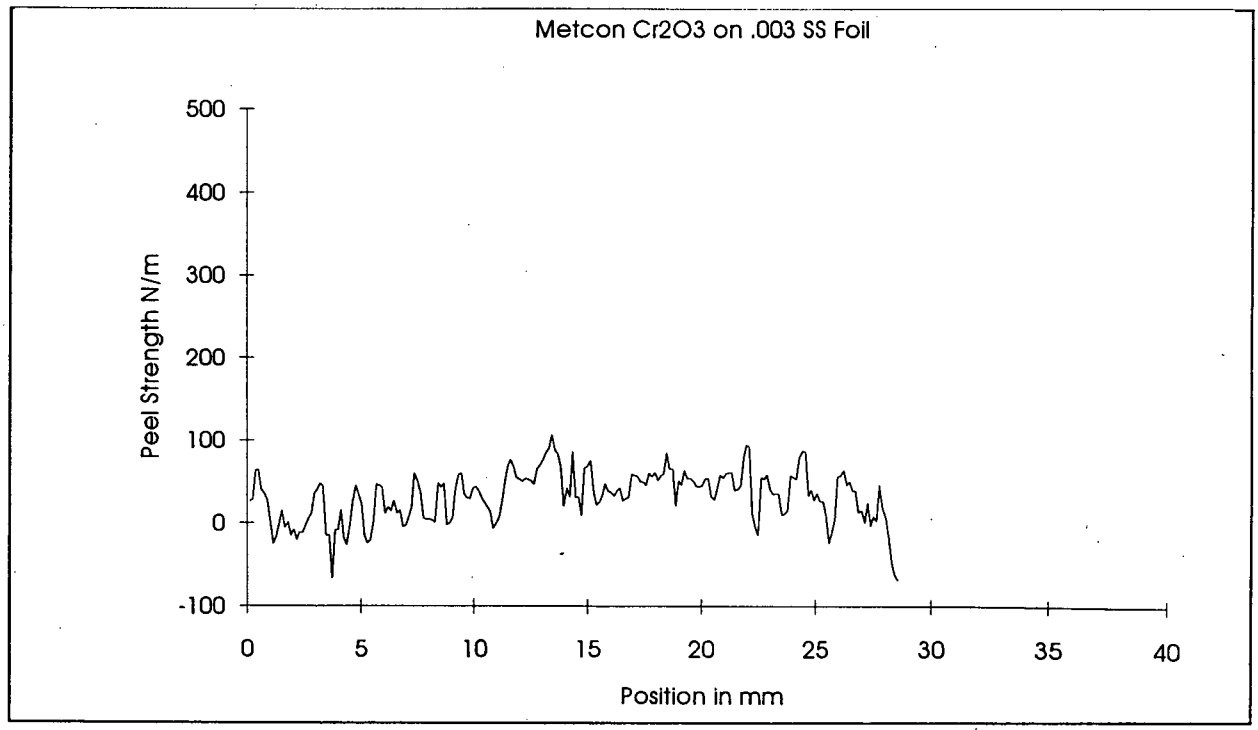

Metcon Cr_2O_3 on .003 SS Foil (052395b)

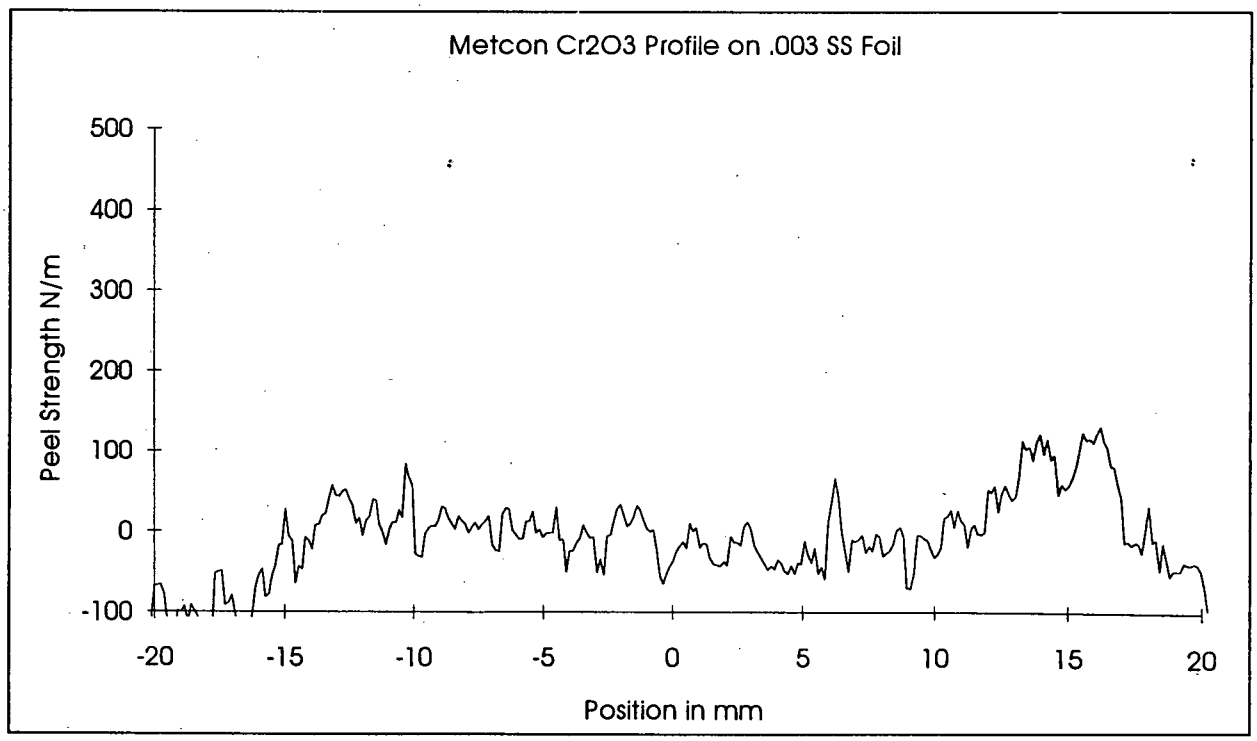

Metcon Cr_2O_3 Profile on .003 SS Foil (052395a)

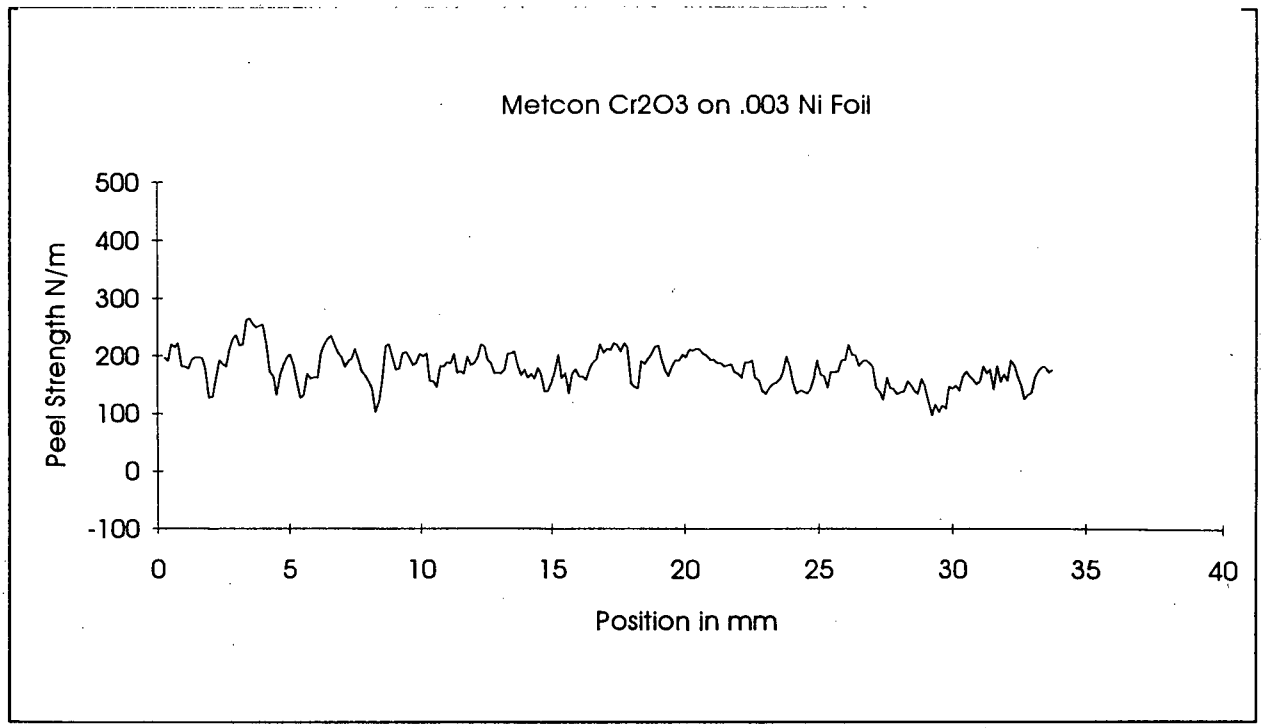

Metcon Cr_2O_3 on .003 Ni Foil (052395b)

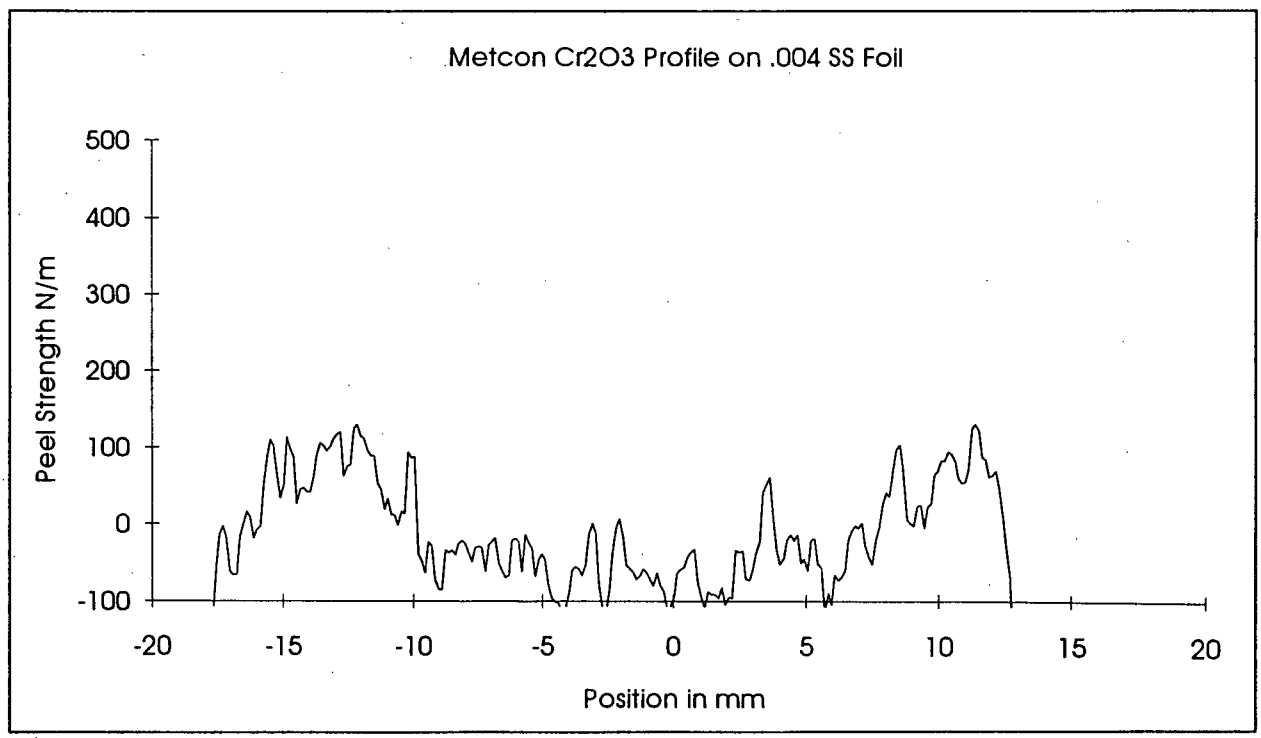

Metcon Cr_2O_3 Profile on .004 SS Foil (052395a)

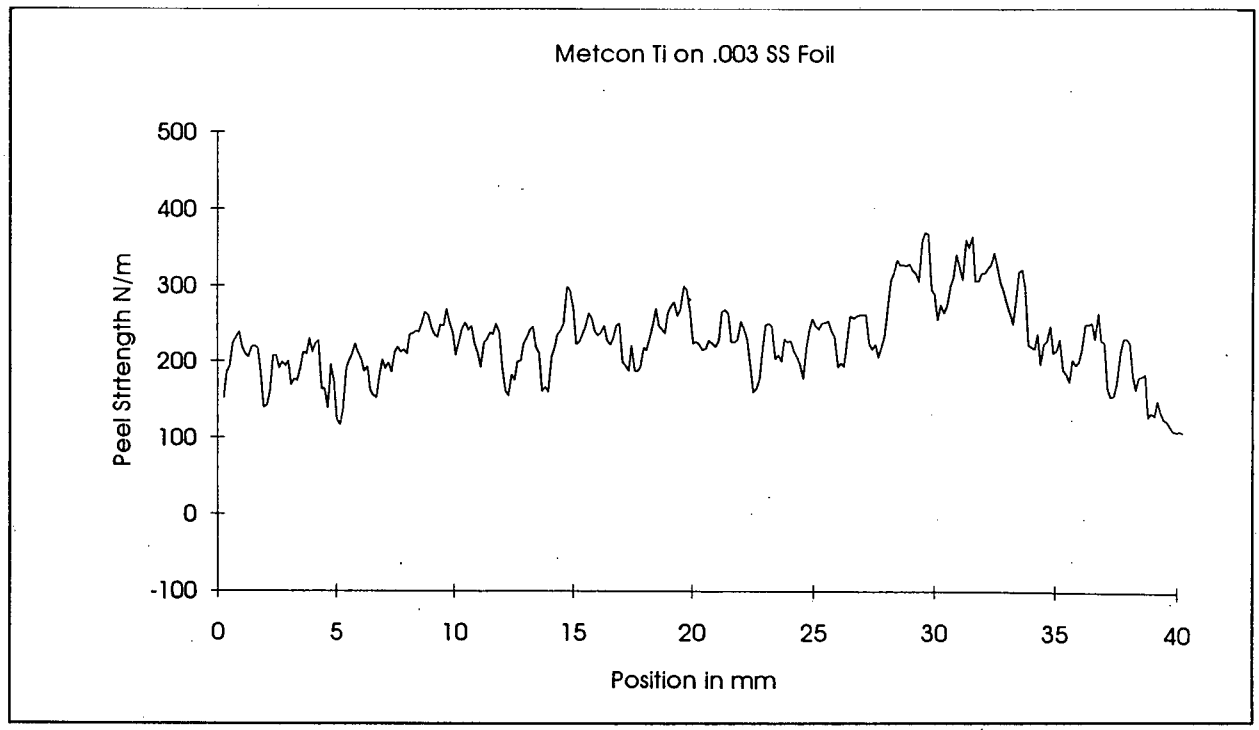

Metcon Ti on .003 SS Foil (052395c)

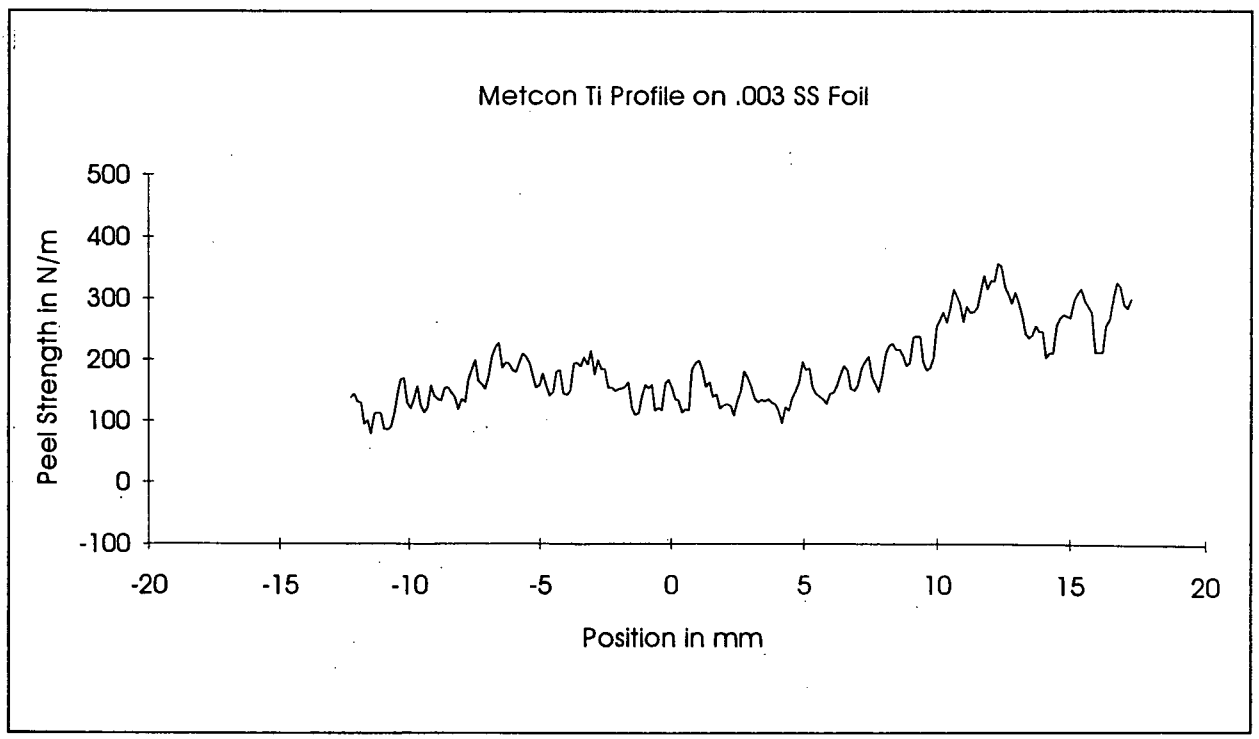

Metcon Ti Profile on .003 SS Foil (052395d)

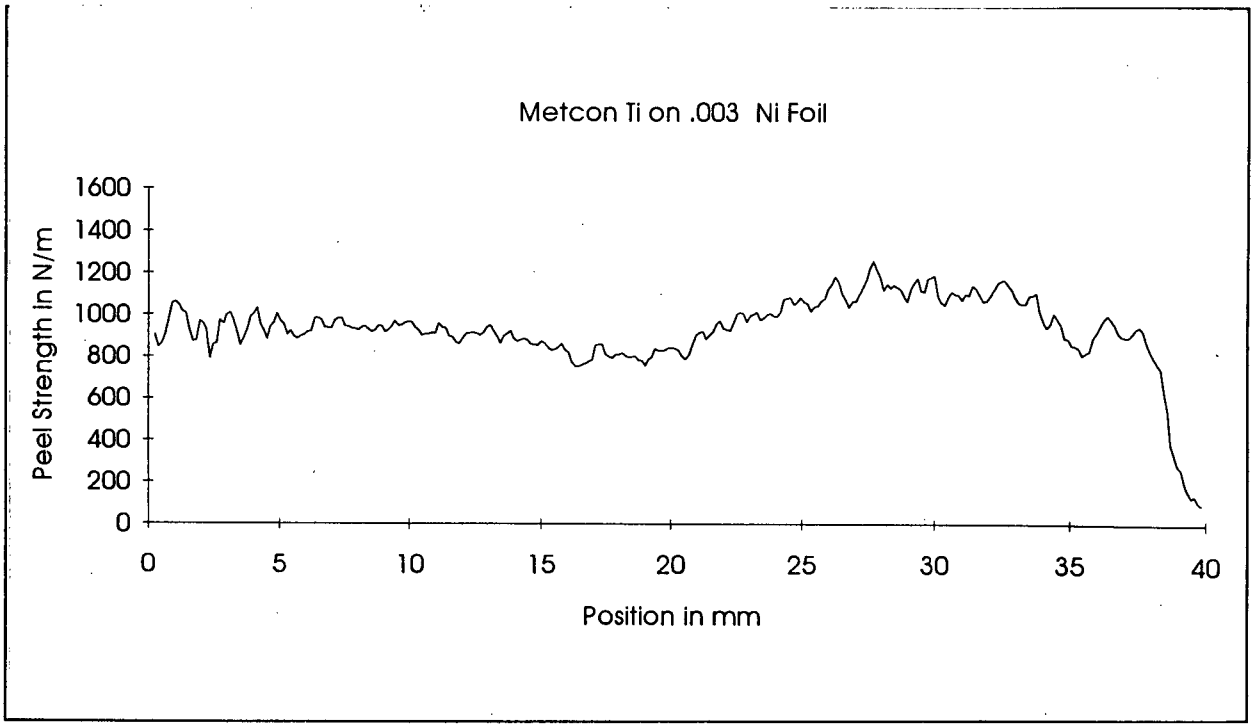

Metcon Ti on .003 Ni Foil (052395c)

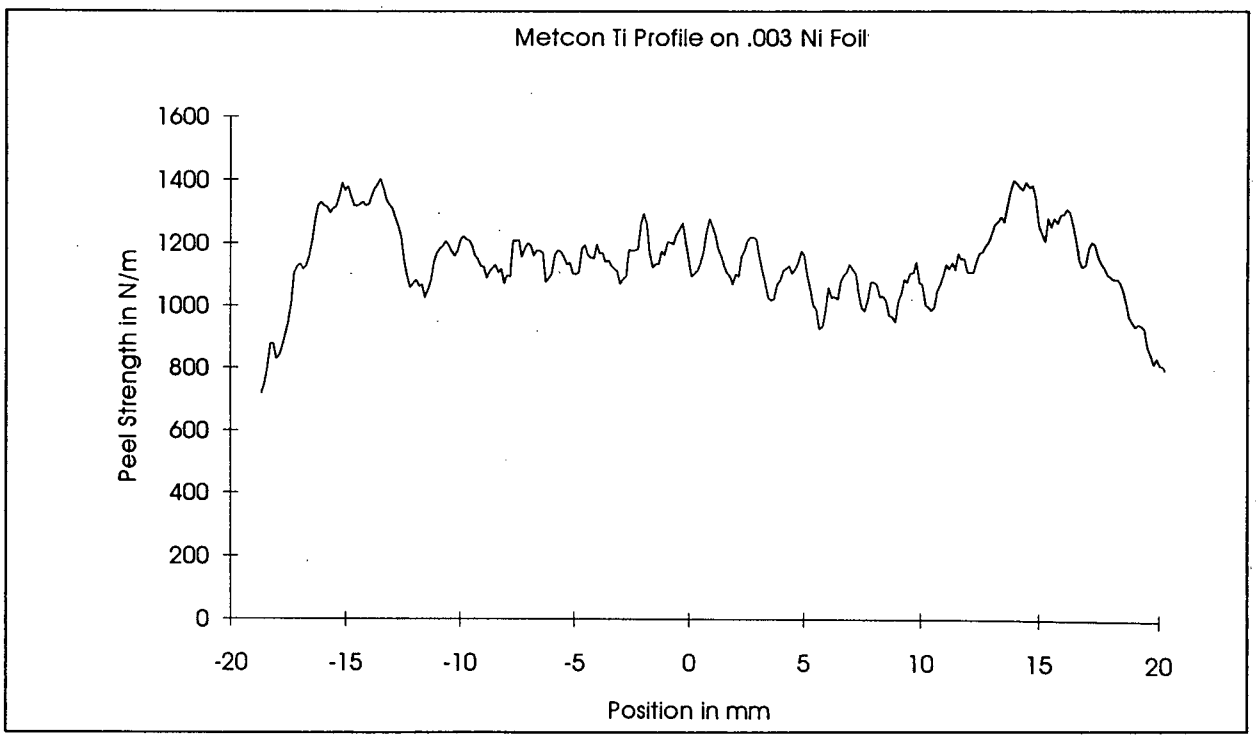

Metcon Ti Profile on .003 Ni Foil (052395d)

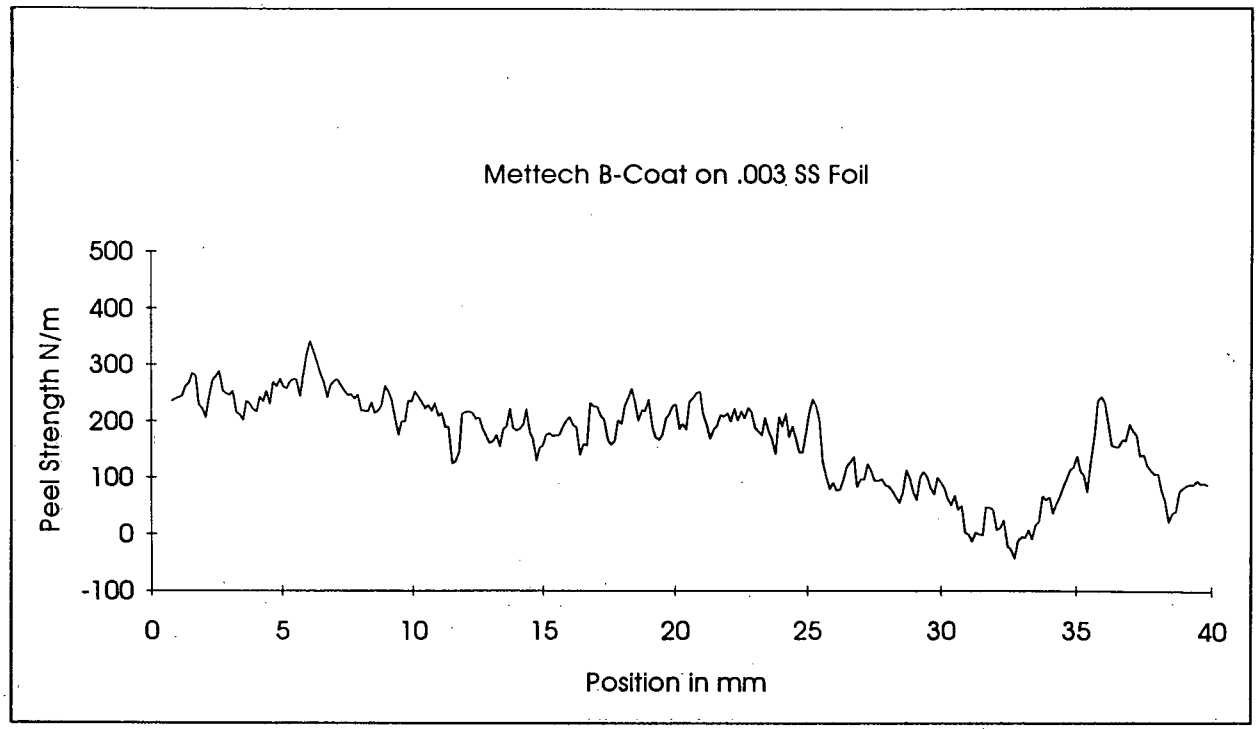

Mettech Bond Coat on .003 SS Foil (052695a)

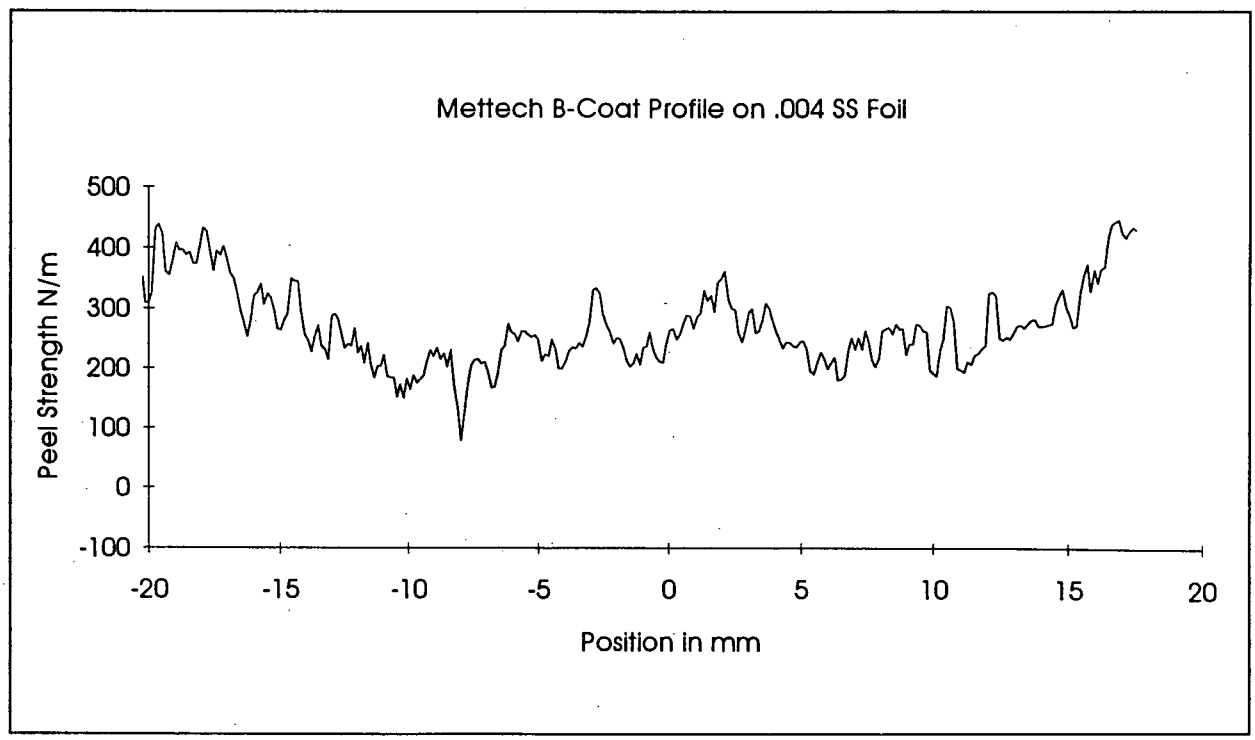

Mettech Bond Coat Profile on .004 SS Foil (052395a)

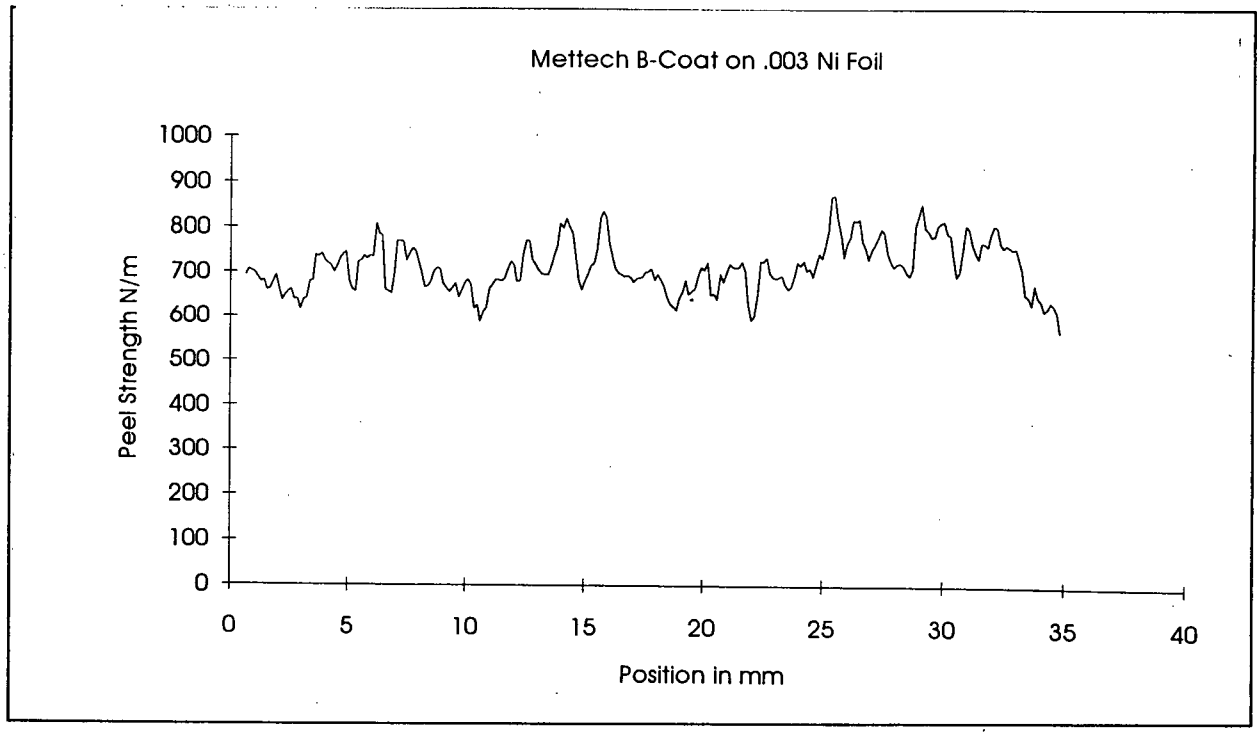

Mettech Bond Coat on .003 Ni Foil (052395a)

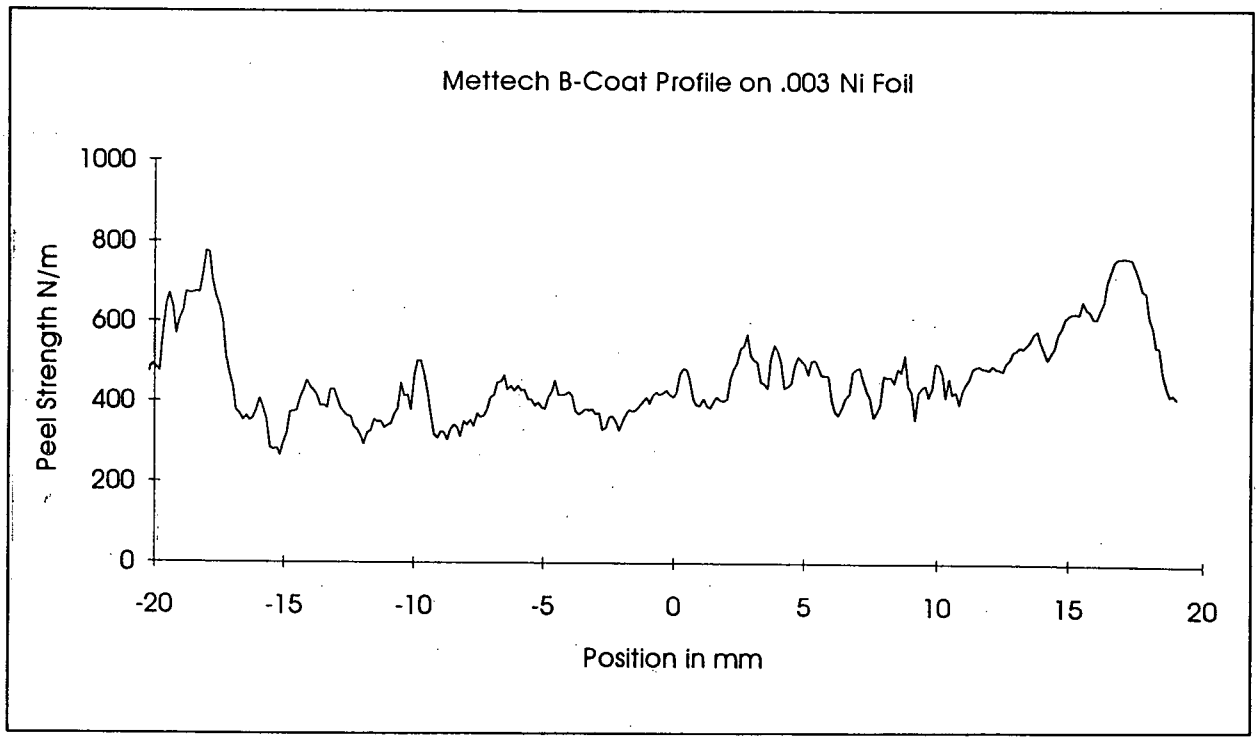

Mettech Bond Coat Profile on .003 Ni Foil (052395b)

Appendix B Test Procedures for Thermal Spray Coatings

Several detailed procedures were develop to test thermal spray coatings using the equipment at the University of British Columbia. In order for these tests to be conducted in a standard fashion these procedures were written. Each consists of a set of instructions outlining the important details of each test.

B.1 Procedure for ASTM C633-79 Pull Test

The following is a brief description of the procedure used to test the adhesion of thermal spray coatings. The fixtures and tensile machine are located in the Frank Forward Building at UBC. These procedures are based on ASTM standard C 633-79 which specifies the requirements for, and the applicability of, the test. People performing the test should be familiar with the standard. It should be noted that the test is crude and produces results with a large scatter. This scatter is due to many variables including: variations in coating properties, misalignment during bonding or pulling, the presence of different types of coating flaws and variations in the glue properties. Due to the this variation a large number of test samples may be needed to obtain significant results. The ASTM recommends at least 5 samples per set for quality control. A list of current references on the bonding of thermal spray coatings and a description of new adhesion measurement techniques are available from Tom Troczynski at UBC Metals and Materials Engineering (604-822-2612).

1. Spray 5 test pieces as described in the standard. A jig for holding the samples is available in room 106b. Use the same spray parameters as will be used in actual manufacturing. The samples should conform to the geometry shown in the standard and should be labeled with an engraver prior to spraying. It should be noted that the test fixture at UBC uses the 0.5 inch UNF thread. It in not in the standard, but recent work suggests that the test pieces should be two inches long instead of one, because the longer samples produce a much more uniform stress field in the coating. Samples of both sizes of cylinder are available in room 106.

   DO NOT TOUCH THE COATED SURFACE at any time after spraying. Grease or other debris will destroy the adhesion of the glue to the coating and invalidate a test. If the coating is dirty or grinding was necessary (as per the standard) it should be cleaned with dry compressed air and then LPS Presolve or other suitable solvent which leaves no residue.

2. Prepare glue blocks. These blocks are identical to the sprayed blocks but can be reused. The old glue should be removed and the glue surface should be recut on a lathe to ensure that it is flat and true. The blocks should be cleaned and degreased. After remachining ethyl alcohol may be used as an initial cleaner. Blow the sample clean with dry compressed air. A second cleaning with LPS Presolve will remove any remaining oil or debris. Grit blast the face of glue blocks and brush off the remaining dust with a clean toothbrush. After cleaning place the samples and glue blocks in the drying oven in

room 106. Check that the temperature in the oven is 65C. The samples should be preheated for 1 hour in the drying oven and glued immediately upon removal.

3. Glue the blocks to the coated samples. At UBC we currently use a thermoset epoxy which cures at 180 C in air. The maximum bond strength achievable will depend on surface preparation and alignment. The 3M epoxy 1386 has been tested to 12000 psi for thin glue layers. NW Mettech has a supply of this adhesive for the purpose of adhesion testing. The glue is spread on each surface to be bonded. Approximately 0.5ml should be used on each surface, but this amount will depend on the roughness and porosity of the coating material. The samples are then held under a low vacuum (-30 in Hg) in a desiccator for 10 min. This step eliminates air bubbles in the glue. Place one edge of the coated block on the edge of the glue block and roughly align them. Push the blocks together from one edge to the other to avoid trapping air in the glue. Wipe off excess glue. Wrap each joint with a layer of teflon tape to prevent the glue from leaving the joint. Place 6 samples at a time in the alignment jigs and place them in the kiln (see Peter Musil for kiln operation) for 3 hours at 180 C.

4 Remove the samples from the kiln and allow to air cool in a dry place. The samples should then be stored overnight room temperature.

5 Remove the samples from the alignment jigs and remove any excess glue with a razor blade, then 60 grit SiC paper, followed by a light polish with 320 grit paper. Care must be taken here not to damage the metal fixtures, coating, glue, or their interfaces.

6 Prepare tensile machine. Use a load cell with a 10000lb full scale load and the Instron machine with the chart recorder. The load cell labeled 233F was calibrated in April 1994 and was found to be accurate over all load scales to 1.3%. If a larger failure load is expected special apparatus may be required. Calibrate and balance the machine as specified in the Instron manual. Use a standard universal in the top of the machine. Make sure that the chart recorder and load cell amplifiers have at least 30 min. to warm up before calibration and balancing. Run the chart recorder in load versus time mode and use a chart speed of 3 cm/min. See Serge Dalliare for Instron operation.

7 Thread the test sample onto the loading fixtures. Screw the sample into the fixture until the thread bottoms out then back off a full turn. Adjust the cross-head position so that the sample are easily placed in the machine. Do not force sample or apply any loads to it after gluing.

8 Start the chart recorder at 3 cm/min. Pull the sample at a cross-head speed of 0.050 in/min. until the joint fails. Note the peak load.

9 Measure the sample diameter and calculate the failure stress. Examine the failure surface. If the glue failed the coating bond strength is only known to be greater than the glue strength as tested in the control sample. If the coating failed then the cohesive strength of the coatings was measured. If the coating-substrate interface failed then the

interfacial bond strength was measured. If any other interface failed or if failure occurred by a combination of the above, no general interpretation is possible.

B.2 Procedure for Peel Test Specimen Preparation

The following procedure is an outline of the steps required to perform an accurate peel test on a thermal spray coating. Various parameters have not been optimized for every foil and test requirement and thus can be varied if problems with the below procedure arise. The thickness and type of foil depend on the conditions of the test. Some foils such as aluminum are difficult to solder and will require some practice and skill.

1 Prepare foil. Cut, using shears, into strips 25 mm by 150 mm. Avoid bending or kinking foil. Do not work the foil. Prepare surface of the foil for soldering. With stainless steel, nickel or copper foils a simple cleaning with alcohol is all that is required. With aluminum or other active metal foils a surface preparation is necessary which depends on the soldering system.

2 Place foil on a flat metal plate. Place a layer of clean paper towel between the foil and plate. Paint Kester liquid acid flux onto a 70 mm portion of the foil starting 20 mm from one end. Use a high power electrical soldering iron (100 Watts) and eutectic Pb-Sn solder (40-60) to coat the first 80 mm of the foil strip with a thin layer of solder. Work the molten solder from on end of the region to the other. Excessive heating of the foil is to be avoided. Ensure that complete wetting has taken place. Remove any solder bumps and all flux. Kerosene works well as a cleaner but must be washed off with alcohol afterwards. Mild detergent may also be used. Rinse sample well in clean water.

3 Heat the premade 25 mm by 65 mm by 8 mm threaded copper block with a thin layer of solder. Use hot plate to heat the block to soldering temperature. Spread the solder across the copper with the end of the solder wire.

4 Paint a layer of acid flux onto the soldered region of the foil. Hold the foil over the copper block and lower one end onto the liquid solder. As the solder on the foil melts continue to lower the foil ensuring that no air is trapped. Place a 25mm by 6.25mm by 100 mm steel block on top of the foil and push down to press out excess solder.

5 Remove the sample from the hot plate and allow it to cool in air. Wash thoroughly in soap and water to remove all flux and dirt. Use a nylon scrubby. If the back plate is stuck to the sample grasp copper with vise grips and gently bang the plate with a hammer until it comes loose.

6 Mask the area of foil not supported by the copper block using high temperature tape. Mask one millimeter along each edge to prevent lifting during grit blasting. Grit blast with fresh 80 or 100 grit Al_2O_3. Hold the gun 80 mm and 45 degrees from the sample and spray in even longitudinal strokes. Note the surface preparation should be determined for each test situation. Because harsh grit blasting may damage a

foil or cause it to lift from the solder it may not be possible to apply some surface treatments which might be more realistic. Without touching the blasted surface, clean the sample thoroughly with dry and clean compressed air. Brush the surface with a clean toothbrush to remove trapped grit.

7 Bolt copper block to spray bar. Note that a UBC we use a standard fixture for holding our samples. Figure 1 shows the assembly. Ensure that the holding bar and aluminum mask are clean and dry before they contact the sample. Mount the sample onto the rotating jig. The jig, holding bars and masks are in room 106.

8 Spray the assembly. For profile samples the flame center should fall on the center of the mask window. Align the gun carefully. Record all spray parameters

9 Remove the copper block from the bar. Clean the soot and dust from the sample. Use alcohol. After most of the dust is gone rinse again in alcohol and blow dry with compressed air. Dry sample for 1 hour in drying oven at 65 C.

10 Roughen and clean a 25 mm by 100 mm by 1 mm aluminum plate. This is best accomplished by cleaning, grit blasting and then cleaning as in step 9. Allow the alcohol to dry completely (5 min. under hot air). Smear the adhesive over coating and foil ensuring that there are no bubbles or unwet spots. Any heat curable epoxy which become rigid after curing will do but 3M 1386 Epoxy has been shown to work well. NW Mettech has a supply of this epoxy. Do the same with the Al plate. Place the plates and samples in a chamber and pump down to a -30 in Hg. Allow to sit until all bubbles are gone. Clamp the plates firmly together and place in a kiln at 180C for 3 hours. See peter Musil for kiln operation. Remove the assembly from the kiln and without letting it cool remove the clamps.

11 Place the copper side of the plate on a hot plate and heat until the foil coating and aluminum sandwich is free. Quickly wipe and solder from the foil with cold steel wool. The copper blocks may be cleaned and reused.

12 Make a mark on the Al plate corresponding to the torch center line with a permanent felt tip pen. Use 60 grit flat wheel to grind the edges parallel and flat. Grind the edges of the samples until the coating can be seen on the ground edge then use a 180 grit wheel to remove .1 mm on each edge. Always have foil side towards the cutting direction.

13 Label each sample with an appropriate name. This is usually the date sprayed followed by a letter indicating which type of coating and a number identifying the sample.

14 Peel on Tensile machine recording force and displacement. The procedure for this is outlined below. Normalize displacement to the crack tip at completion.

B.3 Procedure for Peel Testing

A peel test jig can be found in the cabinet in room 402 on the fourth floor. The jig bolts to the crosshead of a standard Instron testing machine. For use the jig should be clean and the bearings well lubricated with WD40. The load-displacement reading may be recorded on the Instron chart recorder or recorded with the data acquisition system. The literature on the data acquisition system in room 106a The load cell used should be a tension cell which is sensitive in the range 0 to 50 lbs. Most coating will be in the range 0 to 15 lbs. Calibration instructions are available from Serge Dalliare. Care should be taken when interpreting the results as following the procedure below does not guarantee good results. Figure 2 shows the peel jig.

1 Usually the peel test require a load cell which is sensitive to loads between 0 and 50 lbs. Use an appropriate range Calibrate the tensile machine following the machine's instructions. Mount the peeling jig in the machine ensuring that everything is square and solid. Mount a universal joint and a self tightening grip onto the load cell. Zero the load scale.

2 Set up data acquisition system. If using a chart recorder adjust paper and start the recorder. If using a data acquisition computer check all the wires and run the acquisition program.

3 Using crazy glue attach an aluminum tab onto the end of the foil. These aluminum tabs are stored with the jig. When the glue has cured (~10 min.) clip the deadweight cord to the aluminum support plate.

4 Clamp the aluminum tab into the self tightening grips of the Instron. Thread the sample into the test jig as shown in the figure. Be careful not to load the sample in any way. Place a 1 lb. weight on the end of the cord. Check to make sure that nothing is binding and that all the rollers can rotate. Add 6 more lbs to the deadweight.

5 Start the tensile machine and pull at a rate of .2 in/min. As the sample peel watch for any binding kinking or twisting of the foil which would indicate misalignment. Peel for 2mm to initialize cracking.

6 Without stopping the crosshead remove enough weight to achieve the desired backload. In most cases a 3 lb. deadweight will be adequate. For a strongly bonded stiff foil more weight can be used. Be aware that when comparing coatings the same backload should be used.

7 If using the data acquisition system reset the LVDTs and the acquisition. Peel the foil until the end mark crosses the mark on the jig. Stop acquiring data. Place marks on the chart corresponding to the start and finish of the test. Convert the measured displacement to be zero at the crack tip.

8 Remove the specimen from the jig and examine the peeled surface. Ensure that the crack propagated through the coating foil interface and not some other path.

9 The data analysis and calibration is discussed below

10 Tape the foil back onto the substrate and store appropriately.

B.4 Calibration Procedure

In order to obtain the interfacial energy from the peel load a calibration is necessary to determine the amount of energy consumed by friction and plastic work during peeling. This can be accomplished by directly measuring the friction and plastic work in a free standing foil. The calibration involves measuring the force required to bend a foil around the mandrel of the peeling jig as a function of foil tension. The plastic work is constant and the friction increases linearly with load. The friction can be found from the slope of a plot of deadweight versus measured load. The plastic work can be found from the intercept.

1 Make calibration samples in the same manner as the coated specimens. Grit blast them as discussed above. Do not coat the samples. Place them in the kiln while the coated sample are curing. Upon removal from the kiln, heat them and remove the solder in the same way as the coated samples. For every type of foil make at least one calibration sample for every 10 peel tests.

2 Trim 4mm from the edges with shears to provide clean edges. Glue aluminum tabs to the ends of the foil and mount the sample in the jig in the same fashion as a normal peel sample. Place 8 lbs of deadweight at the end of the cord and peel at 0.2in/min for 1 minute to initialize the deformation. Stop the crosshead and remove all but 1lb of deadweight. Again peel for 1 min and record the load cell force. Add 0.5lbs and continue peeling. Repeat the procedure until you reach a 7 lbs total weight.

3 Average the peel load for each dead weight for the last 45 sec of peeling. This allows a steady state to be reached for each load. Plot the deadweight against the average measured force, and calculate the slope and intercept. Measure the sample width.

4 The following relationship exists between the applied load, the friction and the deformation work:

$$F_m = (\mu + 1)D + \Omega w$$

Calculate μ from the slope and divide the intercept by the sample width to obtain (Ω). This is a material property of the foil and can thus be used obtain the peel strength from a test with the same foil material with the same thickness.

5 To convert the measured load in a peel test to a peel strength use the deformation energy and friction from the above calculation to modify the measure peel force in:

$$PeelStrength = \left(\frac{F_m - (1+\mu)D}{w} \right) - (\Omega)$$

6 For a coating with variable adhesion such as a profile sample a plot of peel strength versus position is reported. For a uniform coating the average peel strength over 30 mm of peeling is reported.